HEAT TRANSFER IN NON-NEWTONIAN FLUID FLOW FROM AN OBLIQUE ARRAY OF PLATES OF UNEQUAL LENGTH

by

Ammata Tusnapuckdi

B.S. in M.E., Rangsit University, 1992

M.S. in M.E., Bradley University, 1996

Submitted to the Graduate Faculty of

School of Engineering in partial fulfillment

of the requirements for the degree of

Doctor of Philosophy

University of Pittsburgh

2002

UNIVERSITY OF PITTSBURGH

SCHOOL OF ENGINERING

This dissertation was presented

By

Ammata Tusnapuckdi

It was defended on

March 12th 2002

and approved by

(Signature) _____

Committee Chairperson

(J.L.S. Chen, Professor of Mechanical Engineering)

(Signature) _____

Committee Member

(M. Chyu, Professor of Mechanical Engineering)

(Signature) _____

Committee Member

(P. Smolinski, Professor of Mechanical Engineering)

(Signature) _____

Committee Member

(L. Schaefer, Professor of Mechanical Engineering)

(Signature) _____

Committee Member

(R.M. Enick, Professor of Chemical Engineering)

ACKNOWLEDGMENTS

I would like to express my sincere appreciation and acknowledgement to my advisor, Professor James L.S. Chen, for all the advice and guidance that he provided during my graduate study. Without his help, the completion of this dissertation would not have been possible.

Thanks also to the other members of the dissertation committee, Professor Minking Chyu, Professor Laura Schaefer, Professor Patrick Smolinski, and Professor Robert M Enick for their helpful comments.

I would also like to extend my thanks to my parents and my sister for their continuing support and encouragement during my study.

Finally, and most importantly, I would like to thank my girlfriend, Kuntalee Kuptawathin, for her prayers, patience, encouragement, and understanding that were vital to complete this dissertation.

HEAT TRANSFER IN NON-NEWTONIAN FLUID FLOW FROM AN OBLIQUE ARRAY OF PLATES OF UNEQUAL LENGTH

Ammata Tusnapuckdi, Ph.D.

University of Pittsburgh, 2002

The periodically fully developed laminar heat transfer and pressure drop of arrays with non-uniform plate length aligned at angle to the flow direction of Non-Newtonian and Newtonian fluids are studied by numerical analysis. The body-fitted coordinate system is adopted to retain the corresponding periodic relation of the lines in physical coordinate system and computational domains in body-fitted coordinate system. The computations are carried out in one periodic cycle.

Power law model non-Newtonian fluids are considered. The continuity equation, the x-y momentum equations, and the energy equation with viscous energy dissipation are presented.

The power law scheme, discretization, SIMPLE algorithm, TDMA, Jacobi iterative methods are adopted in the numerical procedure for the integration of the governing equations.

In this dissertation, focus is placed on the effects of the flow index, the generalized Reynolds number, and various geometrical parameters on the flow field and thermal behavior of the flow. The results are obtained and show that the form drag of plate including the inlet and outlet effects gradually becomes significant after a certain value of Reynolds number.

The flow re-circulation has a significant influence on the average heat transfer at higher Reynolds number. The increment of flow index leads to the increase of friction factor but decrease of heat transfer and fluid temperature.

The longer plate causes the increase of the friction factor and heat transfer as well as fluid temperature. The increment of transverse pitch leads to the decrease of both friction factor and heat transfer as well as fluid temperature.

The increment of plate angle leads to the increase of friction factor, average heat transfer, and fluid temperature.

DESCRIPTORS

Body-fitted coordinate system

Heat transfer of non-Newtonian

Interrupted plates

Non-uniform oblique plate

Power law model

Non-Newtonian fluid

TABLE OF CONTENTS

LIST OF FIGURES

LIST OF TABLES

NOMENCLATURE

Symbols

u	axial velocity, m/s
v	transverse velocity, m/s
x, y	coordinate in Cartesian plane
m	consistency index of power-law model
n	flow index
k	thermal conductivity
c_p	specific heat
J	Jacobean of inverse coordinate transformation
P	pressure, Pa
u_m	mean velocity, m/s
L	plate length, m
L_p	streamwise length of one cycle, m
T	temperature, K
T_w	wall temperature, K
T_b	bulk mean temperature, K
T_p	transverse spacing between two adjacent plates, m
Re	generalized Reynolds number
Nu	Nusselt number

f	friction factor per cycle
b	source term

Greek Symbols

α, β, γ	metric coefficients of two coordinate systems
ϕ_u, ϕ_v	contravariant velocity components in ξ, η direction
Π	general dependent variable
θ	plate angle, degree
Θ	dimensionless temperature
ξ, η	coordinates in transformation plane
Ψ	molecular diffusivity of heat
Φ	viscous-energy dissipation

Subscripts

m	mean
ξ, η	partial derivatives with respect to ξ and η
1	long plate
2	short plate

Superscript

*	guessed value
**	value of last iteration time

1. Introduction

Flow interruption at periodic intervals in a flow passage is a well-know technique for enhancing heat transfer. The slit fins used in compact heat exchangers and automobile radiators are an example of this technique [1-3]. Due to the repeated interruption of the thermal boundary layer, the slit fin has a higher local heat transfer coefficient than that without slits [1, 2, 4, 5]

In the case of louvered fins, the fin segments are positioned obliquely to the flow direction; additional heat transfer enhancement can be obtained because of the impinging effect and the vorticity and turbulence created in the flow. The heat transfer and pressure drop characteristics mainly depend on the geometric factor as well as dynamic parameters. The former includes the positioning of the fin segments (i.e., plates), the transverse pitch between two adjacent plates, and the inclined angle of the plates [6-9].

Non-Newtonian flow behavior is typically observed in concentrated suspensions and in high molecular-weight materials [27, 28]. One of the best opportunities to observe Non-Newtonian behavior may be found in the kitchen. Salad dressings, butter, whipped cream, and doughs are examples of non-Newtonian fluids

Most biologically important fluids contain high molecular-weight components and are, therefore, non-Newtonian fluids. The rheology of blood has received much study. Blood is rheologically complex on two counts: first, it is a suspension because erythrocytes with characteristic dimensions of several micrometers are present in excess

of 40 % by volume, and second, the suspending fluid itself exhibits non-Newtonian behavior because of the presence of high molecular-weight protein.

In many chemical and processing industries, the products such as polymer, foods, and plastics exhibit non-Newtonian behavior. The understanding of such non-Newtonian fluids is important because of their growing technology applications.

The objective of this work is to numerically analyze the forced convection heat transfer of power-law non- Newtonian fluids flowing along an array of non-uniform plate length positioned obliquely to the flow direction. The analysis is started with the formulation of the problem. Through a coordinate transformation, the governing equations with appropriate boundary conditions are numerically calculated and transformed to a problem similar to the one with forced convection flow through an array of parallel plates.

Results of velocity fields, friction factor, temperature profile, and heat transfer are obtained for variation of non-Newtonian fluids (pseudoplastic and dilatant). The effects of the Reynolds number, plate angle, ratio of plate length, ratio of transverse pitch to streamwise length of one cycle, and the flow index on the thermofluid characteristics are examined in detail.

2. Literature Review

Huang and Tao [1] did an experimental study on heat transfer and pressure drop characteristics for arrays of non-uniform plate length positioned obliquely to the flow direction. They investigated experimentally arrays of non-uniform plates, aligned at an angle of 25 degree to the flow direction. They found that for most cases studied, the thermal performance of the array with a non-uniform plate length was better than that of the array with a uniform plate length.

Lee [2] studied experimentally heat transfer and pressure drop characteristics of an array of plates aligned at angles to the flow direction in a rectangular duct. An array of plates, aligned at various angles of 20-35 degree to the direction of air flow in a rectangular, straight duct, was investigated in the range of Reynolds numbers between 350 and 5000. He found that the average heat transfer coefficient at low Reynolds numbers (less than 1200) is nearly independent of the angle of alignment with respect to the air flow direction. At higher Reynolds numbers (greater than 1500), the average heat transfer coefficient deviated significantly from the theory. The pressure drop measurement through the array of the plate showed that the flow pattern was a function of only the plate angle and independent of the Reynolds number.

Wang and Tao [3] studied heat transfer and fluid flow characteristics of plate array aligned at various angles to the flow direction. They investigated numerically in the range of Reynolds numbers between 50 and 2300 using body-fitted coordinated system

and at angle of 15, 25, and 35 degrees. They found that both the intensity of the heat transfer and the pressure drop increase with the increases of oblique angle and plate length.

Yan et al. [4] experimentally investigated heat transfer and pressure drop performance for arrays of staggered plates aligned with air flows. The experimental results showed that in the fully developed region of uniform arrays, the values of the ratio of heat transfer factor and friction factor (j/f) for plate length equal to 22, 44, and 66 were almost the same at the same Reynolds number. For the non-uniform periodic arrays, the fully developed region of heat transfer was achieved from the second period.

Sparrow et al. [5] studied heat transfer and fluid flow of interrupted wall channels with application to heat exchangers. The basic heat transfer and pressure drop results were employed to investigate whether an interrupted wall channel experienced an augmented heat transfer rate as compared with that for a parallel plate channel. The results showed that the heat transfer performance of the interrupted wall channel was clearly superior to that of a parallel plate channel.

Sparrow and Liu [6] studied heat transfer, pressure drop, and performance relationships for in-line staggered and continuous plate heat exchangers. The results were compared to that of the cases with segmented plate arrays and with parallel-plate channels. It was found that the heat transfer effectiveness of the segmented plate arrays was appreciably higher than that of the parallel plate channels.

Sparrow and Cur [7] studied experimentally on heat transfer and pressure drop for a pair of collinear interrupted plate aligned with the flow. It was found that the Nusselt number increased substantially with thickness at the higher Reynolds numbers

but decreased moderately with thickness at low Reynolds numbers. It was also found that the Nusselt numbers were relatively insensitive to thickness at smaller spacing but became more sensitive as the spacing increases and thicker plates promoted higher heat transfer coefficients.

Amano [8] studied numerically the laminar and turbulent heat transfer in a periodically corrugated wall channel. The Reynolds numbers were considered from 10-25,000. It was observed that the effect of the step ratio on the local Nusselt number was minor. Moreover, it was found that both skin friction and heat transfer patterns change drastically from laminar to turbulent flows.

Lee [9] studied heat transfer and pressure drop characteristics of an assembly of partially segmented plates. The segmented plates, which inclined at 25 degree to the flow, were investigated experimentally in the range of Reynolds numbers between 900 and 4000. He found that the heat transfer coefficient was a strong function of the segmented to total plate width ratio and it decreased as the segmented to total plate width ratio decreased.

Lang and Zhang [10] investigated the effect of oblique angles of interrupted plate lengths for louvered fins in a compact heat exchanger. He found that oblique angles of interrupted plate lengths increased the efficiency and thermal performance of a compact heat exchanger.

Pang et al. [11] studied numerically the heat transfer in fully developed fluid flow past arrays of interrupted plates positioned convergently and divergently along the flow direction. The obliquely positioned plates were simulated by a succession of steps. By adequately choosing the computation domain and appropriately assigning the initial

values of velocity and temperature, they found that the thermal performance of the obliquely positioned arrays of plates was better than that of a corresponding plane straight duct.

Patankar and Prakash [12] analyzed the effect of plate thickness on laminar flow and heat transfer in interrupted plate passages. The flow field was found to be quite complex. It contained recirculation zones behind the trailing edges of the plates, and there occurred significant defection of the through flow. The heat transfer from the thick plates did not improve sufficiently where the pressure drop for a given flow rate was greatly increased.

Wang et al. [13] studied numerically the periodically fully developed laminar heat transfer and pressure drop along arrays of non-uniform plate length aligned at an angle of 25 degree to air flow direction in the range of Reynolds numbers from 50-1700. The body-fitted coordinated system was adopted in their investigation to retain the corresponding periodic relation of the lines in physical and computational domains. The numerical results showed that both heat transfer and pressure drop increased with the increase in the length ratio of the long plate to the short plate and decreased with the increase in the ratio of transverse pitch to the longitudinal pitch.

Wieting [14] reported empirical correlations for heat transfer and friction characteristics of rectangular offset fin-plate in heat exchangers. Empirical relationships were developed by correlating experimental heat transfer and flow friction data from 22 rectangular offset fin-plate in heat exchanger configurations. The relationships could predict heat transfer and friction characteristics quite well.

Xiao and Tao [15] studied the effect of fin spacing on heat transfer and pressure drop of two row corrugated fin and tube heat exchangers. They experimentally investigated heat transfer coefficients and friction factors for corrugated fin and tube heat exchangers with different fin spacing. It was found that with increased fin spacing both the Sherwood number and the friction factor increased.

3. Analysis

The problem analyzed is schematically shown in Fig. 1. As seen there, a two-dimensional array of non-uniform plate length with constant wall temperature T_w is positioned obliquely to the flow direction.

The configuration studied can be specified by the following parameters: The periodic axial length L_p, the plate lengths L_1, L_2, the transverse space between the plates T_p, the plate angle θ.

The engineering background of this study is the heat transfer in Non-Newtonian fluid flow past louvered fins used in automobiles and other heat exchangers where the fins are formed by slitting a continuous thin copper plate and then turning the slit segments to an angle.

In this work the flow is two-dimensional, $L_p = L_1 + L_2$, $L_2 = 15mm$, steady state, laminar, and periodically fully developed. The fluid properties are assumed to be constant and the body force is neglected. The surface plate temperature is maintained at a constant temperature (T_w). The viscous energy dissipation is considered. Parametric studies of the following cases are performed:

1. The effect of flow index (n), equal to 1.2, 1.0, and 0.5, at $\theta = 25$ on the friction factor, temperature profile, and average heat transfer for each plate length ratio (L1/L2):

L1/L2 = 2.5	Tp/Lp = 0.571	Tp = 30 mm
L1/L2 = 2.0	Tp/Lp = 0.667	Tp = 30 mm
L1/L2 = 1.5	Tp/Lp = 0.800	Tp = 30 mm

2. The effect of flow index (n), equal to 1.2, 1.0, and 0.5 on temperature profile for different plate angle at Re = 300:

L1/L2 = 2.5	Tp/Lp = 0.571	θ = 5
L1/L2 = 2.5	Tp/Lp = 0.571	θ = 25
L1/L2 = 2.5	Tp/Lp = 0.571	θ = 30

3. The effect of flow index (n), equal to 1.2, 1.0, and 0.5 on temperature profile for different Reynolds number at θ = 25:

L1/L2 = 2.5	Tp/Lp = 0.571	Re = 100
L1/L2 = 2.5	Tp/Lp = 0.571	Re = 300
L1/L2 = 2.5	Tp/Lp = 0.571	Re = 900

4. The effect of plate length ratio at $\theta = 25$ and Re = 300 on the temperature profile for each flow index (n), equal to 1.2, 1.0, and 0.5:

L1/L2 = 2.5	Tp/Lp = 0.571	Tp = 30 mm
L1/L2 = 2.0	Tp/Lp = 0.667	Tp = 30 mm
L1/L2 = 1.5	Tp/Lp = 0.800	Tp = 30 mm

5. The effect of flow index (n), equal to 1.2, 1.0, and 0.5 at $\theta = 25$ and Re = 300 on the temperature profile for different transverse pitch spacing:

L1/L2 = 2.5	Tp/Lp = 0.571	Tp = 30 mm
L1/L2 = 2.5	Tp/Lp = 1.143	Tp = 60 mm
L1/L2 = 2.5	Tp/Lp = 1.905	Tp = 100 mm

6. The effect of plate length ratio at $\theta = 25$ on the friction factor and average heat transfer for each flow index (n), equal to 1.2, 1.0, and 0.5:

L1/L2 = 2.5	Tp/Lp = 0.571	Tp = 30 mm
L1/L2 = 2.0	Tp/Lp = 0.667	Tp = 30 mm
L1/L2 = 1.5	Tp/Lp = 0.800	Tp = 30 mm

7. The effect of transverse pitch ratio (T_p / L_p) at $\theta = 25$ on the friction factor and average heat transfer for each flow index (n), equal to 1.2, 1.0, and 0.5:

L1/L2 = 2.0	Tp/Lp = 0.571	Tp = 30 mm
L1/L2 = 2.0	Tp/Lp = 0.556	Tp = 25 mm
L1/L2 = 2.0	Tp/Lp = 0.444	Tp = 20 mm

8. The effect of plate angle (θ) at Re = 300 on the friction factor and the average heat transfer.

In the computation domain as shown in Fig. 2, the fluid flow and heat transfer can be specified by the following governing equations:

The continuity equation is essentially the equation for the conservation of mass; it is derived by a mass balance on the fluid entering and leaving a volume element taken in the flow field.

$$\frac{\partial u}{\partial x} + \frac{\partial v}{\partial y} = 0 \tag{1}$$

Equation (1) is the continuity equation in rectangular coordinate for the steady, two-dimension flow of an incompressible fluid.

The momentum equations are derived from Newton's second law of motion [16-19] which states that mass times the acceleration in given direction is equal to the external forces acting on the body in the same direction.

The external forces acting on a volume element in the flow field are considered to consist of the surface forces and body forces. The body forces will be neglected in this thesis.

The power law model for the non-Newtonian fluids can be defined by the following relationships [20]:

$$\tau = -\left[m \left| \sqrt{\frac{1}{2}(\Delta : \Delta)} \right|^{n-1} \right] \Delta$$

where

$$\Delta = \left(\frac{\partial u_i}{\partial x_j} \right) + \left(\frac{\partial u_j}{\partial x_i} \right)$$

$$\frac{1}{2}(\Delta : \Delta) = \left[2\left(\left(\frac{\partial u}{\partial x} \right)^2 + \left(\frac{\partial v}{\partial y} \right)^2 \right) + \left(\frac{\partial u}{\partial y} + \frac{\partial v}{\partial x} \right)^2 \right]$$

Then, the momentum equations for power law non-Newtonian fluid [20] can be defined by the following equations:

x -Momentum:

$$\rho(u\frac{\partial u}{\partial x} + v\frac{\partial u}{\partial y}) = \frac{\partial}{\partial x}\left[m \left[\left| 2\left(\left(\frac{\partial u}{\partial x} \right)^2 + \left(\frac{\partial v}{\partial y} \right)^2 \right) + \left(\frac{\partial u}{\partial y} + \frac{\partial v}{\partial x} \right)^2 \right|^{\frac{n-1}{2}} \right] \frac{\partial u}{\partial x} \right] + \frac{\partial}{\partial y}\left[m \left[\left| 2\left(\left(\frac{\partial u}{\partial x} \right)^2 + \left(\frac{\partial v}{\partial y} \right)^2 \right) + \left(\frac{\partial u}{\partial y} + \frac{\partial v}{\partial x} \right)^2 \right|^{\frac{n-1}{2}} \right] \frac{\partial u}{\partial y} \right] - \frac{\partial P}{\partial x} \quad (2)$$

y-Momentum:

$$\rho(u\frac{\partial v}{\partial x} + v\frac{\partial v}{\partial y}) = \frac{\partial}{\partial x}\left[m \left[\left| 2\left(\left(\frac{\partial u}{\partial x} \right)^2 + \left(\frac{\partial v}{\partial y} \right)^2 \right) + \left(\frac{\partial u}{\partial y} + \frac{\partial v}{\partial x} \right)^2 \right|^{\frac{n-1}{2}} \right] \frac{\partial v}{\partial x} \right] + \frac{\partial}{\partial y}\left[m \left[\left| 2\left(\left(\frac{\partial u}{\partial x} \right)^2 + \left(\frac{\partial v}{\partial y} \right)^2 \right) + \left(\frac{\partial u}{\partial y} + \frac{\partial v}{\partial x} \right)^2 \right|^{\frac{n-1}{2}} \right] \frac{\partial v}{\partial y} \right] - \frac{\partial P}{\partial y} \quad (3)$$

where m is the consistency index and n is flow index [20].

The temperature distribution in the flow field is governed by the energy equation, which can be derived by writing an energy balance according to the first law of thermodynamics for a differential volume element in the flow field [16-19].

If radiation is absent and there are no distributed energy source in the fluid, the energy equation is:

$$\rho c_p \left(u \frac{\partial T}{\partial x} + v \frac{\partial T}{\partial y}\right) = k\left(\frac{\partial^2 T}{\partial x^2} + \frac{\partial^2 T}{\partial y^2}\right) + m\left[\left|2\left(\left(\frac{\partial u}{\partial x}\right)^2 + \left(\frac{\partial v}{\partial y}\right)^2\right) + \left(\frac{\partial u}{\partial y} + \frac{\partial v}{\partial x}\right)^2\right|^{\frac{n-1}{2}}\right]\Phi \tag{4}$$

where

$$\Phi = 2\left(\left(\frac{\partial u}{\partial x}\right)^2 + \left(\frac{\partial v}{\partial y}\right)^2\right) + \left(\frac{\partial u}{\partial y} + \frac{\partial v}{\partial x}\right)^2$$

Equation (4) is the energy equation including viscous energy dissipation, Φ, [19, 21].

Since the geometry of the physical model is an array of oblique plates as shown in Fig.1, the computational domain (see Fig. 2) has two types of boundary conditions consisting of plate surface boundary condition and periodic boundary condition.

The periodic boundary conditions can be defined as follows:

$$u(x,y)\,|_{AG} = u(x,y)\,|_{FL}$$

$$v(x,y)\,|_{AG} = v(x,y)\,|_{FL}$$

$$\Theta(x,y)\,|_{AG} = \Theta(x,y)\,|_{FL}$$

$$u(x,y)\,|_{BC} = u(x,y)\,|_{HI}$$

$$v(x,y)\,|_{BC} = v(x,y)\,|_{HI}$$

$$T(x,y)\,|_{BC} = T(x,,y)\,|_{HI}$$

$$u(x,y)\,|_{DE} = u(x,y)\,|_{JK}$$

$$v(x, y)|_{DE} = v(x, y)|_{JK}$$

$$T(x, y)|_{DE} = T(x, y)|_{JK}$$

The boundary conditions at the surface of the solid plate:

$$u(x, y) = 0$$

$$v(x, y) = 0$$

$$T(x, y) = T_w$$

where the dimensionless temperature [13, 22] is defined as

$$\Theta(x, y) = \frac{(T(x, y) - T_w)}{(T_b(x) - T_w)} \tag{5}$$

where

$T_b(x)$ is the bulk mean temperature of fluid.

Fig. 2 shows that the computation domain has an irregular shape and Fig. 3 shows the typical grid generated in physical model. The body-fitted coordinate system will be generated to solve this problem by transformed physical coordinate system (x, y) to generalized coordinate system (ξ, η).

To evaluate the spatial derivative of the dependent variable in the governing equations, a numerical method is adopted. The two most popular methods are polynomial approximations such as finite elements and finite differences with generalized coordinate transformations. In this thesis, the finite differences method is adopted.

In terms of the two generalized coordinates (ξ, η), the spatial derivative of the dependent variable become

$$\frac{\partial}{\partial x} = \frac{\partial}{\partial \xi}\xi_x + \frac{\partial}{\partial \eta}\eta_x$$
$$\frac{\partial}{\partial y} = \frac{\partial}{\partial \xi}\xi_y + \frac{\partial}{\partial \eta}\eta_y \tag{6}$$

The components of the coordinate transformation are given by the use of the chain rule and the Cramers rule as a function of the metrics [23]:

$$\xi_X = J^{-1}(y_\eta)$$

$$\xi_Y = -J^{-1}(x_\eta)$$

$$\eta_X = -J^{-1}(y_\xi)$$

$$\eta_Y = J^{-1}(x_\xi)$$

where:

$$J = x_\xi y_\eta - x_\eta y_\xi \tag{7}$$

is the Jacobean of transformation and is equivalent to the volume of the cell when evaluated at the cell center.

Introducing the following dimensionless variables:

$$U = \frac{u}{u_m}$$

$$V = \frac{v}{u_m}$$

$$X = \frac{x}{L_2}$$

$$Y = \frac{y}{L_2}$$

$$\rho^* = \frac{\bar{\rho}}{\rho}$$

$$\bar{P} = \frac{P - P_{rc}}{\rho u_m^2}$$

where the quantity ρu_m^2 represents the double of the dynamic head [19].

The continuity and momentum equations in dimensionless form become

Continuity:

$$\frac{\partial}{\partial \xi}(\phi_U) + \frac{\partial}{\partial \eta}(\phi_V) = 0 \tag{8}$$

x-Momentum:

$$\frac{\partial}{\partial \xi}(\phi_U U) + \frac{\partial}{\partial \eta}(\phi_V U) = [\frac{\partial}{\partial \xi}[\frac{A}{J\,\mathrm{Re}}(\alpha\frac{\partial U}{\partial \xi} - \beta\frac{\partial U}{\partial \eta})] + \frac{\partial}{\partial \eta}[\frac{A}{J\,\mathrm{Re}}(-\beta\frac{\partial U}{\partial \xi} + \gamma\frac{\partial U}{\partial \eta})]] + (\frac{\partial P}{\partial \eta}Y_\xi - \frac{\partial P}{\partial \xi}Y_\eta) \tag{9}$$

y-Momentum:

$$\frac{\partial}{\partial \xi}(\phi_U V) + \frac{\partial}{\partial \eta}(\phi_V V) = [\frac{\partial}{\partial \xi}[\frac{A}{J\,\mathrm{Re}}(\alpha\frac{\partial V}{\partial \xi} - \beta\frac{\partial V}{\partial \eta})] + \frac{\partial}{\partial \eta}[\frac{A}{J\,\mathrm{Re}}(-\beta\frac{\partial V}{\partial \xi} + \gamma\frac{\partial V}{\partial \eta})]] + (\frac{\partial P}{\partial \xi}X_\eta - \frac{\partial P}{\partial \eta}X_\xi) \tag{10}$$

where

$\mathrm{Re} = \frac{\rho u_m^{2-n} L_2^n}{m}$ is the generalized Reynolds number

$$A = \left[\left| \begin{array}{l} 2\left(\left(\frac{\partial U}{\partial \xi}\frac{Y_\eta}{J} - \frac{\partial U}{\partial \eta}\frac{Y_\xi}{J} \right)^2 + \left(\frac{\partial V}{\partial \eta}\frac{X_\xi}{J} - \frac{\partial V}{\partial \xi}\frac{X_\eta}{J} \right)^2 \right) + \left(\frac{\partial U}{\partial \eta}\frac{X_\xi}{J} - \frac{\partial U}{\partial \xi}\frac{X_\eta}{J} \right)^2 + \\ \left(2\left(\frac{\partial U}{\partial \eta}\frac{X_\xi}{J} - \frac{\partial U}{\partial \xi}\frac{X_\eta}{J} \right)\left(\frac{\partial V}{\partial \xi}\frac{Y_\eta}{J} - \frac{\partial V}{\partial \eta}\frac{Y_\xi}{J} \right) \right) + \left(\frac{\partial V}{\partial \xi}\frac{Y_\eta}{J} - \frac{\partial V}{\partial \eta}\frac{Y_\xi}{J} \right)^2 \end{array} \right|^{\frac{n-1}{2}} \right] \tag{11}$$

The energy equation remains in dimensional form.

Energy:

$$\frac{\partial}{\partial \xi}(\phi_U T) + \frac{\partial}{\partial \eta}(\phi_V T) = \frac{\partial}{\partial \xi}[\frac{\Psi}{J}(\alpha \frac{\partial T}{\partial \xi} - \beta \frac{\partial T}{\partial \eta})] + \frac{\partial}{\partial \eta}[\frac{\Psi}{J}(-\beta \frac{\partial T}{\partial \xi} + \gamma \frac{\partial T}{\partial \eta})] + \frac{Bm\,\Phi}{\rho c_p} \tag{12}$$

where

$$B = \left[\left| \begin{array}{l} 2\left(\left(\frac{\partial u}{\partial \xi}\frac{y_\eta}{J} - \frac{\partial u}{\partial \eta}\frac{y_\xi}{J} \right)^2 + \left(\frac{\partial v}{\partial \eta}\frac{x_\xi}{J} - \frac{\partial v}{\partial \xi}\frac{x_\eta}{J} \right)^2 \right) + \left(\frac{\partial u}{\partial \eta}\frac{x_\xi}{J} - \frac{\partial u}{\partial \xi}\frac{x_\eta}{J} \right)^2 + \\ \left(2\left(\frac{\partial u}{\partial \eta}\frac{x_\xi}{J} - \frac{\partial u}{\partial \xi}\frac{x_\eta}{J} \right)\left(\frac{\partial v}{\partial \xi}\frac{y_\eta}{J} - \frac{\partial v}{\partial \eta}\frac{y_\xi}{J} \right) \right) + \left(\frac{\partial v}{\partial \xi}\frac{y_\eta}{J} - \frac{\partial v}{\partial \eta}\frac{y_\xi}{J} \right)^2 \end{array} \right|^{\frac{n-1}{2}} \right] \tag{13}$$

$$\Phi = \left[\left| \begin{array}{l} 2\left(\left(\frac{\partial u}{\partial \xi}\frac{y_\eta}{J} - \frac{\partial u}{\partial \eta}\frac{y_\xi}{J} \right)^2 + \left(\frac{\partial v}{\partial \eta}\frac{x_\xi}{J} - \frac{\partial v}{\partial \xi}\frac{x_\eta}{J} \right)^2 \right) + \left(\frac{\partial u}{\partial \eta}\frac{x_\xi}{J} - \frac{\partial u}{\partial \xi}\frac{x_\eta}{J} \right)^2 + \\ \left(2\left(\frac{\partial u}{\partial \eta}\frac{x_\xi}{J} - \frac{\partial u}{\partial \xi}\frac{x_\eta}{J} \right)\left(\frac{\partial v}{\partial \xi}\frac{y_\eta}{J} - \frac{\partial v}{\partial \eta}\frac{y_\xi}{J} \right) \right) + \left(\frac{\partial v}{\partial \xi}\frac{y_\eta}{J} - \frac{\partial v}{\partial \eta}\frac{y_\xi}{J} \right)^2 \end{array} \right| \right] \tag{14}$$

$$\Psi = \frac{k}{\rho c_p}$$

$$\phi_u = UY_\eta - VX_\eta$$

$$\phi_v = VX_\xi - UY_\xi$$

$$\alpha = X_\eta^2 + Y_\eta^2$$

$$\beta = X_\xi X_\eta + Y_\xi Y_\eta$$

$$\gamma = X_\xi^2 + Y_\xi^2$$

$$J = X_\xi Y_\eta - X_\eta Y_\xi$$

According to the energy equation in the body-fitted coordinate system, equation (12), the energy equation can not be conducted to dimensionless form because in the body-fitted coordinate system the bulk mean temperature ($T_b(\xi)$) appeared in the equation (15) for the definition of the dimensionless temperature $\Theta(\xi,\eta)$ is not a constant but a functioned of ξ.

At the inlet and outlet temperature of computational domain in Fig. 4, the periodic condition is valid only for the dimensionless form because the requirement to satisfy the fully developed condition. However in the calculation procedure for energy equation, the dimensional form of inlet and out temperatures must be calculated by first, solving the dimensionless temperature $\Theta(\xi,\eta)$ shown in equation (15) with the local dimensional temperatures at the cycle inlet and outlet given by equation (25) and (26) respectively.

Then, substitute the relationship of bulk mean temperatures at the cycle inlet and outlet and use composite trapezoid rule to obtain the final set of linear equations of dimensional inlet and outlet temperatures. Finally, solve those set of linear equations of dimensional inlet and outlet temperatures by use Jacobi iterative method.

The periodic boundary conditions can be defined as follows:

$$U(\xi,\eta)|_{AG} = U(\xi,\eta)|_{FL}$$

$$V(\xi,\eta)|_{AG} = V(\xi,\eta)|_{FL}$$

$$\Theta(\xi,\eta)|_{AG} = \Theta(\xi,\eta)|_{FL}$$

$$U(\xi,\eta)|_{BC} = U(\xi,\eta)|_{HI}$$

$$V(\xi,\eta)|_{BC} = V(\xi,\eta)|_{HI}$$

$$T(\xi,\eta)|_{BC} = T(\xi,\eta)|_{HI}$$

$$U(\xi,\eta)|_{DE} = U(\xi,\eta)|_{JK}$$

$$V(\xi,\eta)|_{DE} = V(\xi,\eta)|_{JK}$$

$$T(\xi,\eta)|_{DE} = T(\xi,\eta)|_{JK}$$

The boundary conditions at the surface of the solid plate:

$$U(\xi,\eta) = 0$$

$$V(\xi,\eta) = 0$$

$$T(\xi,\eta) = T_w$$

where the dimensionless temperature[13,22] is defined as follows:

$$\Theta(\xi,\eta) = \frac{(T(\xi,\eta) - T_w)}{(T_b(\xi) - T_w)} \tag{15}$$

where

$T_b(\xi)$ is the bulk mean temperature of fluid.

$$T_b(\xi) = \frac{\int_{\eta_1}^{\eta_{M1}} T(\xi,\eta)u(\xi,\eta)\sqrt{\alpha}\,d\eta}{\int_{\eta_1}^{\eta_{M1}} u(\xi,\eta)\sqrt{\alpha}\,d\eta}$$

The local heat flux is computed by Fourier's law of heat conduction [13]. The value of heat flux at the plate surface is determined by

$$q_{n_1} = -k\left.\frac{\gamma T_\eta - \beta T_\xi}{J\sqrt{\gamma}}\right|_{\eta=\eta_1} \tag{16}$$

$$q_{n_2} = -k\left.\frac{\gamma T_\eta - \beta T_\xi}{J\sqrt{\gamma}}\right|_{\eta=\eta_{MM1}} \tag{17}$$

The average heat flux of the plate surface is determined by

$$q_m = \frac{\int_{\xi_A}^{\xi_b} q_{n_2}\sqrt{\gamma}d\xi + \int_{\xi_C}^{\xi_D} q_{n_2}\sqrt{\gamma}d\xi + \int_{\xi_E}^{\xi_F} q_{n_2}\sqrt{\gamma}d\xi + \int_{\xi_G}^{\xi_H} q_{n_2}\sqrt{\gamma}d\xi + \int_{\xi_I}^{\xi_J} q_{n_2}\sqrt{\gamma}d\xi + \int_{\xi_K}^{\xi_L} q_{n_2}\sqrt{\gamma}d\xi}{\int_{\xi_A}^{\xi_B}\sqrt{\gamma}d\xi + \int_{\xi_C}^{\xi_D}\sqrt{\gamma}d\xi + \int_{\xi_E}^{\xi_F}\sqrt{\gamma}d\xi + \int_{\xi_G}^{\xi_H}\sqrt{\gamma}d\xi + \int_{\xi_I}^{\xi_J}\sqrt{\gamma}d\xi + \int_{\xi_K}^{\xi_L}\sqrt{\gamma}d\xi} \tag{18}$$

The plate average heat transfer coefficient of one cycle is computed by

$$h_m = \frac{q_m}{\{[T_b(\xi_{FL}) - T_b(\xi_{AG})]/[\ln[T_w - T_b(\xi_{AG})] - \ln[T_w - T_b(\xi_{FL})]]\}} \tag{19}$$

The plate average Nusselt number is defined as

$$Nu = \frac{h_m L_2}{k} \tag{20}$$

Where the plate length L_2 is taken as the characteristic dimension.

The plate pressure drop friction factor of one cycle is determined by

$$f = \frac{(p_m(\xi_{AG}) - p_m(\xi_{FL})}{(\rho u_m^2/2)} \tag{21}$$

4. Numerical Procedure

The discretization of the equations in the computation domain is performed on the staggered grid by using the finite volume approach. The convection-diffusion terms of momentum equations are treated by the power-law profile of Patankar [24] and the energy equation is treated by the upwind scheme of Patankar [24]. A SIMPLE solution algorithm in the computation domain is adopted to deal with the linkage between pressure and velocities. Because the grid is non-orthogonal, the pressure correction equations contain cross derivatives, which lead to a nine- point formulation. In this thesis, the cross derivatives are incorporated into the source term, and a five –point solver is used to solve the algebraic equations.

As for the implementation of the periodic boundary condition in the computational domain, the interpolation method proposed by Wang and Tao [3] is used.

For the η - direction, the following linear interpolation is used:

$$\Pi(i,1) = \Pi(i, MM_1) = \frac{(\Pi^{**}(i,2) + \Pi^{**}(i, MM_2))}{2} \tag{22}$$

where "**" represents the value from previous iteration, and MM_1, MM_2 are the last and second to last indices in the η - direction.

In the implementation of the periodic boundary condition in ξ - direction, the following linear interpolation is used:

$$\Pi(\xi_{A-G},\eta) = \Pi(\xi_{F-L},\eta) = \frac{(\Pi^{**}(\xi_{1-1},\eta) + \Pi^{**}(\xi_{2-2},\eta))}{2} \tag{23}$$

where ξ_{1-1} and ξ_{2-2} are positions corresponding to the line 1-1 and 2-2 in Fig. 4. It should be noted that in order to restrict the computation to just one cycle, the linear interpolation method for implementation of the periodic boundary condition is adopted, otherwise the computation domain must be extended in both η and ξ direction.

As far as the temperature is concerned, the periodic boundary conditions at the cycle inlet and outlet are valid only for the dimensionless value because the inlet temperature and the outlet temperature is formed fully developed condition that is the relative shape of the inlet temperature profile and outlet temperature profile no longer changes and the flow is said to be thermally fully developed [16, 25]. Thus, the interpolation values determined by equation (23) are taken as the dimensionless temperatures at the cycle inlet and outlet for next iteration [13].

$$\Theta(\xi_{AG},\eta) = \Theta(\xi_{FL},\eta) = \frac{1}{2}\left(\frac{T(\xi_{1-1},\eta) - T_w}{T_b(\xi_{1-1}) - T_w} + \frac{T(\xi_{2-2},\eta) - T_w}{T_b(\xi_{2-2}) - T_w}\right) \tag{24}$$

The local temperatures at the cycle inlet and outlet are calculated by

$$T(\xi_{AG},\eta) = T_w + \Theta(T_b(\xi_{AG}) - T_w) \tag{25}$$

$$T(\xi_{FL},\eta) = T_w + \Theta(T_b(\xi_{FL}) - T_w) \tag{26}$$

4.1 The Staggered Grid Strategy

The staggered grid strategy is that each dependent variable is employed to a different grid point. For control volume approach of axial velocity (u), the center grid point in this control volume is staggered to the right of point (P) and located in the middle

between point (P) and point (E) as shown in Fig. 5. For control volume approach of transverse velocity (v), the center grid point in this control volume is staggered up from point (P) and located in the middle between point (P) and point (N) as shown in Fig. 6.

For control volume approach of pressure and temperature, the center grid point in this control volume is still at point (P) as shown in Fig. 7. In the case of velocity components, there is a significant benefit to be obtained by arranging them on grids that are different form the grid used for all other variables. The benefit is that the difficulties in x-y momentum equations due to the pressure term will totally disappear.

The staggered grid strategy for the velocity components was first used in the MAC method and the SIMPLE procedure of Patankar [24].

In the staggered grid, the velocity components are calculated for the points that lie on the face of the control volumes. Thus the x-direction velocity u is calculated at the faces that are normal to the x direction. The location for u is shown in Fig. 5 by short arrows, while the main grid point is shown by point (P). This figure shows that, with respect to the main grid points, the u locations are staggered only in the x-direction.

The velocity v in the y- direction is handled in a similar manner. The location for velocity v is shown in Fig. 6. This figure shows that, with respect to the main grid point, the v locations are staggered only in the y-direction.

In this thesis, the location of u and v are exactly on midway between two main grid points.

The geometry functions that describe the relationship between the physical coordinate system and the generalized coordinate system can be found in Fig. 8.

4.2 The Discretization of Momentum Equations

The momentum equation can be solved only when the pressure field is given or is somehow estimated. Unless the correct pressure field is employed, the resulting velocity field will not satisfy the continuity equation. Such an imperfect velocity field based on a guessed pressure field p^* will be denoted by u^*, v^*, which are obtained from the solution of the following discretization equations:

$$a_e u_e^* = \sum a_{nb} u_{nb}^* + (p_P^* - p_E^*) A_e \tag{27}$$

$$a_n v_n^* = \sum a_{nb} v_{nb}^* + (p_P^* - p_N^*) A_n \tag{28}$$

4.3 The Pressure and Velocity Corrections

To improve the guessed pressure p^* such that the resulting starred velocity field will progressively get closer to satisfying the continuity equation, the correct pressure is proposed and obtained from

$$p = p^* + p' \tag{29}$$

where p' is the pressure correction [24].

The velocity correction can be introduced in a similar manner:

$$u_e = u_e^* + d_e (p_P' - p_E') \tag{30}$$

$$v_n = v_n^* + d_n (p_P' - p_N') \tag{31}$$

where:

$$d_e = \frac{A_e}{a_e}$$

$$d_n = \frac{A_n}{a_n}$$

4.4 The Pressure Correction Equation

The pressure correction is obtained from the continuity equation by integrating the continuity equation over the control volume [24] which is shown in Fig. 7.

$$a_P p'_P = a_E p'_E + a_W p'_W + a_N p'_N + a_S p'_S + b \tag{32}$$

The pressure correction is needed to calculate the next iteration of pressure and velocity components.

4.5 The Discretization of Energy Equation

The discretization of the energy equation is an equation that can solve temperature distribution in computational domain. It can be obtained by using the control volume approach for temperature as shown in Fig. 7. The numerical integration and upwind scheme are performed on the main grid.

The temperature distribution is obtained from the solution of the following discretization equation:

$$a_e T = \sum a_{nb} T_{nb} + S \tag{33}$$

where T is the temperature distribution and S is the source term.

4.6 The SIMPLE Algorithm

The procedure that was developed for the calculation of the flow field has been given by the name of **SIMPLE,** which stands for Semi-Implicit Method for Pressure-

Linked Equations [24]. To solve the discretization equation of velocity fields and temperature distribution for each iteration of the SIMPLE algorithm, the TDMA algorithm is adopted.

The sequence of SIMPLE operations are given as follows:

1. Guess the pressure field p^*
2. Solve the momentum equations given by equations (27) and (28) to obtain u^*, v^*.
3. Solve the p' equation.
4. Calculate p from equation (29) by adding p' to p^*.
5. Calculate u, v from their starred values using the velocity correction formulas given by equations (30) and (31) respectively.
6. Treat the corrected pressure p as a new guessed pressure p^*, repeat to step 2 until a converged solution is obtained.
7. Solve the discretization equation for temperature distribution. However, it is better to calculate it after a converged solution for the flow field has been obtained.

5. Results and Discussion

The discretized governing equations for non-Newtonian fluids have been solved numerically to determine velocity field and temperature profile. The effects of power law index (n), generalized Reynolds number (Re), and geometrical parameters such as plate length ratio (L1/L2), transverse pitch ratio (Tp/Lp), and plate angle (θ) on the flow and thermal behavior have been analyzed. Results are presented in graphical and tabulated forms.

5.1 Flow Field

The velocity fields in Fig. 9 – Fig. 10 for pseudoplastic fluid (n < 1), Fig. 11 – 12 for Newtonian Fluid (n = 1), and Fig. 13 – 14 for dilatant fluid (n > 1) show how the flow pattern changes with an increasing Reynolds number for $L_1 / L_2 = 2.5$ and $T_p / L_p = 0.571$. There are three panels in each figure, among which the center panel is the whole long plate (L_1), with the left and the right panels are the two parts of the short plates (L_2). The flow field characteristics shown in the three figures may be summarized as follows: first, in the flow field at the leeward side and windward side of long plate, there is one circulating zone for each side, and at the second windward side of short plate there is one circulating zone. For the cases with a given geometry the increase in Reynolds number leads to an increase in circulating intensity.

From these results, it can also be seen that the fluid velocity is increased when the flow index is increased at the same Reynolds number because of the viscosity term in the momentum equations. Physically, the higher viscosity fluids flow slower than the lower viscosity fluids at the same Reynolds number.

5.2 The Friction Factor

From the results shown in the odd figure numbers from Figs. 15-37, a general feature may be noted: with increases in the Reynolds number, the values of friction factor decreases. This is the flow region where the pressure drop is mainly caused by the surface friction effect. The form drag of the plate (including the inlet and outlet effects) gradually becomes significant with the further increase of Reynolds number, and finally, it becomes predominant, leading to a constant value of friction factor (f) for each case.

5.2.1 The Effect of Flow Index (n)

The effects of flow index (n) on friction factor for each plate length ratio (L_1 / L_2) and transverse pitch ratio (T_p / L_P) is shown in Fig.15, Fig.17, and Fig.19, where the friction factor is expressed as a function of Reynolds number.

These three figures show that the friction factor increases with increasing flow index (n). That is the friction factor of dilatant fluids are higher than both Newtonian and pseudoplastic fluids at the same generalized Reynolds number with pseudoplastic fluids having the smallest values. Physically, the pseudoplastic fluids may be employed as a friction – reducing agent.

5.2.2 The Effect of Plate Length Ratio (L1/L2)

The results of the effect of plate length ratio (L_1 / L_2) on the friction factor for each flow index (n) and transverse pitch ratio (T_p / L_P) are presented in Fig. 21, Fig. 23, and Fig. 25, where the friction factor is expressed as a function of Reynolds number.

From these results, it can be seen that the friction factor is increased as plate length ratio is increased at a given Reynolds number and flow index. This is because increased long plate (L_1) leads to increase both friction effect and plate form drag, thus the total cycle pressure drop increase.

5.2.3 The Effect of Transverse Pitch Ratio (Tp/Lp)

The results of the effect of transverse pitch ratio (T_p / L_P) on the friction factor for each flow index (n) and plate length ratio (L_1 / L_2) are presented in Fig. 27, Fig. 29, and Fig. 31, where the friction factor is expressed as a function of Reynolds number.

From these results, it can be seen that the friction factor is increased as transverse pitch ratio is decreased at the same Reynolds number. The decrement of the transverse pitch (T_p) results in a decrease of the gap between upper plate and bottom plate, therefore it causes the decrease of the pressure at the outlet.

5.2.4 The Effect of Plate Angle (θ)

The results of the effect of plate angle (θ) on the friction factor for each flow index (n), plate length ratio (L_1 / L_2), and of transverse pitch ratio (T_p / L_P) are presented

in Fig. 33, Fig. 35, and Fig. 37, where the friction factor is expressed as a function of plate angle (θ) at Reynolds number 300.

From the results, it can be seen that the friction factor is higher as the plate angle (θ) increases. At Reynolds number of 300, the pressure at the outlet is dropped when the plate angle (θ) increases because the increment of plate angle (θ) leads to increase obstruction to the flow.

5.3 The Average Heat Transfer

From the results shown in the even figure numbers from Figs. 16-38, the following trend may be noted: when the Reynolds number is small, the plate average Nusselt number increases slowly, which is similar to the character of fully developed laminar heat transfer in a continuous duct. In the higher Reynolds number region (Re >400), the increase of Reynolds number yields more steeply appreciable increase in Nusselt number. Moreover, between Re = 400 and 500, it can be seen that the average heat transfer suddenly jumps. This may indicate the strong effect of the re-circulating flow on heat transfer in this range of Reynolds number.

5.3.1 The Effect of Flow Index (n)

The results of the effect of flow index (n) on the average heat transfer for each plate length ratio (L_1 / L_2) and transverse pitch ratio (T_p / L_P) are presented in Fig. 16, Fig. 18, and Fig. 20, where the plate average Nusselt number is expressed as a function of Reynolds number.

These three figures show that as the flow index decreases the value of Nusselt number is slightly increased at the same Reynolds number. Thus, the thermal performance of pseudoplastic fluids is better than Newtonian and dilatant fluids respectively.

5.3.2 The Effect of Plate Length Ratio (L1/L2)

The results of the effect of plate length ratio (L_1 / L_2) on the average heat transfer for each flow index (n) and transverse pitch ratio (T_p / L_P) are presented in Fig. 22, Fig. 24, and Fig. 26, where the plate average Nusselt number is plotted as a function of Reynolds number.

From these results, it can be seen that Nusselt number is increased as plate length ratio is increased at the same Reynolds number and flow index. This is because that the increase of long plate (L_1) leads to the increase in heat transfer area, thus the total cycle heat transfer increases.

5.3.3 The Effect of Transverse Pitch Ratio (Tp/Lp)

The results of the effect of transverse pitch ratio (T_p / L_P) on the average heat transfer for each flow index (n) and plate length ratio (L_1 / L_2) are presented in Fig. 28, Fig. 30, and Fig. 32, where the plate average Nusselt number is expressed as a function of Reynolds number.

From these results, it can be seen that the Nusselt number increases as transverse pitch ratio decreases at the same Reynolds number. The decrement of the transverse pitch

(T_p) leads to the decrease of a gap between upper plate and bottom plate, therefore it indicates the strong effect of re-circulating flow on heat transfer.

5.3.4 The Effect of Plate Angle (θ)

The results of the effect of plate angle (θ) on the average heat transfer for each flow index (n), plate length ratio (L_1 / L_2), and of transverse pitch ratio (T_p / L_P) are presented in Fig. 34, Fig. 36, and Fig. 38, where the average heat transfer is plotted as a function of plate angle (θ) at Reynolds number 300.

From these results, it can be seen that Nusselt number increase with increasing plate angle (θ). The rise of the higher heat transfer rate stems from a stronger re-circulation flow with the increase of plate angle (θ).

5.4 The Temperature Profile.

The results of temperature profile at the leading edge, middle, and tailing edge of long plate (L1) are presented. The length of long plate (L1) is changed when the plate length ratio is changed since the short plate (L2) is fixed at L2 = 15 mm. When long plate (L1) is longer, the heat transfer area is increased.

From the results shown in all figure numbers from Figs. 39-80, a general feature may be noted as follows: for the temperature profile at the leading edge of long plate (L1), it can be seen that trough is shifted to the right since the effect of the left upper re-circulating flow and the rush-in effect of the fluid flow.

For the temperature profile at the middle of long plate (L1), it can be seen that the fluid temperature rapidly decreases because the boundary layer flow at the leading edge of the plate does not last long downward over the plate surface as it meets a counter stream on the plate surface.

For the temperature profile at tailing edge of long pate (L1), it can be seen that the fluid temperature increases again, basically because of the rushing – out effect and effect of the right bottom re-circulating flow.

5.4.1 The Effect of Plate Length Raito (L1/L2)

The effects of plate length ratio (L1/L2) on the temperature profile at Re = 300, θ = 25, and Tp = 30 mm are presented in Fig. 39 – 41 for n = 0.5, Fig. 42 – 44 for n = 1.0, and Fig. 45-47 for n = 1.2.

From these results, they can be seen that the increment of plate length ratio (L1/L2) leads to the increase of fluid temperature since plate has more area to transfer heat to fluid.

5.4.2 The Effect of Flow Index (n) at Different Plate Length Ratio and Transverse Pitch Spacing (Tp)

The effects of flow index (n) on the temperature profile for θ = 25, and Tp = 30 mm are presented in Fig. 48 – 50 for L1/L2 = 2.5, Fig. 51 – 53 for L1/L2 = 2.0, and Fig. 54-56 for L1/L2 = 1.5 at Re = 300.

The effects of flow index (n) on the temperature profile at L1/L2 = 2.5, Re = 300, and θ = 25 are presented in Fig. 57-59 for Tp = 60 mm and Fig. 60-62 for Tp = 100 mm.

From these results, it can be seen that the increment of flow index results in the decrease in fluid temperature. The wider of the transverse pitch spacing causes the fluid temperature to decrease as expected.

5.4.3 The Effect of Reynolds Number (Re)

The results for the effect of Reynolds number on temperature profile at θ = 25, and Tp = 30 mm, and L1/L2 = 2.5 are presented in Fig. 63-65 for n = 0.5, Fig. 66-68 for n = 1.0, and Fig. 69-71 for n = 1.2.

From the results, the temperature is higher when Reynolds number is increased. It means that the fluid temperature is higher when the fluid flows faster at the same flow index.

5.4.4 The Effect of Plate Angle (θ)

The results for the effect of plate angle (θ) on the temperature profile for L1/L2 = 2.5, Re = 300, and Tp = 30 mm are presented in Fig. 72-74 for n = 0.5, Fig. 75-77 for n =1.0, and Fig. 78-80 for n = 1.2.

From results, they can be seen that the increment of plate angle (θ) leads to increases of fluid temperature.

5.5 Figures

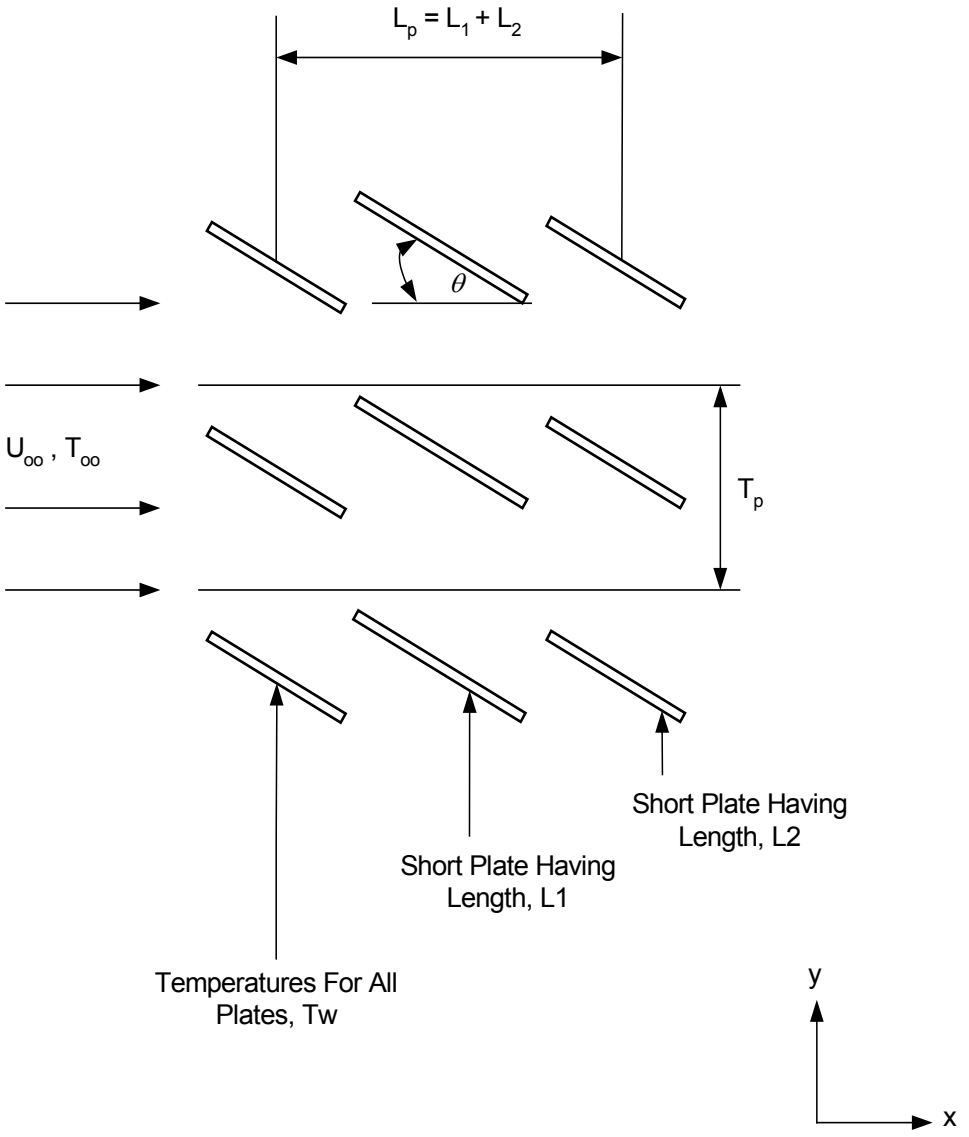

Figure 1. Physical Model

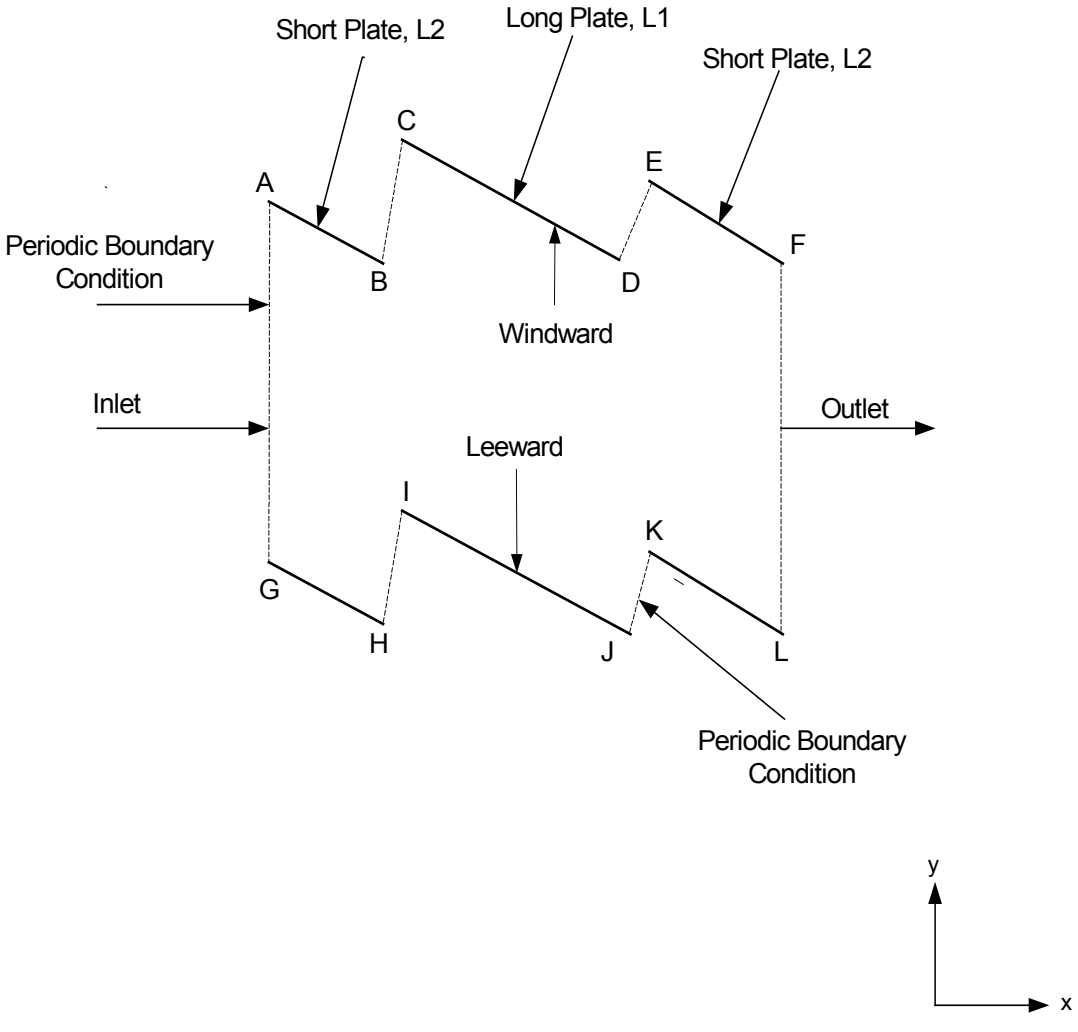

Figure 2. Computational Domain

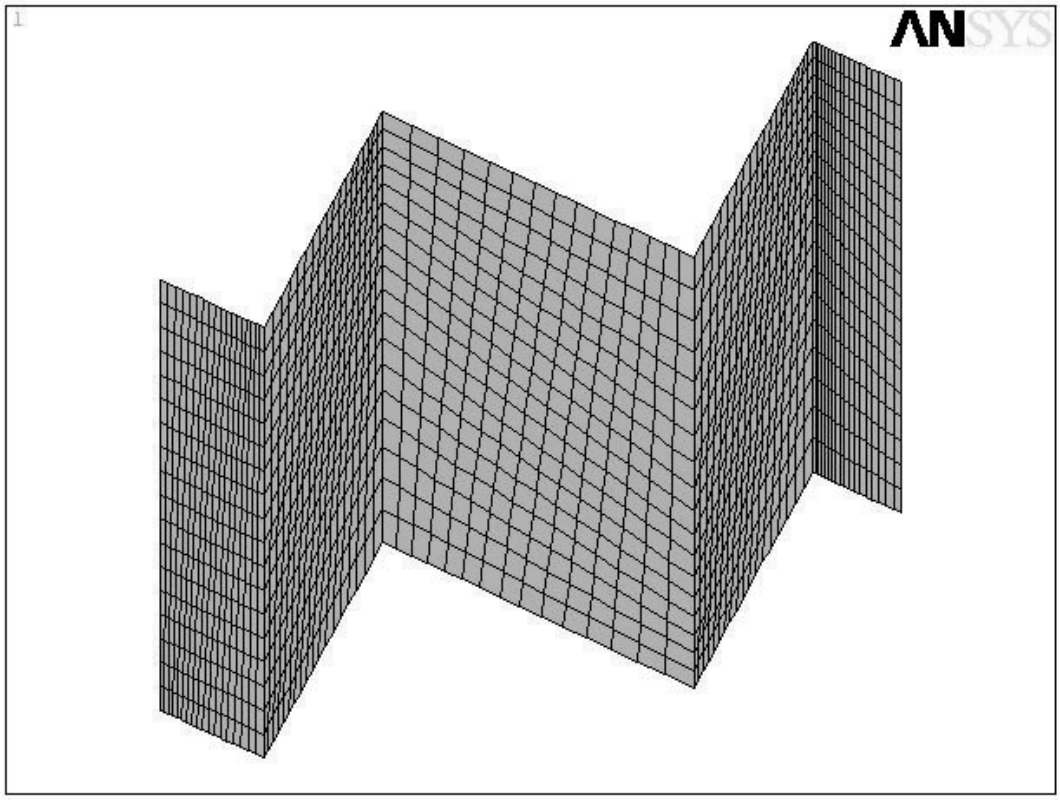

Figure 3. Typical Grid Mesh

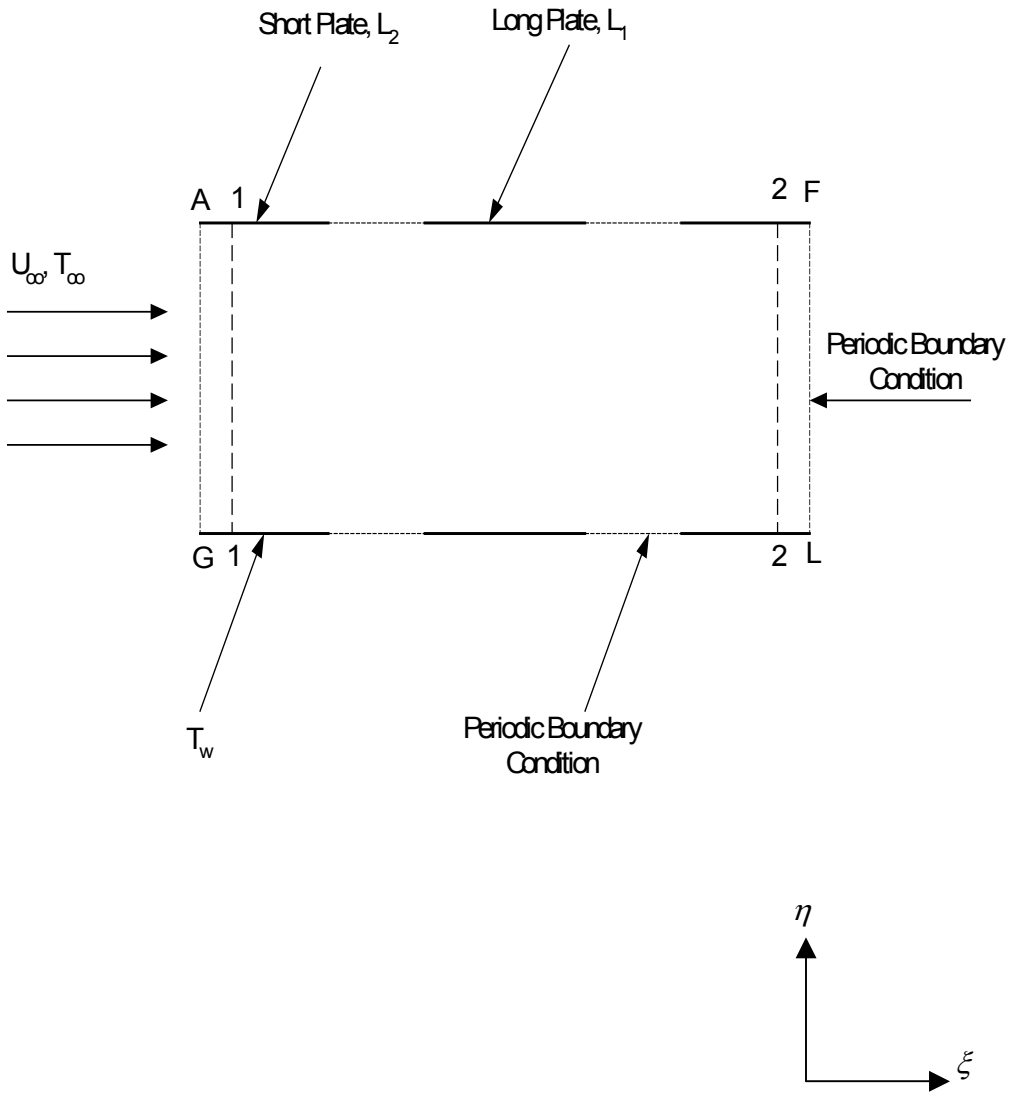

Figure 4. Computational Domain in Generalized Coordinate System

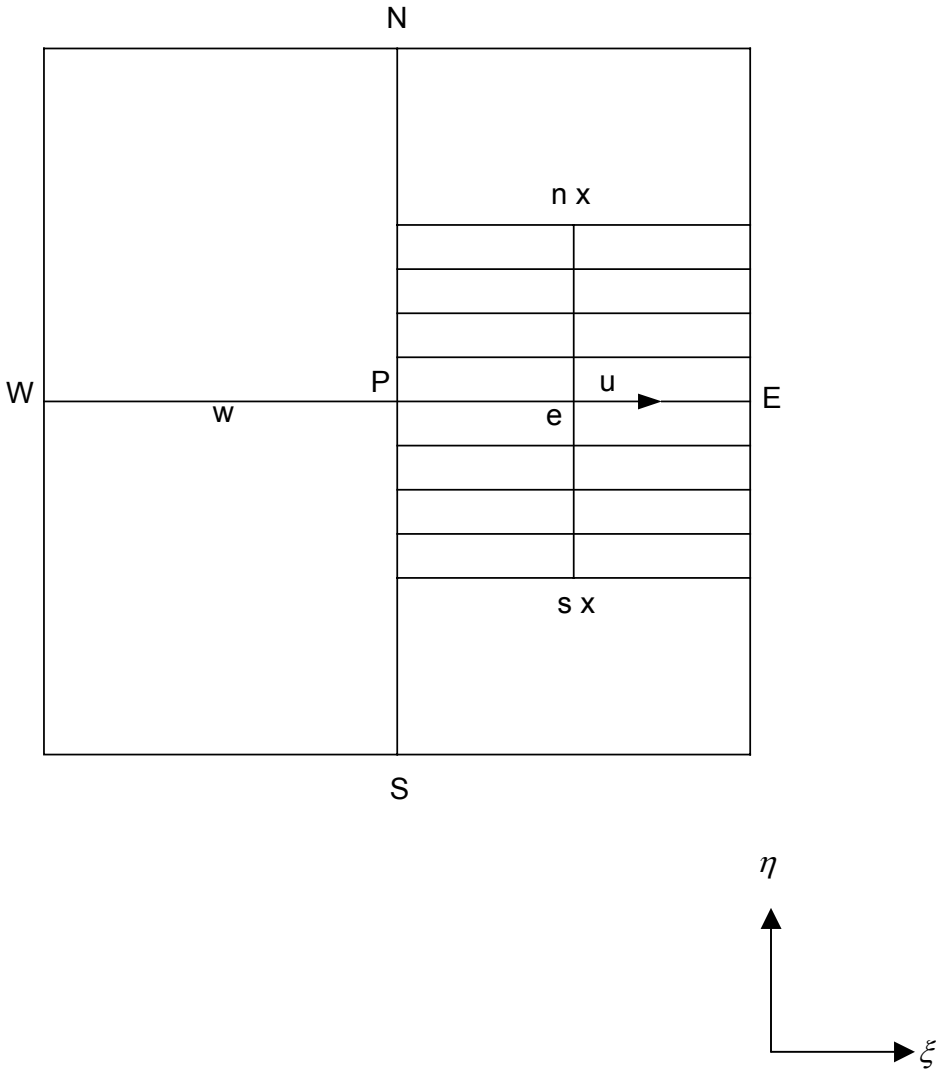

Figure 5. Staggered Control Volume for Axial Velocity (u)

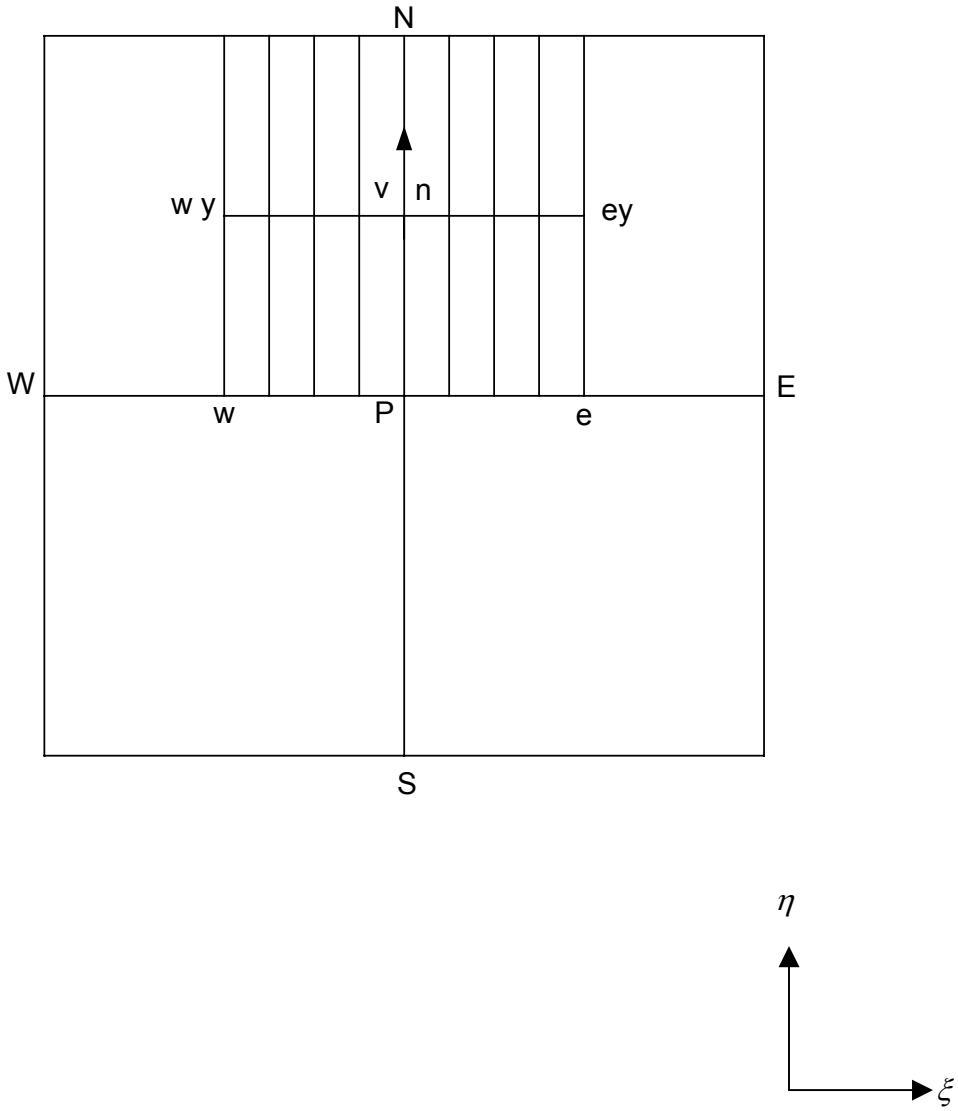

Figure 6. Staggered Control Volume for Transverse Velocity (v)

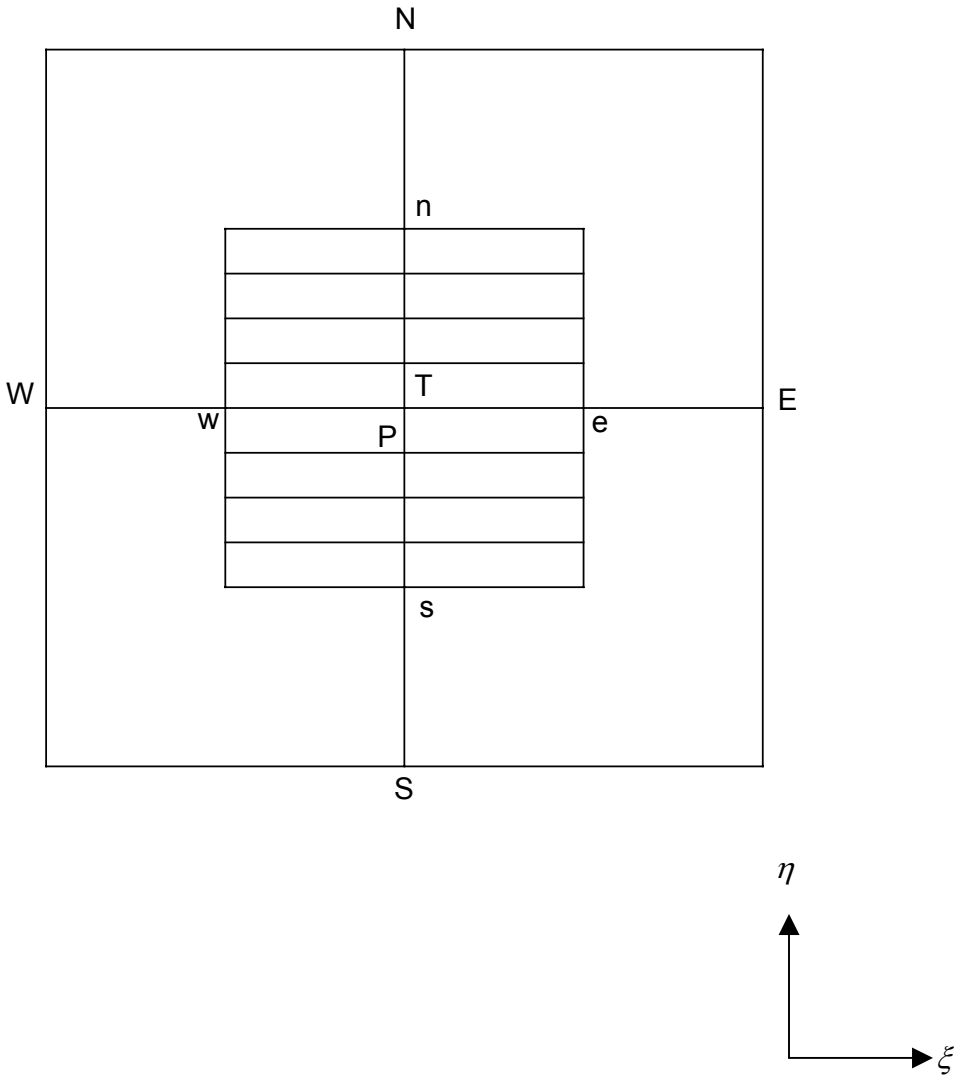

Figure 7. Staggered Control Volume for Pressure or Temperature (P or T)

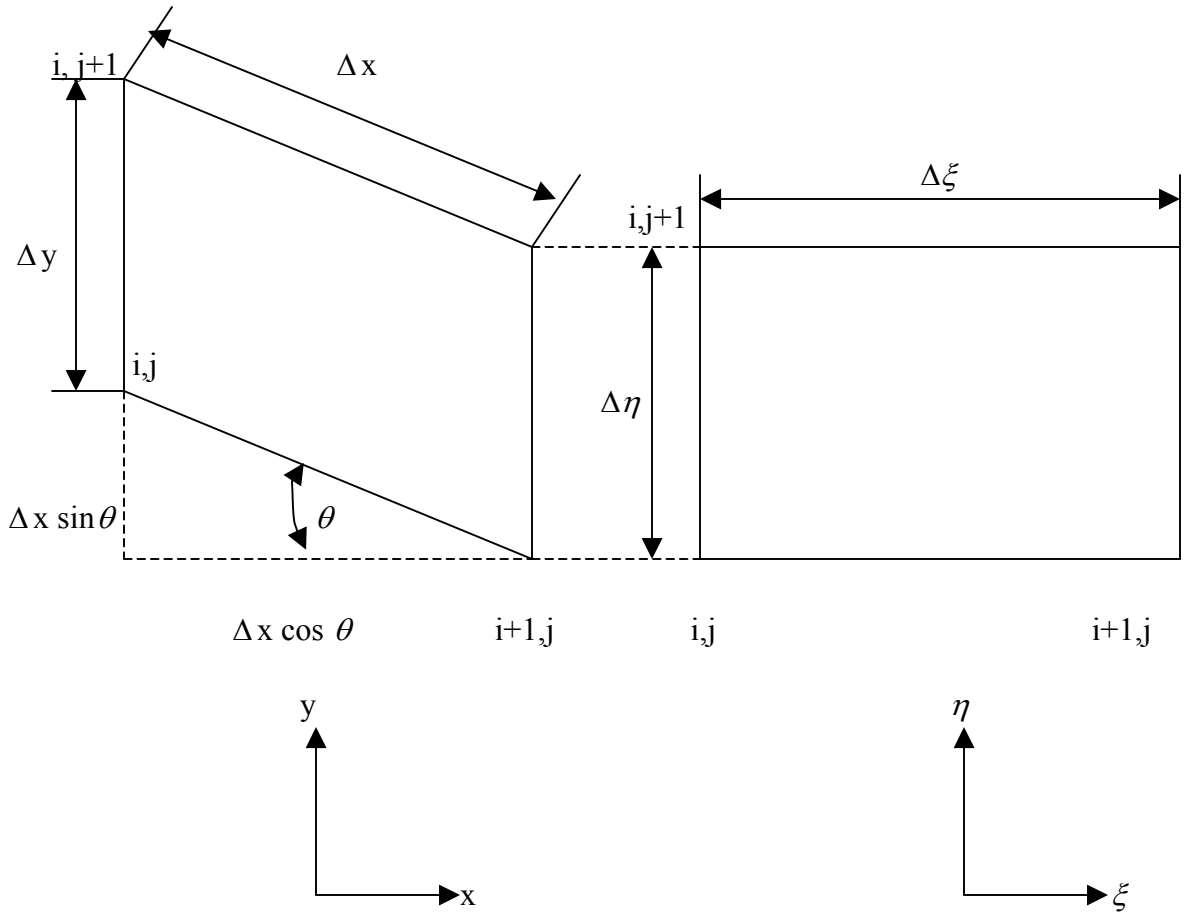

Figure 8. Element Analysis

Let Δx in physical coordinate system = $\Delta\xi$ in generalized coordinate system

Let Δy x in physical coordinate system = $\Delta\eta$ in generalized coordinate system

Number of grid point in physical coordinate system is equal to number of grid point in generalized coordinate system.

$$x_{j+1} - x_j = x_j - x_{j-1} = 0$$

$$y_{j+1} - y_j = y_j - y_{j-1} = \Delta y = \Delta\eta$$

$$x_{i+1} - x_i = x_i - x_{i-1} = \Delta x \cos\theta = \Delta\xi \cos\theta$$

$$y_{i+1} - y_i = y_i - y_{i-1} = \Delta x \sin\theta = \Delta\xi \sin\theta$$

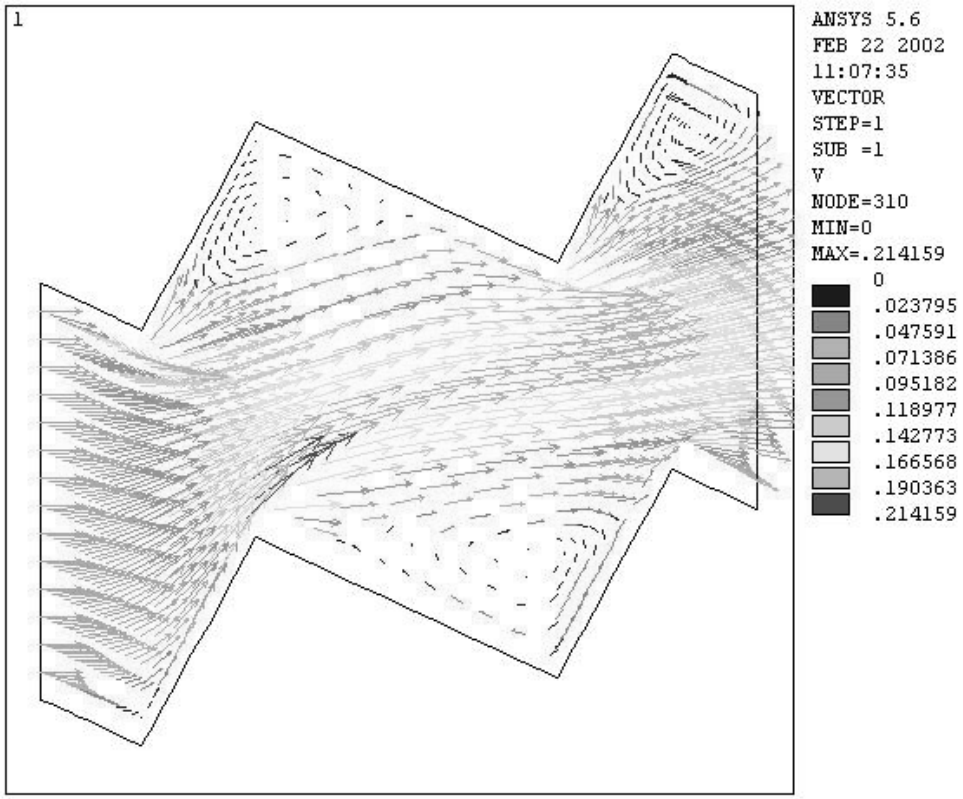

Figure 9. Flow Pattern of The Pseudoplastic Fluid (n = 0.5) at Re = 200

(L1/L2 = 2.5, Tp /Lp = 0.571, and θ = 25)

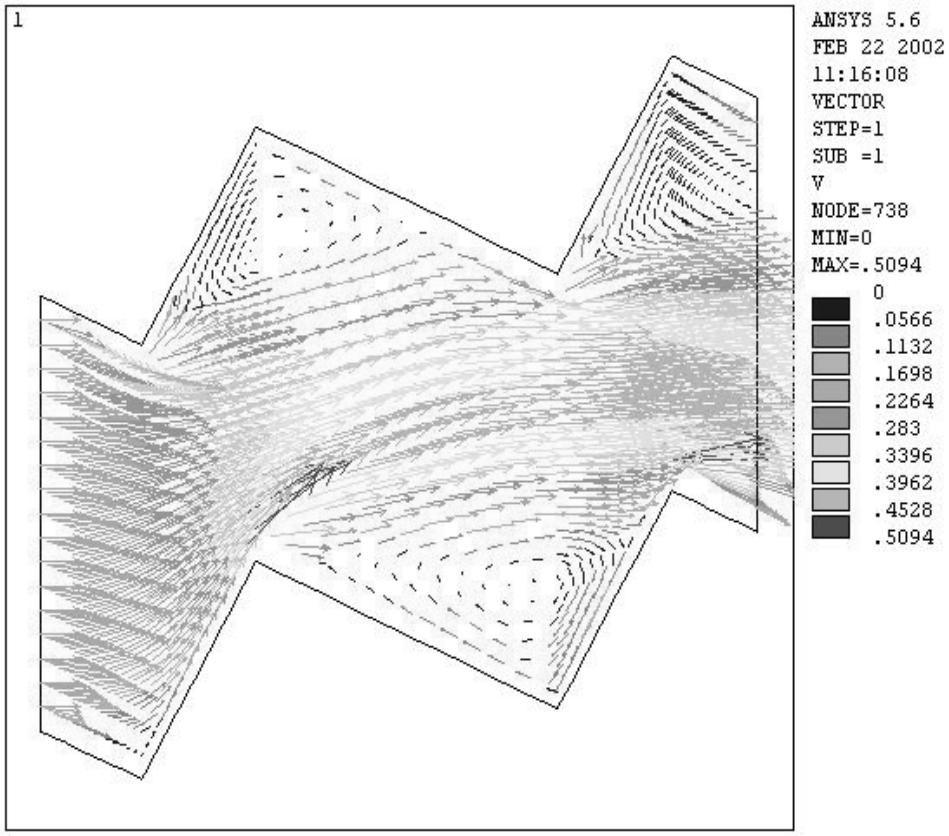

Figure 10. Flow Pattern of The Pseudoplastic Fluid (n = 0.5) at Re = 700

(L1/L2 = 2.5, Tp /Lp = 0.571, and θ = 25)

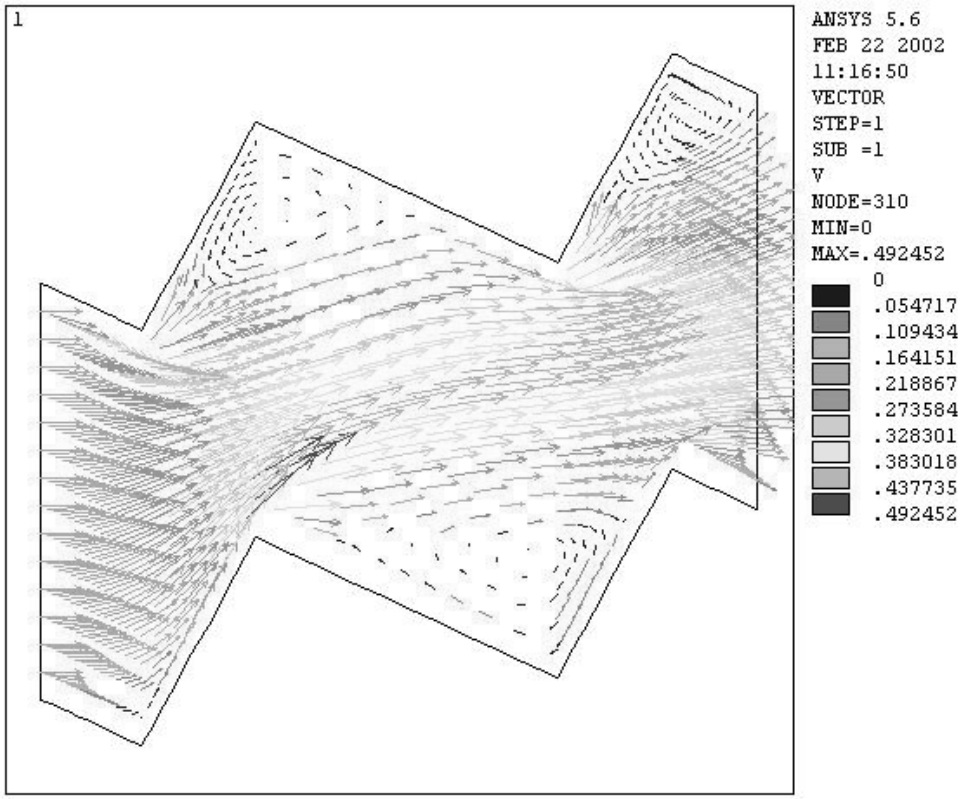

Figure 11. Flow Pattern of The Newtonian Fluid (n = 1.0) at Re = 200

(L1/L2 = 2.5, Tp /Lp = 0.571, and θ = 25)

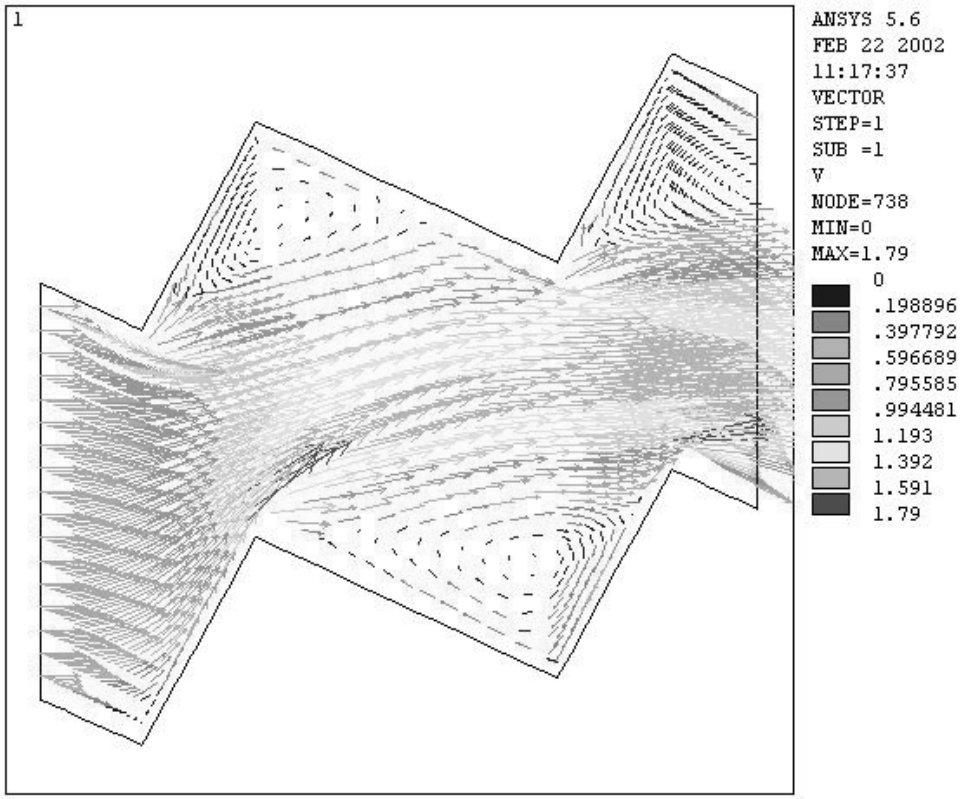

Figure 12. Flow Pattern of The Newtonian Fluid (n = 1.0) at Re = 700

(L1/L2 = 2.5, Tp /Lp = 0.571, and θ = 25)

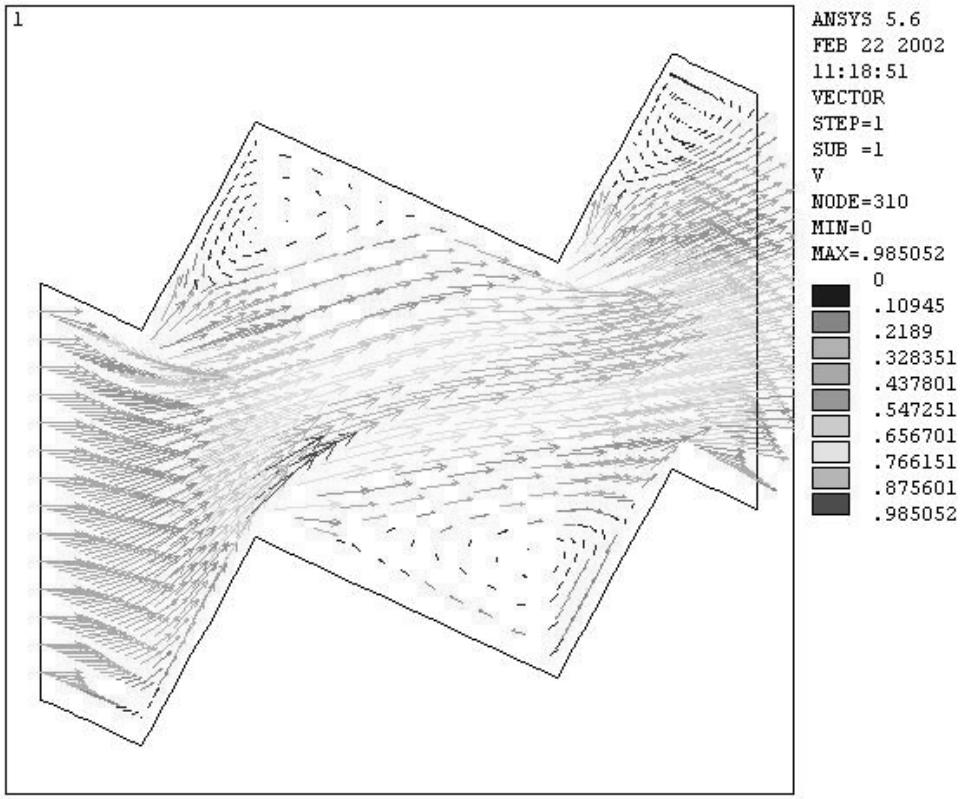

Figure 13. Flow Pattern of The Dilatant Fluid (n = 1.2) at Re = 200

(L1/L2 = 2.5, Tp /Lp = 0.571, and θ = 25)

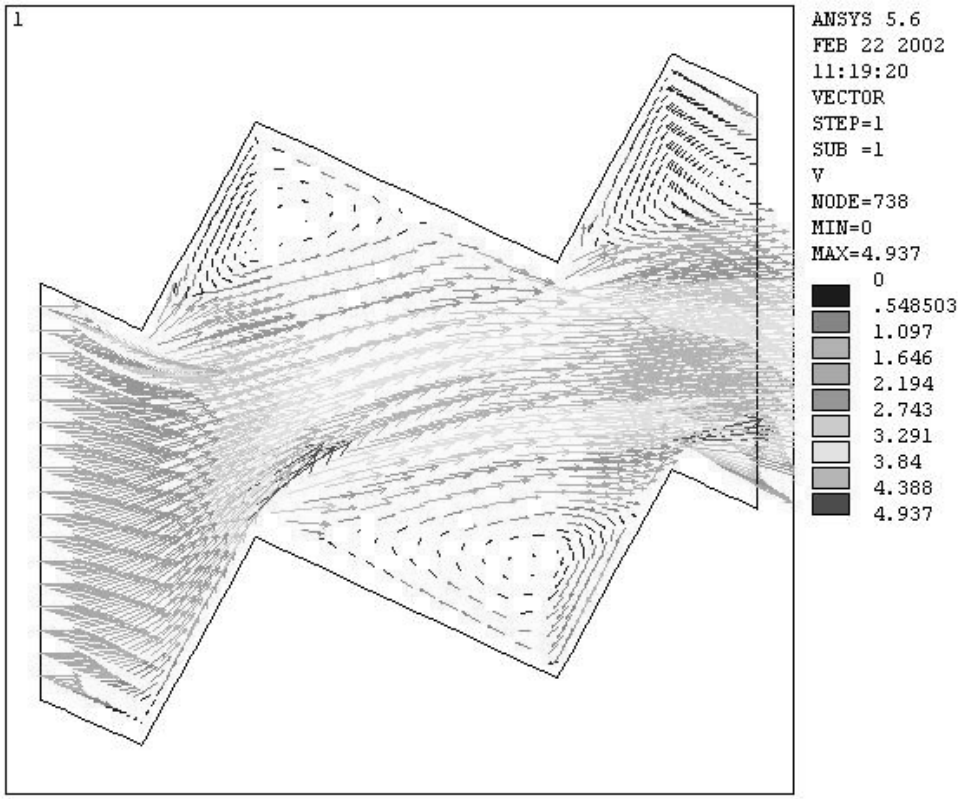

Figure 14. Flow Pattern of The Dilatant Fluid (n = 1.2) at Re = 700

(L1/L2 = 2.5, Tp /Lp = 0.571, and θ = 25)

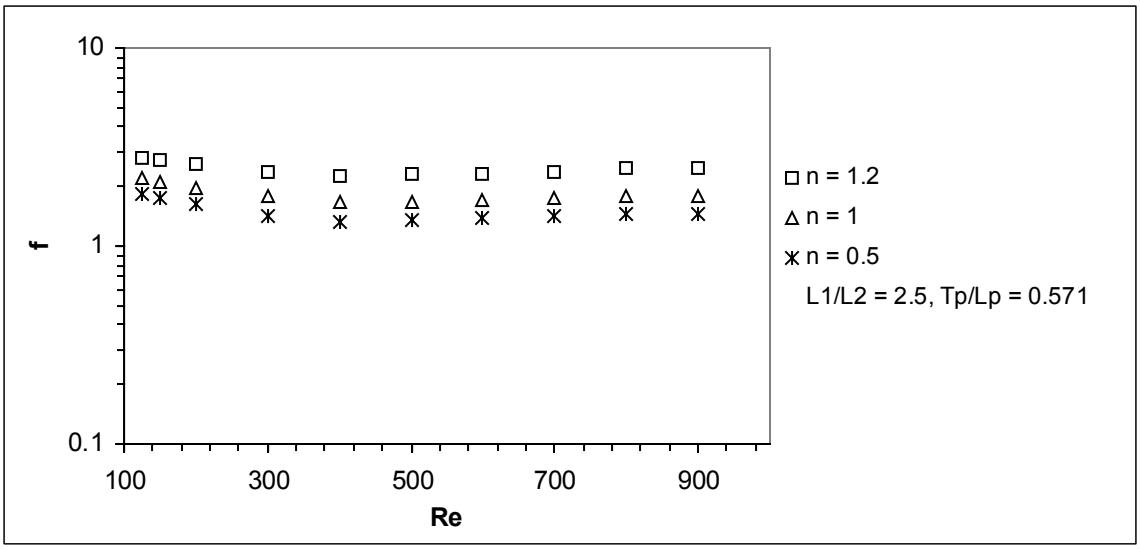

Figure 15. The Effect of Flow Index on Friction Factor for $\theta = 25$

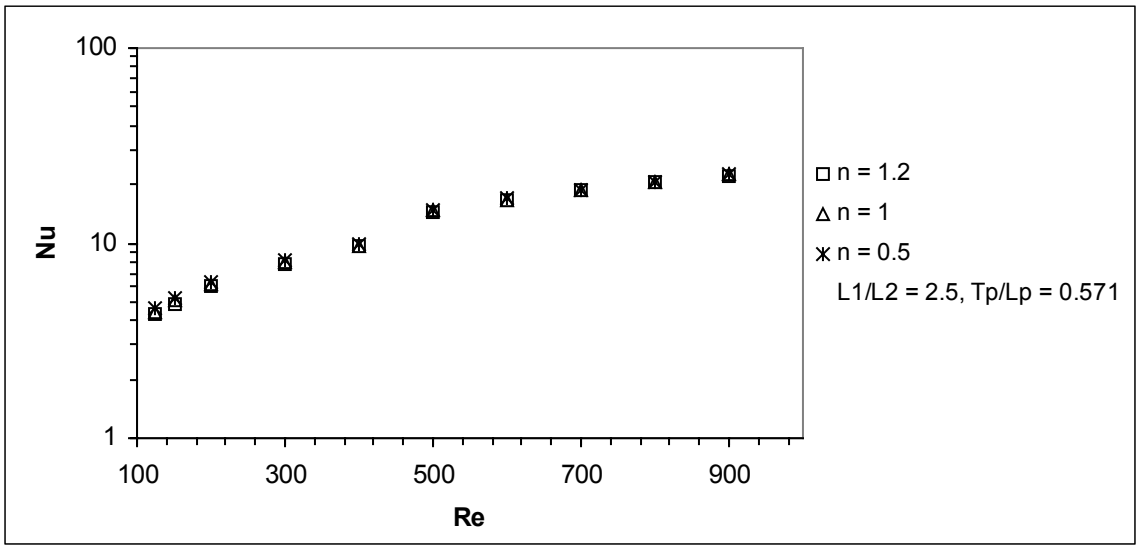

Figure 16. The Effect of Flow Index on Nu for $\theta = 25$

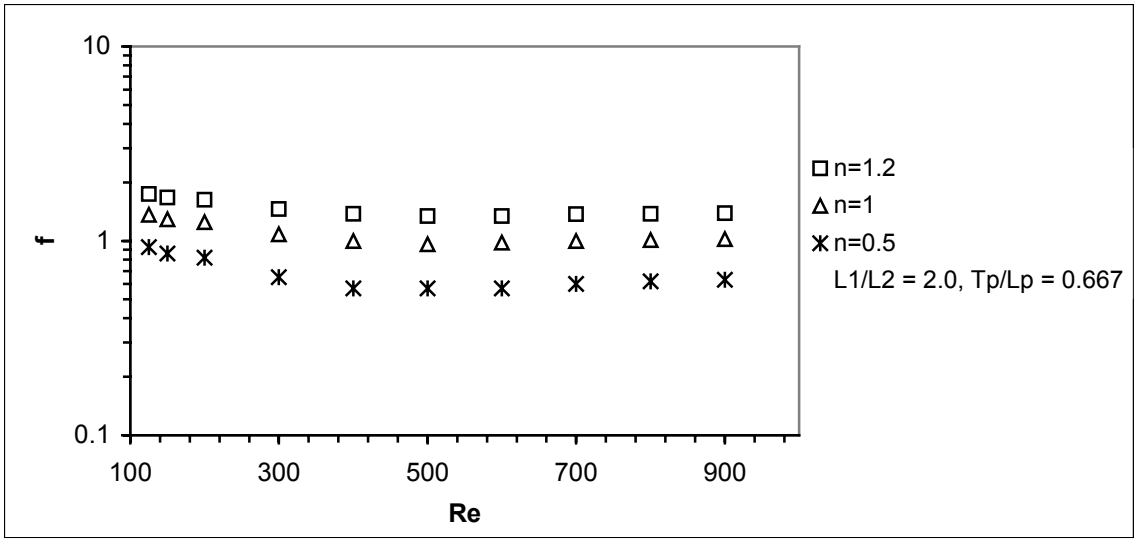

Figure 17. The Effect of Flow Index on Friction Factor for $\theta = 25$

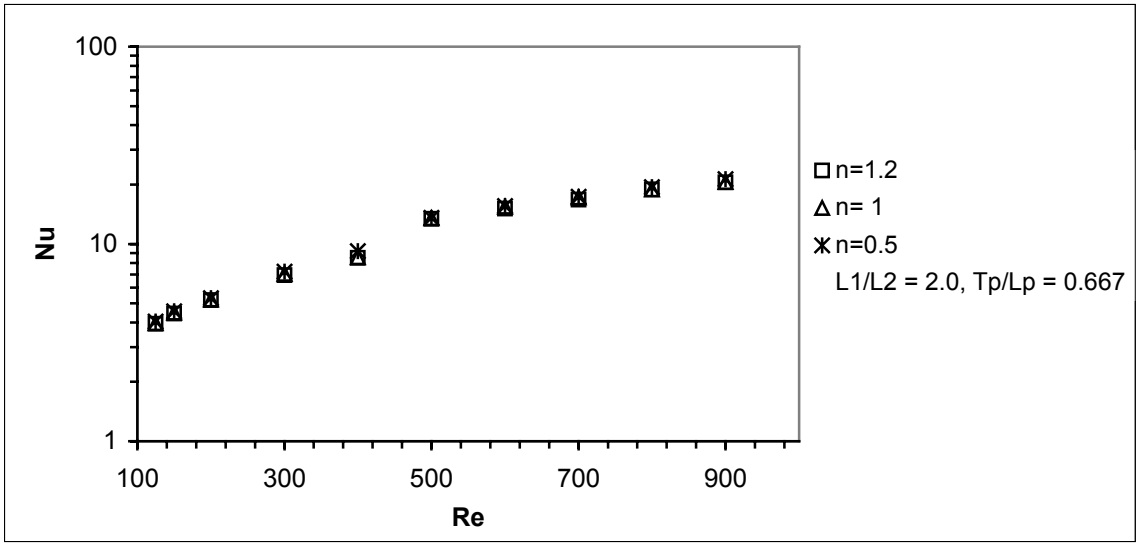

Figure 18. The Effect of Flow Index on Nu for $\theta = 25$

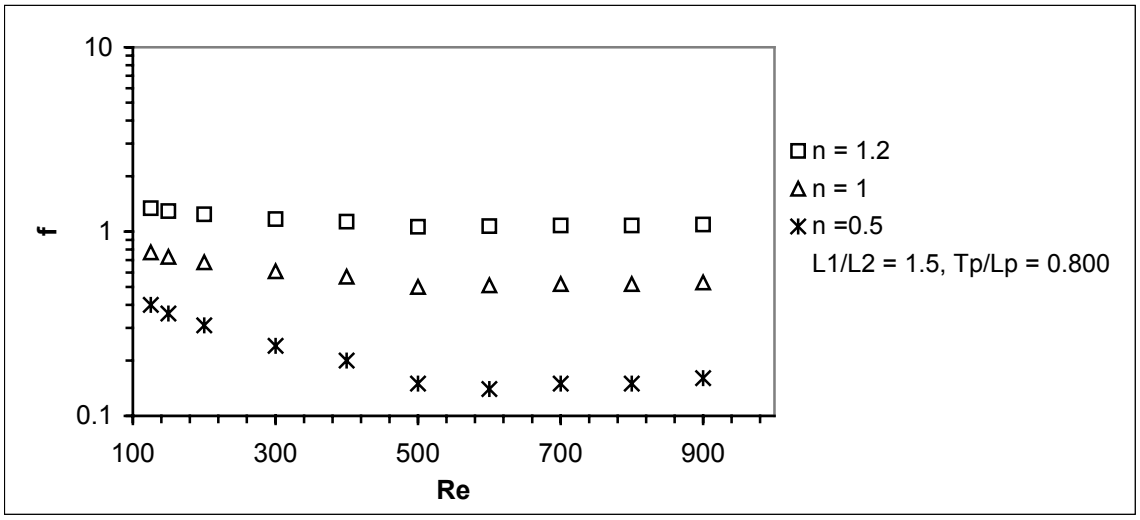

Figure 19. The Effect of Flow Index on Friction Factor for $\theta = 25$

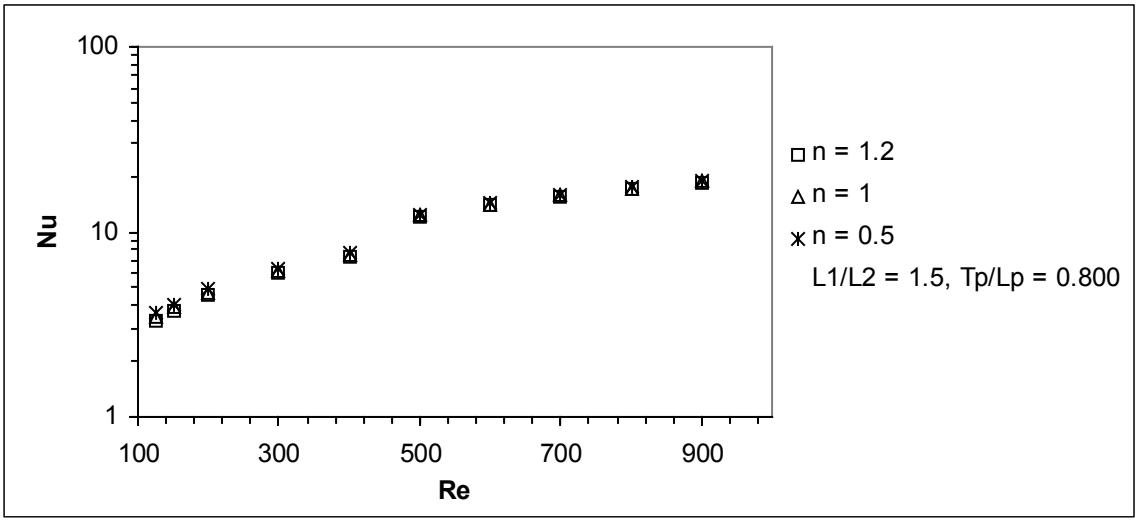

Figure 20. The Effect of Flow Index on Nu for $\theta = 25$

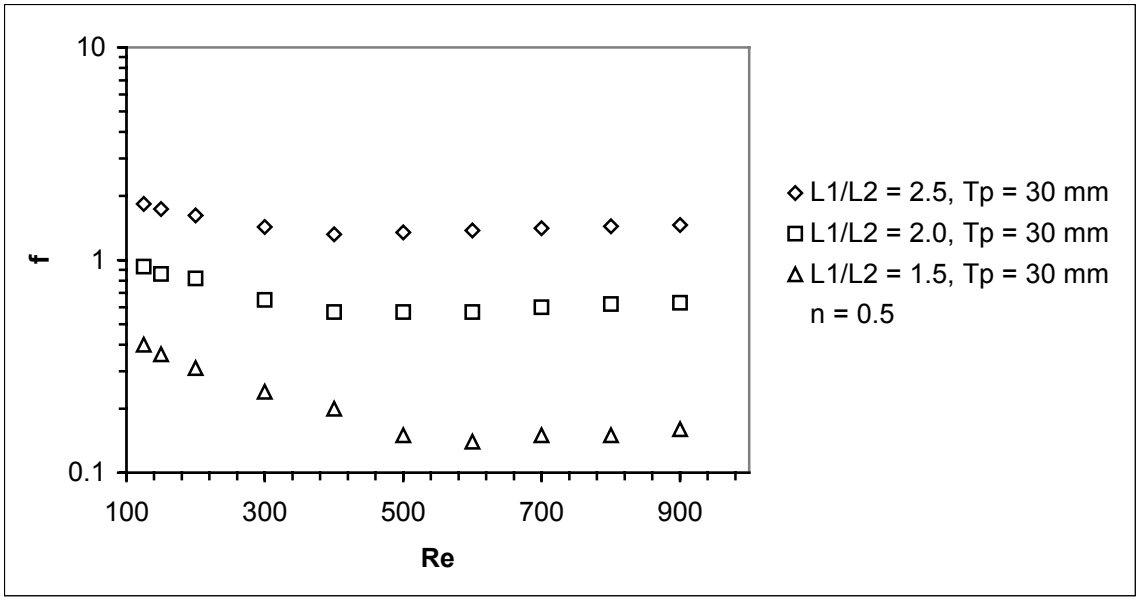

Figure 21. The Effect of Plate Length Ratio on Friction Factor for $\theta = 25$

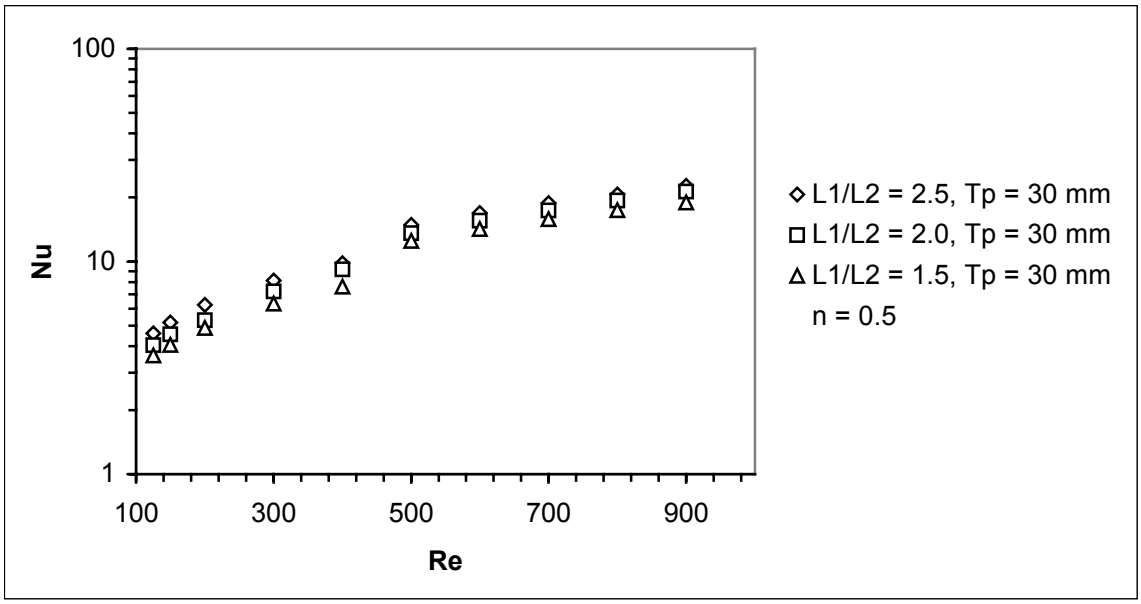

Figure 22. The Effect of Plate Length Ratio on Nu for $\theta = 25$

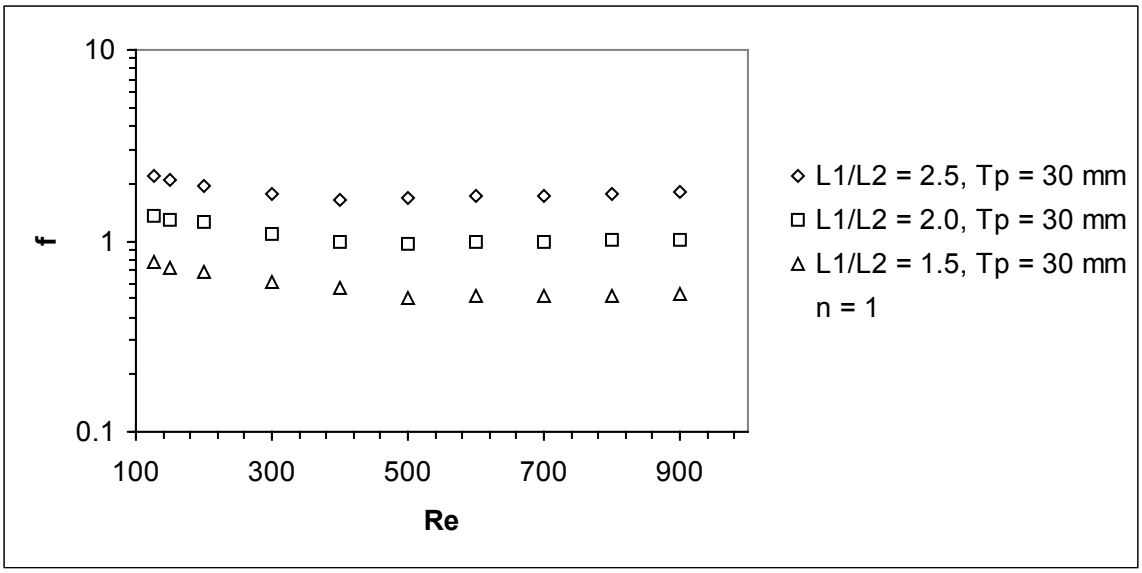

Figure 23. The Effect of Plate Length Ratio on Friction Factor for $\theta = 25$

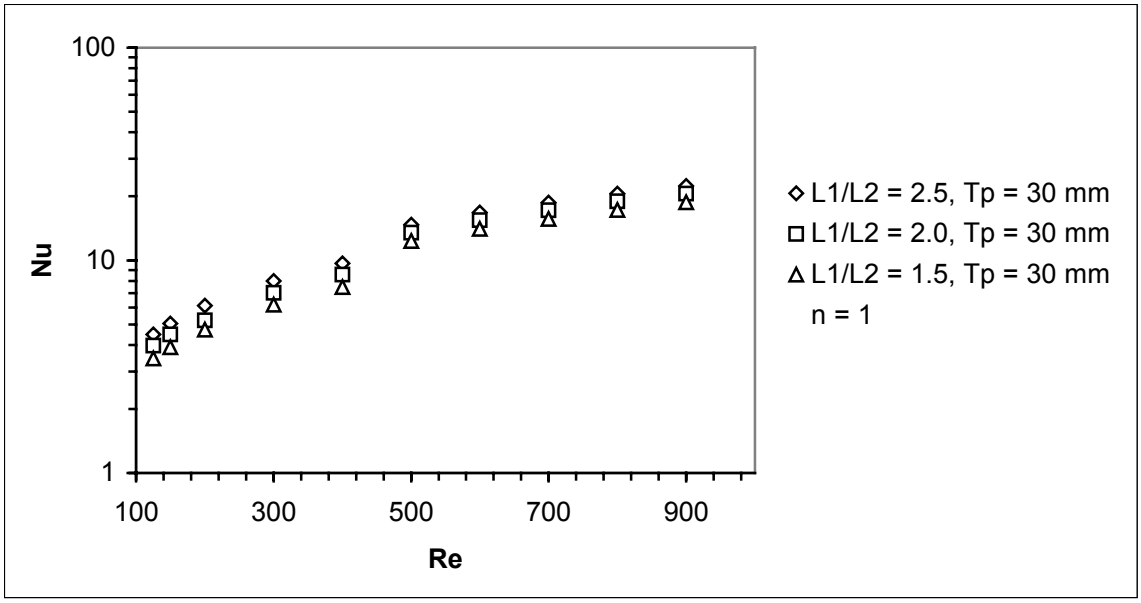

Figure 24. The Effect of Plate Length Ratio on Nu for $\theta = 25$

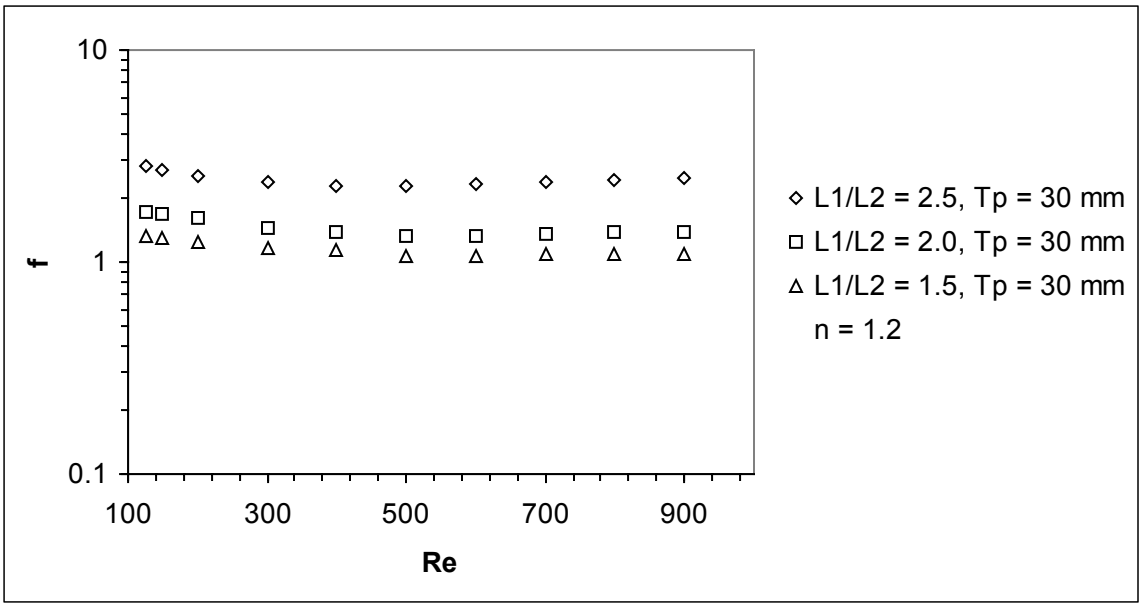

Figure 25. The Effect of Plate Length Ratio on Friction Factor for $\theta = 25$

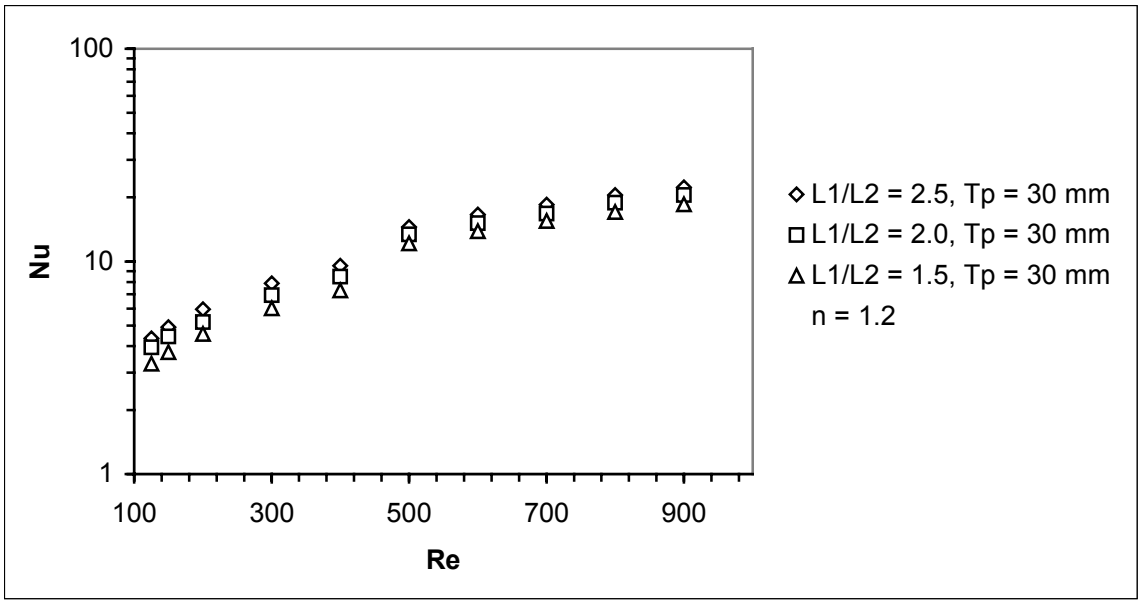

Figure 26. The Effect of Plate Length Ratio on Nu for $\theta = 25$

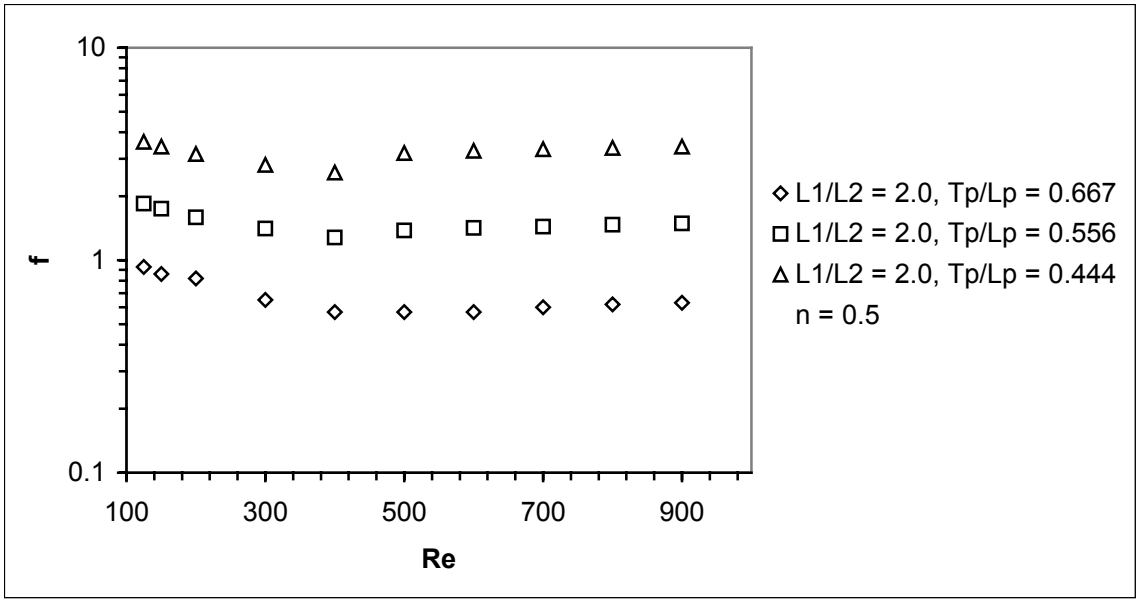

Figure 27. The Effect of Transverse Pitch on Friction Factor for $\theta = 25$

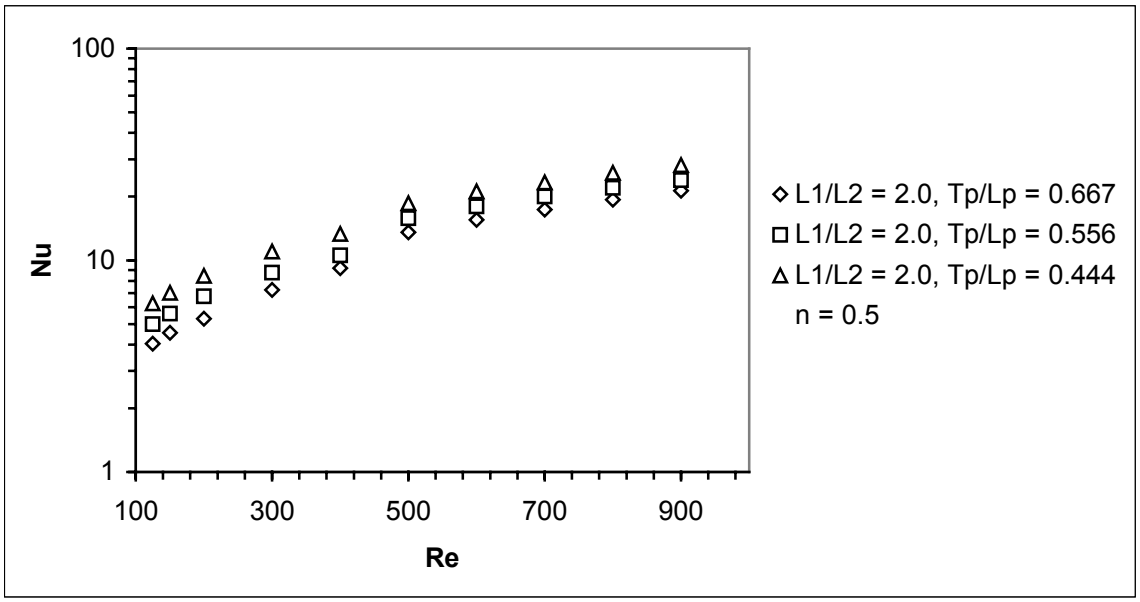

Figure 28. The Effect of Transverse Pitch on Nu for $\theta = 25$

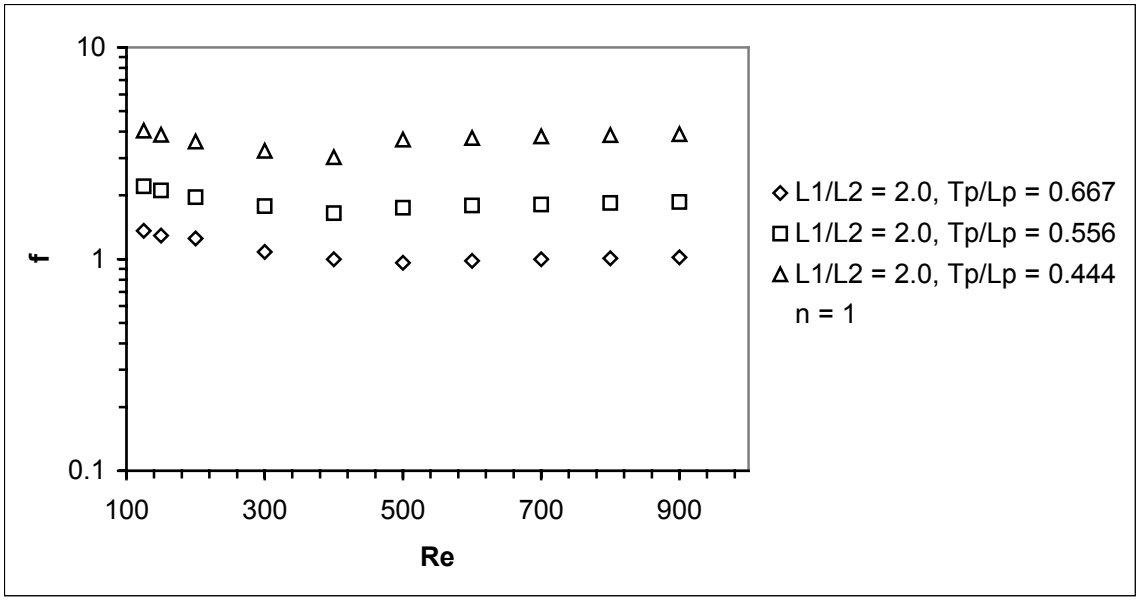

Figure 29. The Effect of Transverse Pitch on Friction Factor for $\theta = 25$

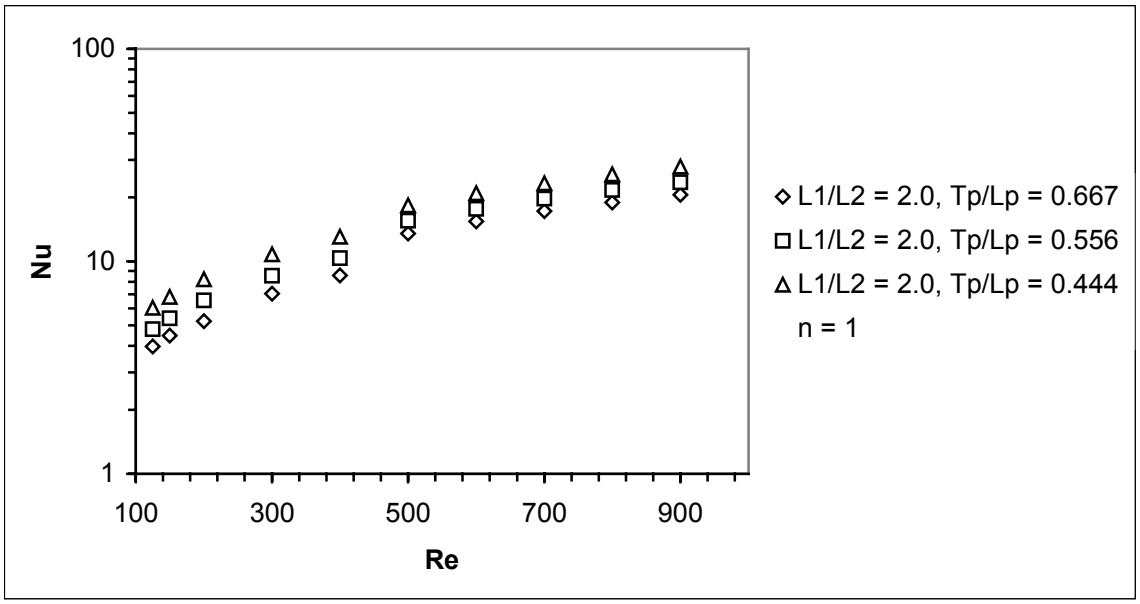

Figure 30. The Effect of Transverse Pitch on Nu for $\theta = 25$

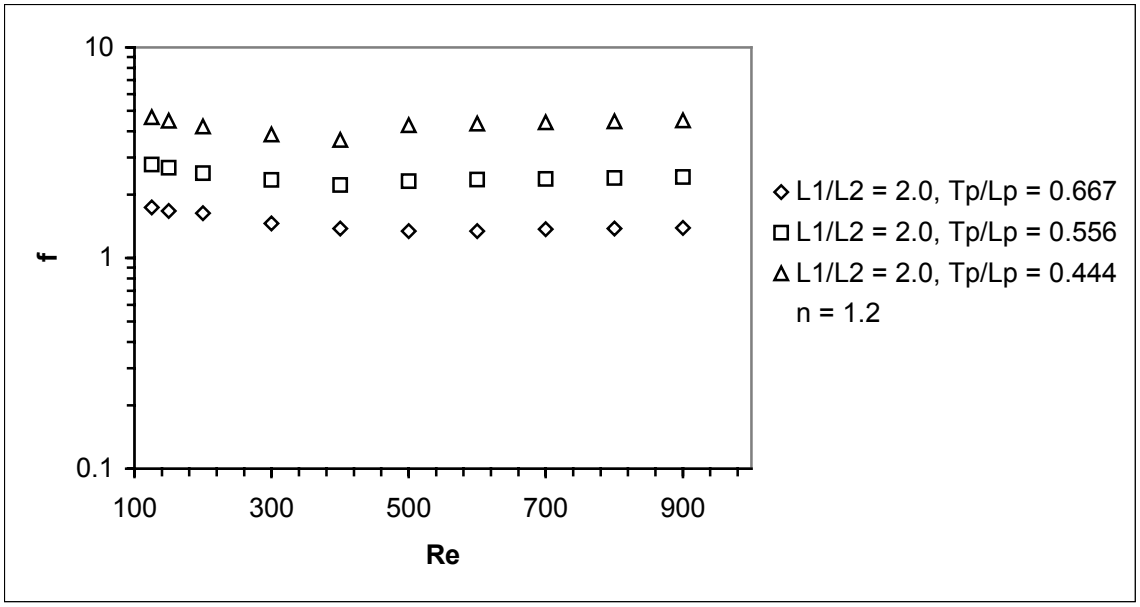

Figure 31. The Effect of Transverse Pitch on Friction Factor for $\theta = 25$

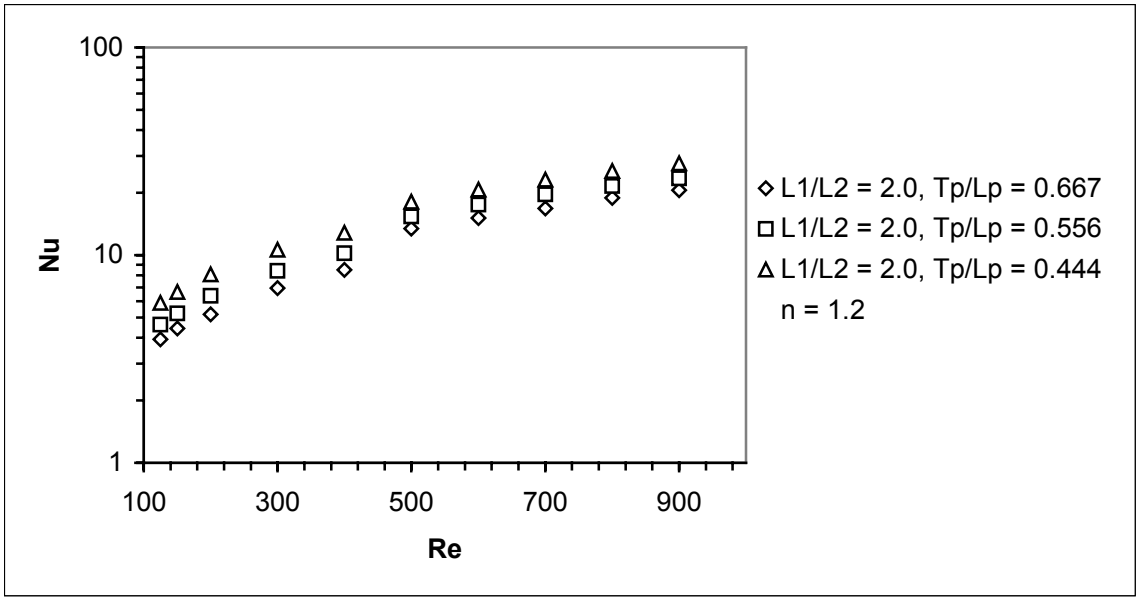

Figure 32. The Effect of Transverse Pitch on Nu for $\theta = 25$

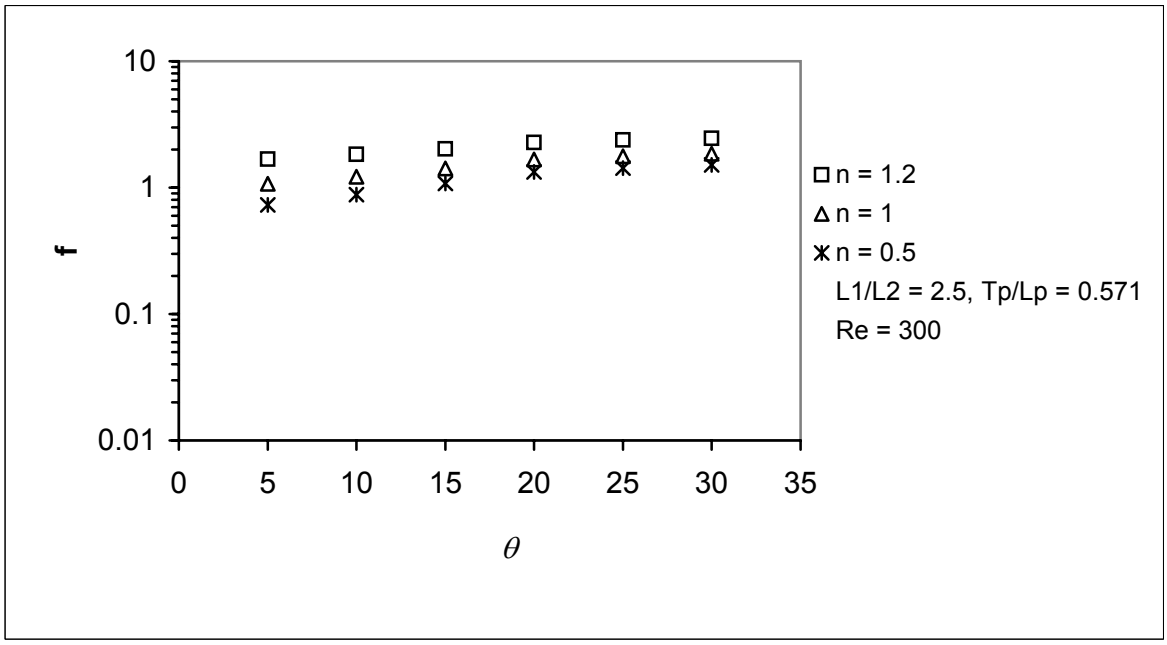

Figure 33. The Effect of Plate Angle θ on Friction Factor

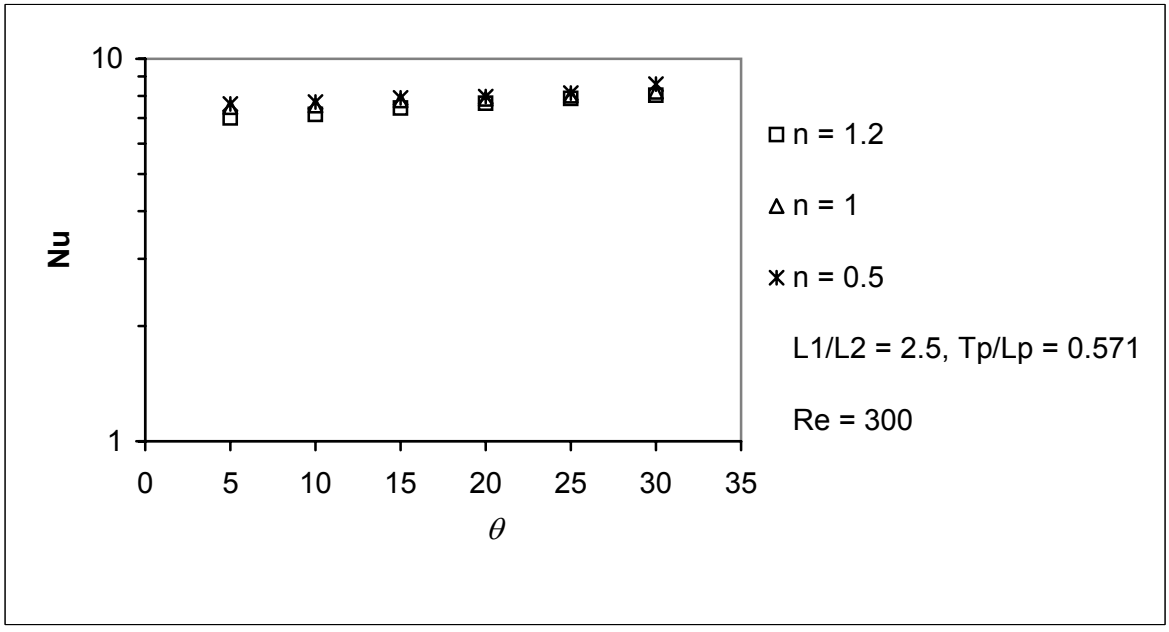

Figure 34. The Effect of Plate Angle θ on Nu

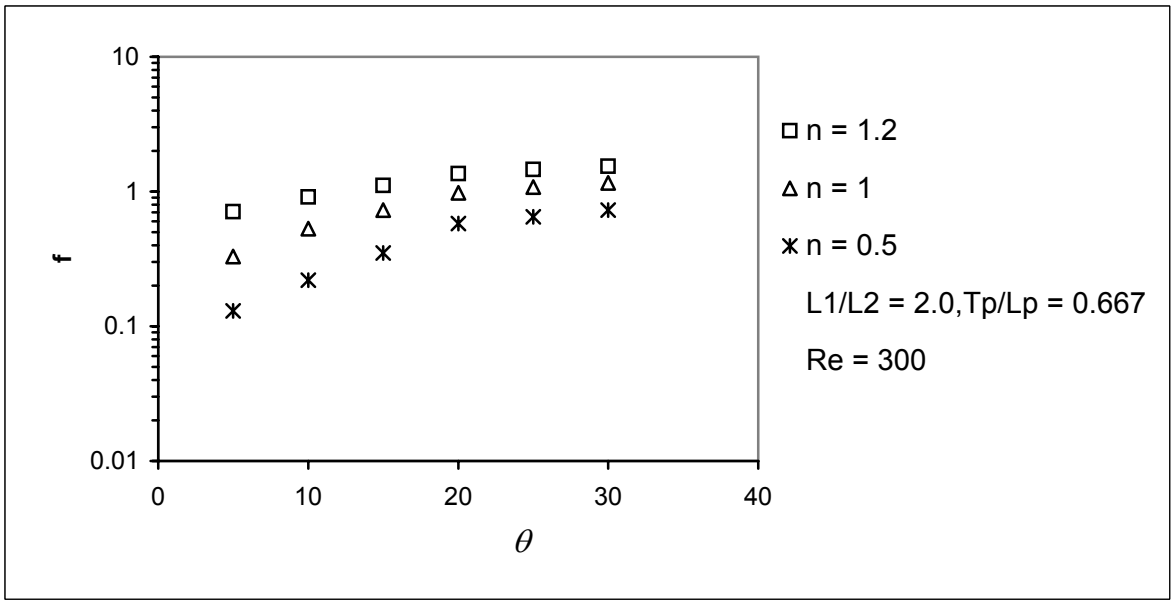

Figure 35. The Effect of Plate Angle θ on Friction Factor

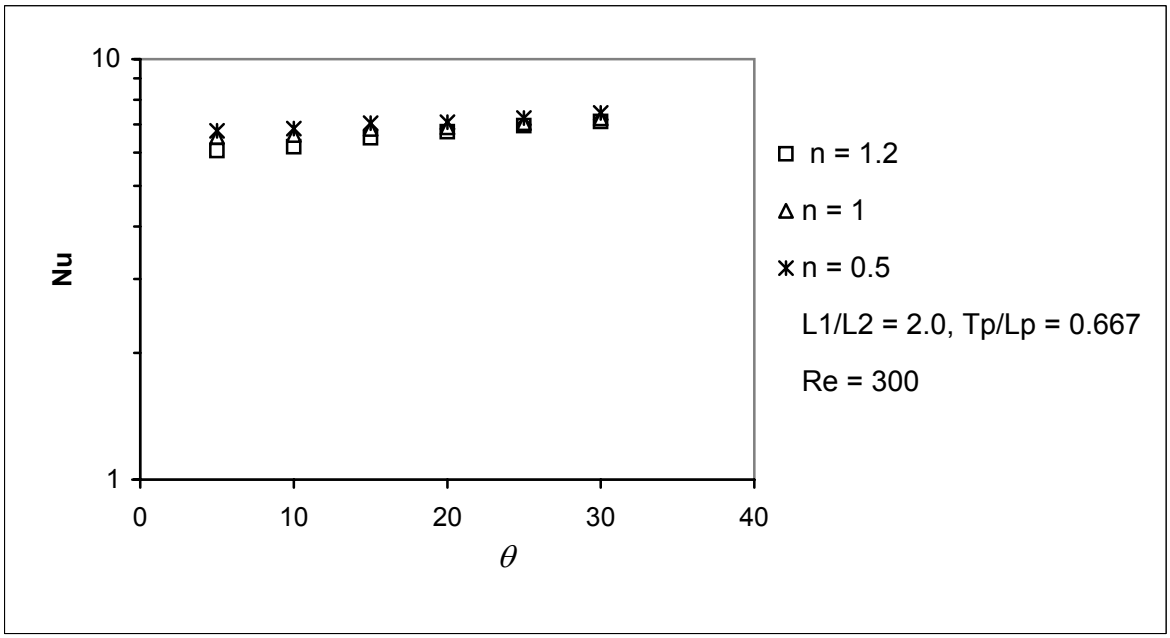

Figure 36. The Effect of Plate Angle θ on Nu

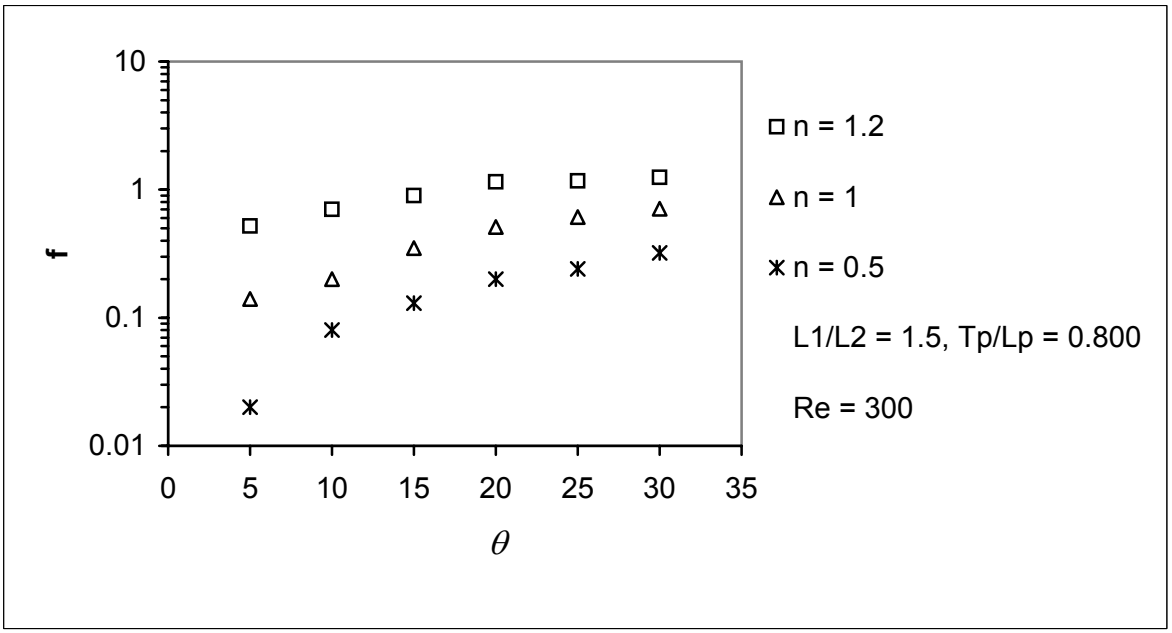

Figure 37. The Effect of Plate Angle θ on Friction Factor

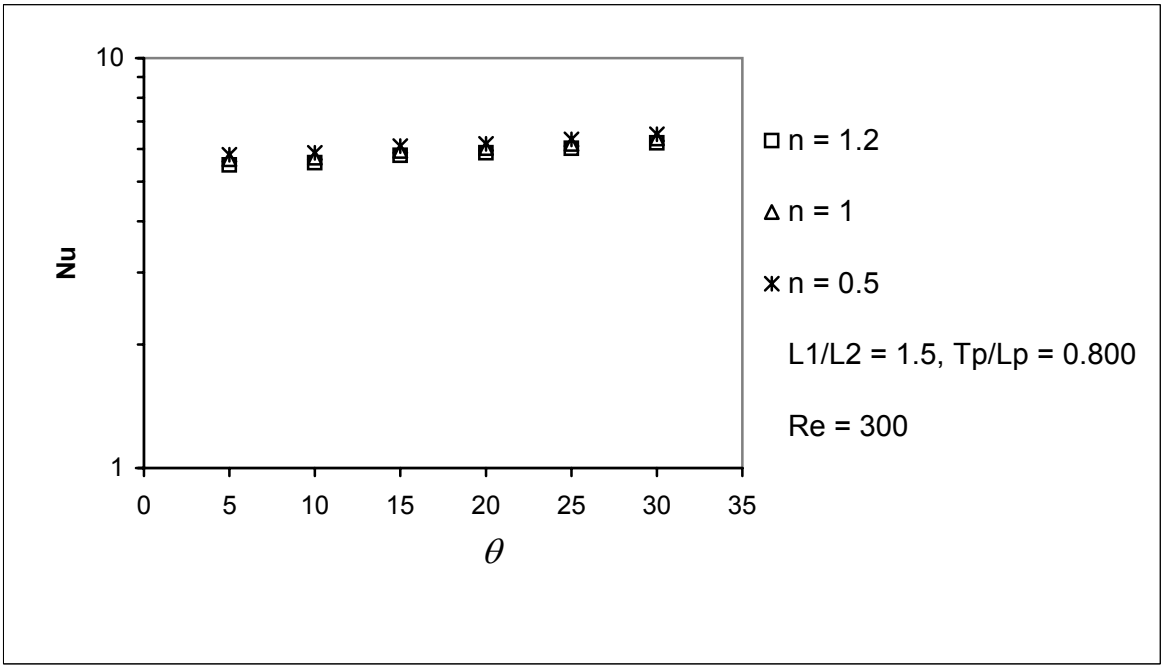

Figure 38. The Effect of Plate Angle θ on Nu

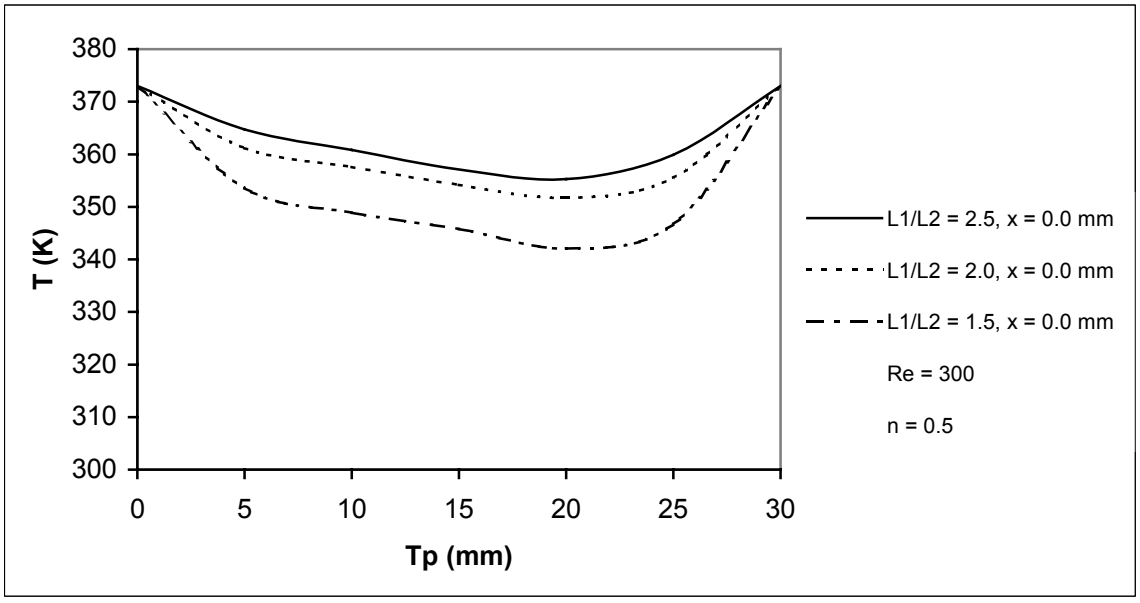

Figure 39. The Effect of Plate Length Ratio on Temperature Profile at Leading Edge (x = 0.0) of Long Plate (L1) for n = 0.5 and $\theta = 25$

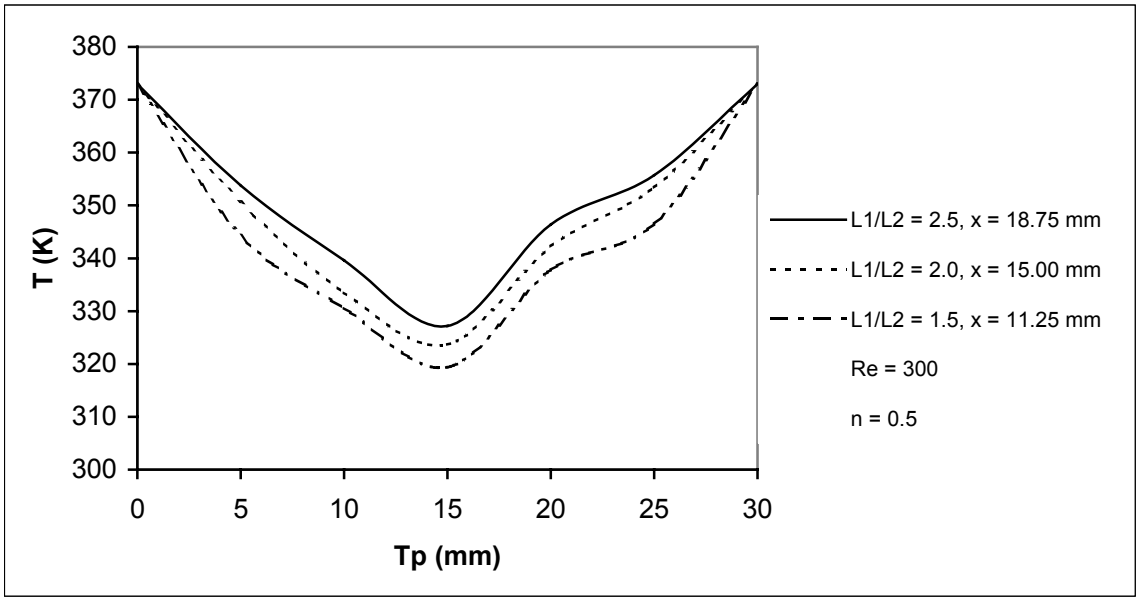

Figure 40. The Effect of Plate Length Ratio on Temperature Profile at Middle of Long Plate (L1) for n = 0.5 and $\theta = 25$

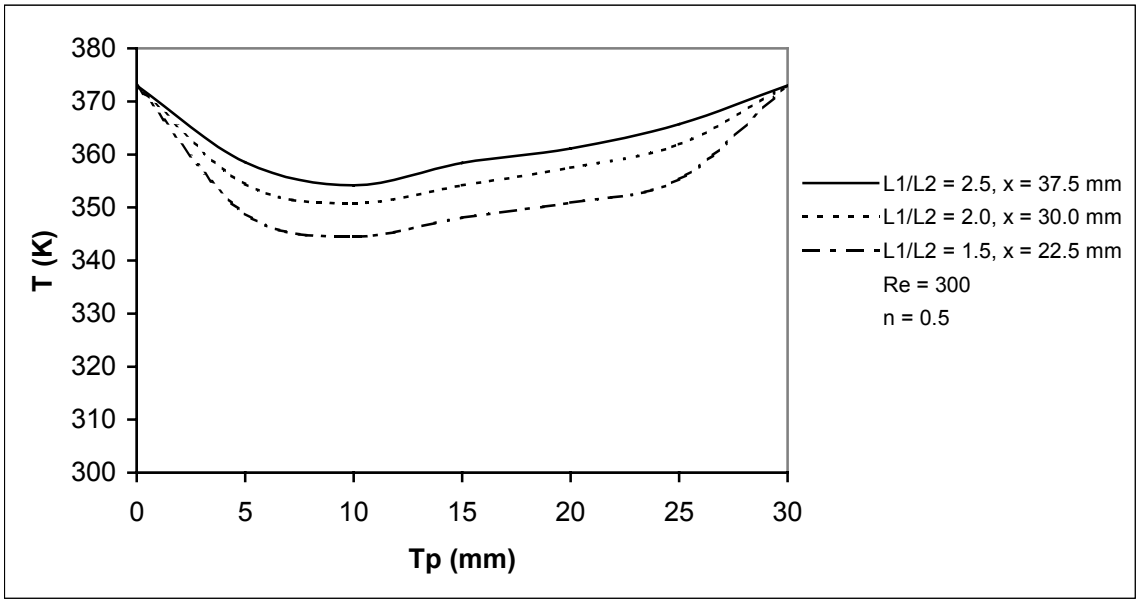

Figure 41. The Effect of Plate Length Ratio on Temperature Profile at Tailing Edge of Long Plate (L1) for n = 0.5 and $\theta = 25$

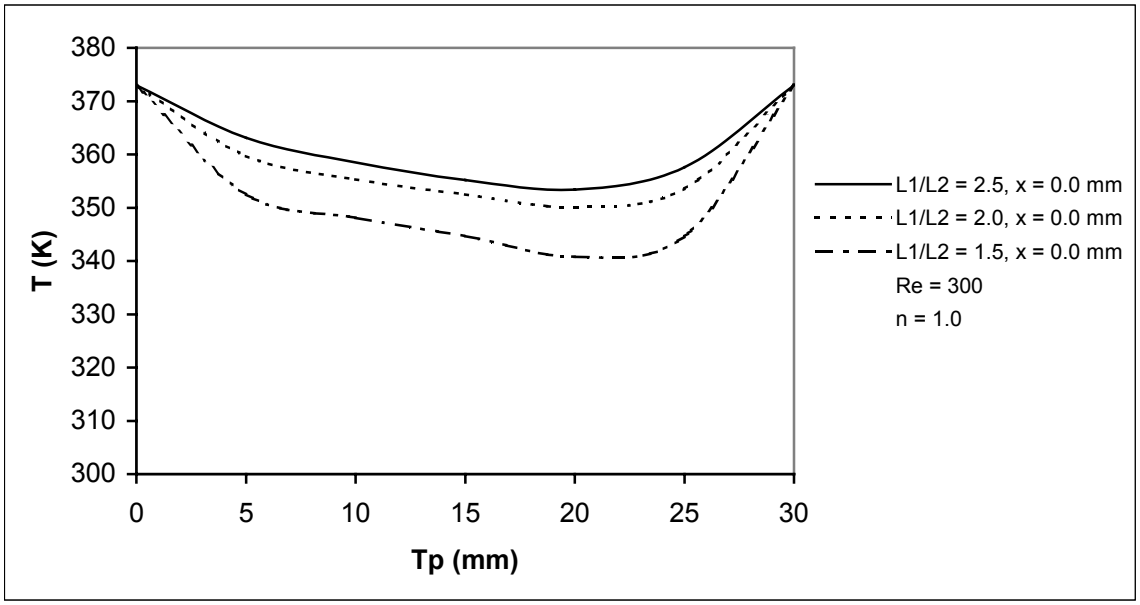

Figure 42. The Effect of Plate Length Ratio on Temperature Profile at Leading Edge (x = 0.0) of Long Plate (L1) for n = 1.0 and $\theta = 25$

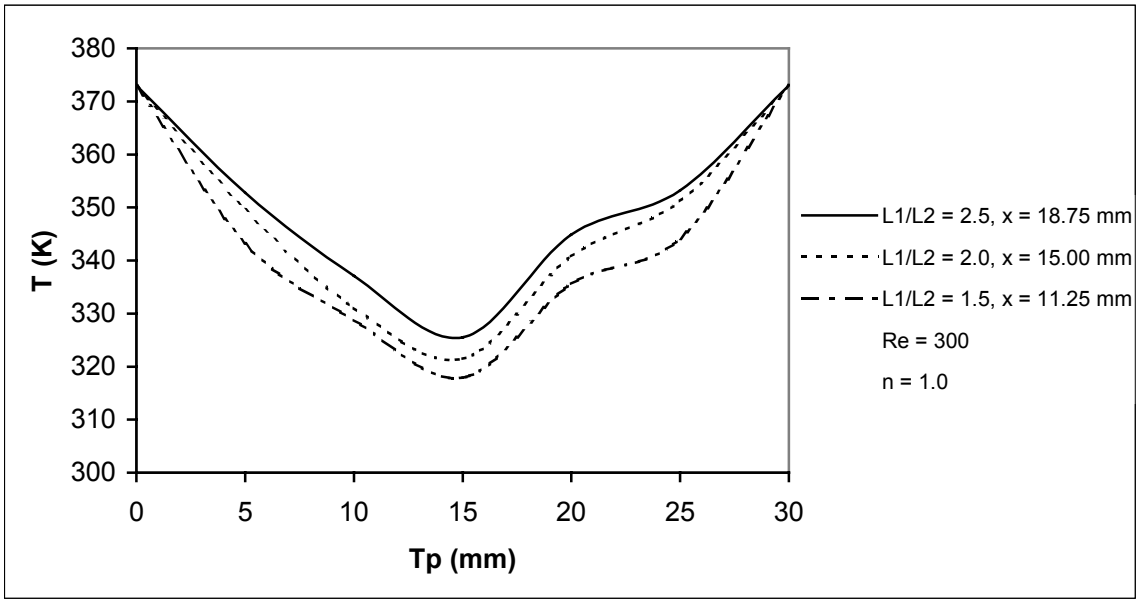

Figure 43. The Effect of Plate Length Ratio on Temperature Profile at Middle of Long Plate (L1) for n = 1.0 and $\theta = 25$

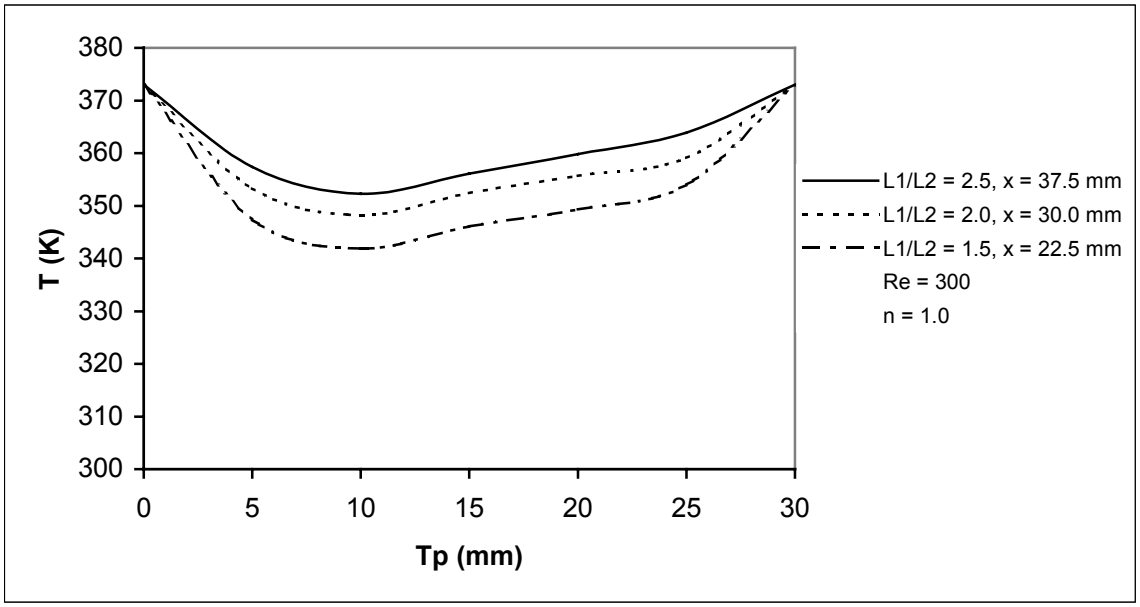

Figure 44. The Effect of Plate Length Ratio on Temperature Profile at Tailing Edge of Long Plate (L1) for n = 1.0 and $\theta = 25$

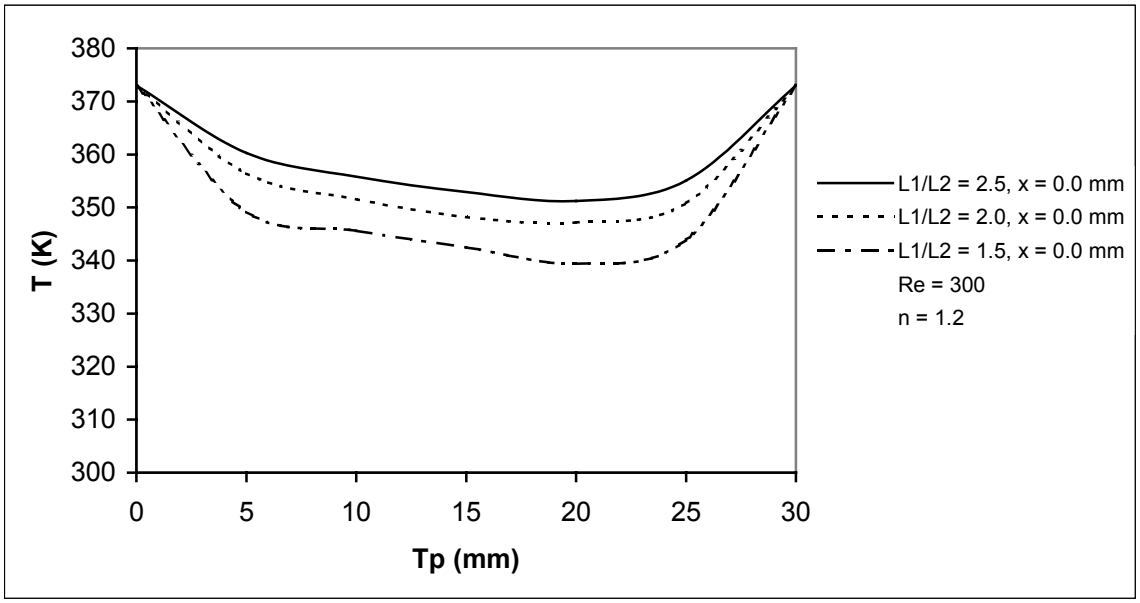

Figure 45. The Effect of Plate Length Ratio on Temperature Profile at Leading Edge (x = 0.0) of Long Plate (L1) for n = 1.2 and $\theta = 25$

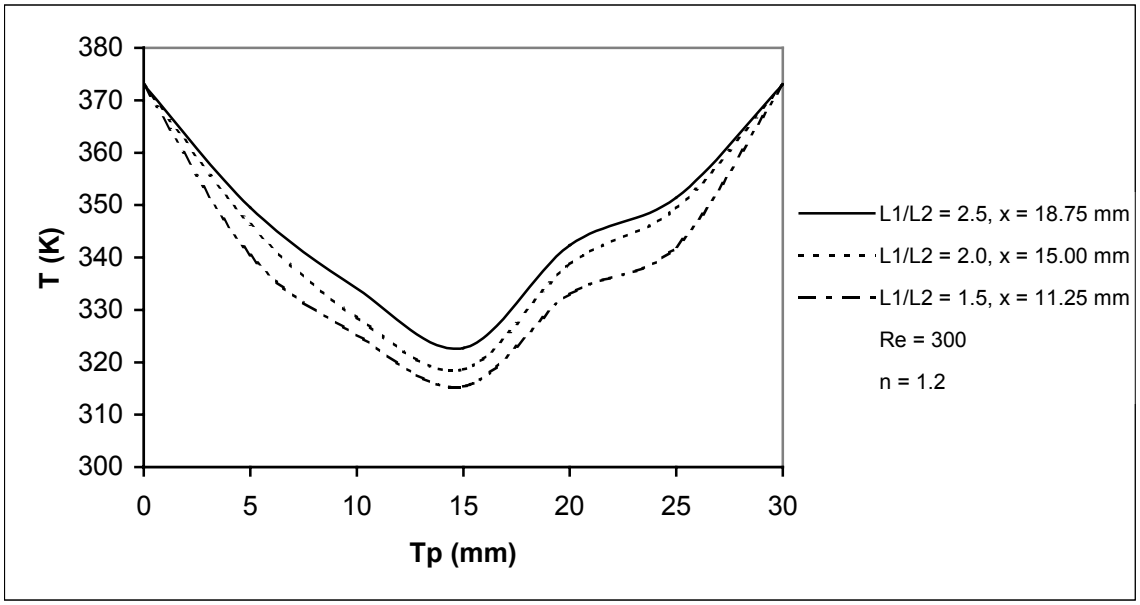

Figure 46. The Effect of Plate Length Ratio on Temperature Profile at Middle of Long Plate (L1) for n = 1.2 and $\theta = 25$

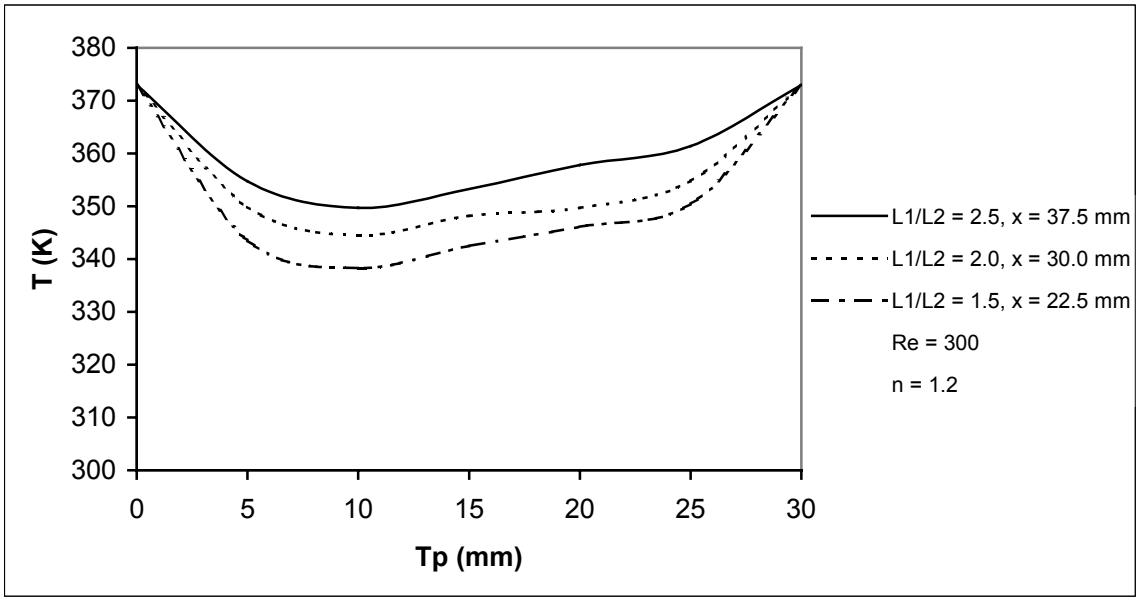

Figure 47. The Effect of Plate Length Ratio on Temperature Profile at Tailing Edge of Long Plate (L1) for n = 1.2 and $\theta = 25$

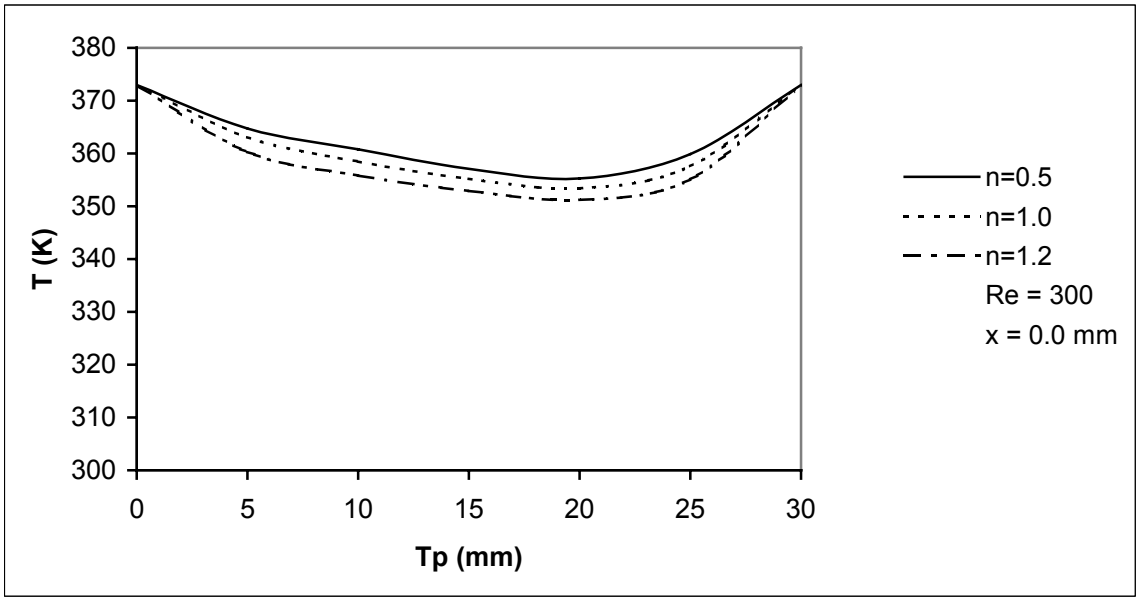

Figure 48. The Effect of Flow Index on Temperature Profile at Leading Edge (x = 0.0) of Long Plate (L1) for L1/L2 = 2.5, Tp = 30 mm, and $\theta = 25$

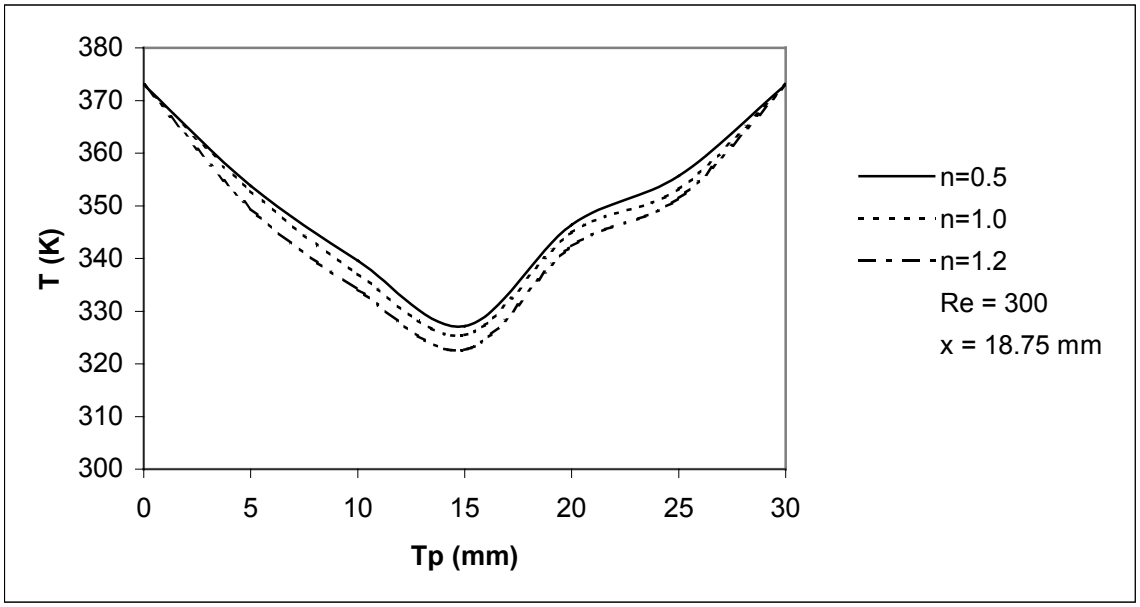

Figure 49. The Effect of Flow Index on Temperature Profile at Middle (x = 18.75) of Long Plate (L1) for L1/L2 = 2.5, Tp = 30 mm, and $\theta = 25$

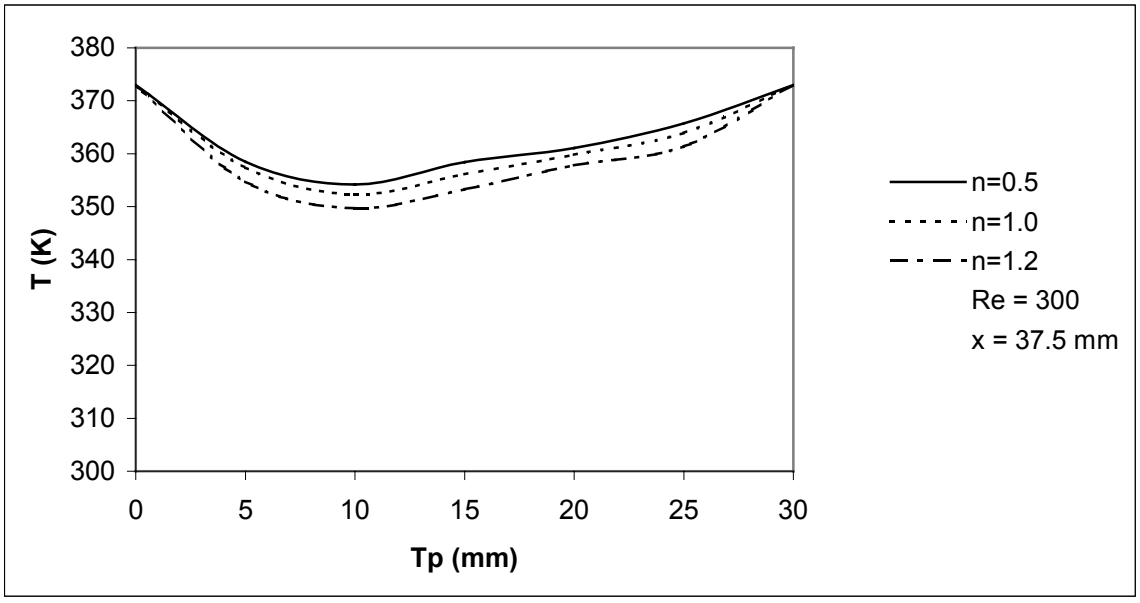

Figure 50. The Effect of Flow Index on Temperature Profile at Tailing Edge (x = 37.5) of Long Plate (L1) for L1/L2 = 2.5, Tp = 30 mm, and $\theta = 25$

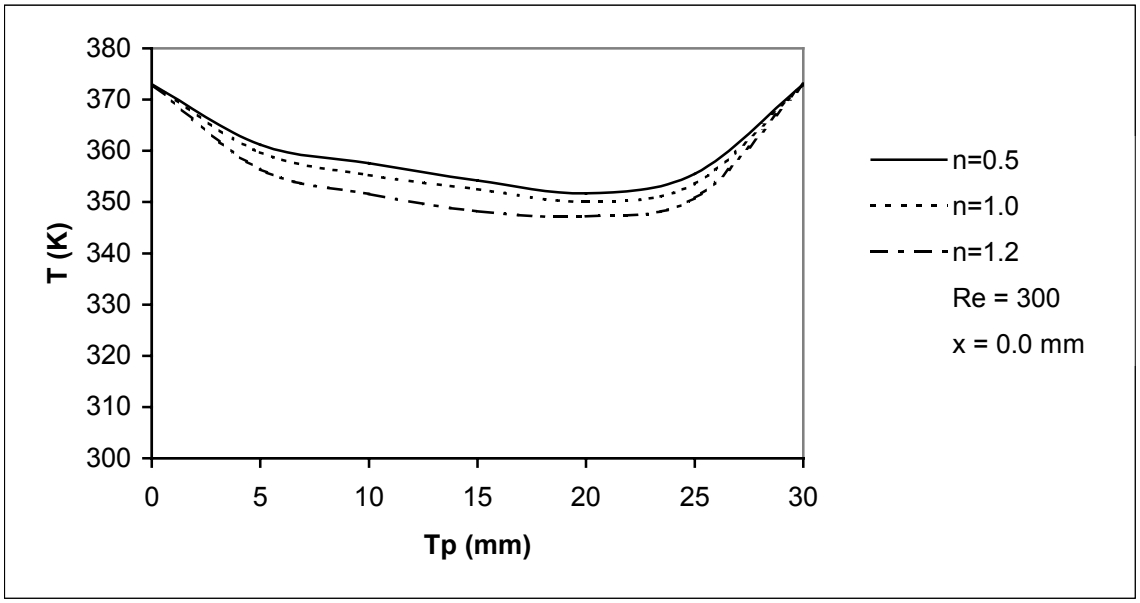

Figure 51. The Effect of Flow Index on Temperature Profile at Leading Edge (x = 0.0) of Long Plate (L1) for L1/L2 = 2.0, Tp = 30 mm, and $\theta = 25$

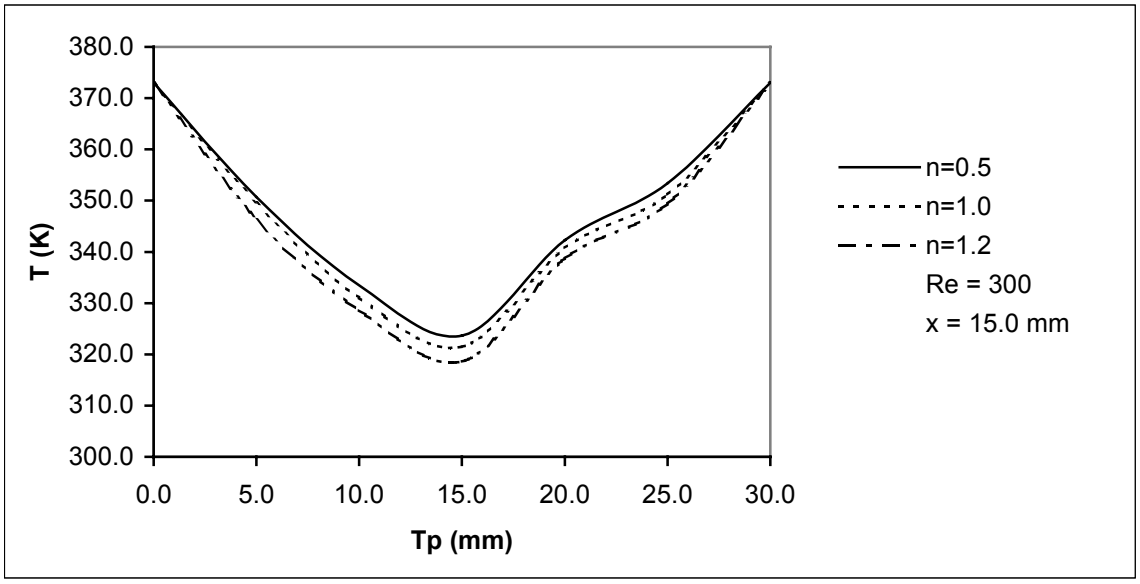

Figure 52. The Effect of Flow Index on Temperature Profile at Middle (x = 15.00) of Long Plate (L1) for L1/L2 = 2.0, Tp = 30 mm, and $\theta = 25$

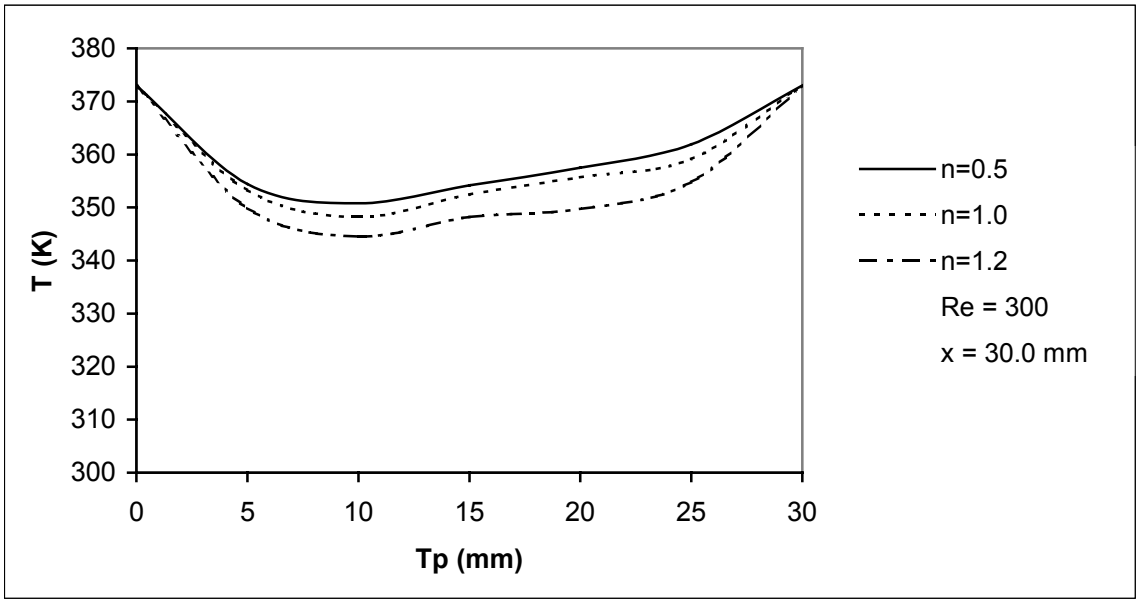

Figure 53. The Effect of Flow Index on Temperature Profile at Tailing Edge (x = 30.0) of Long Plate (L1) for L1/L2 = 2.0, Tp = 30 mm, and $\theta = 25$

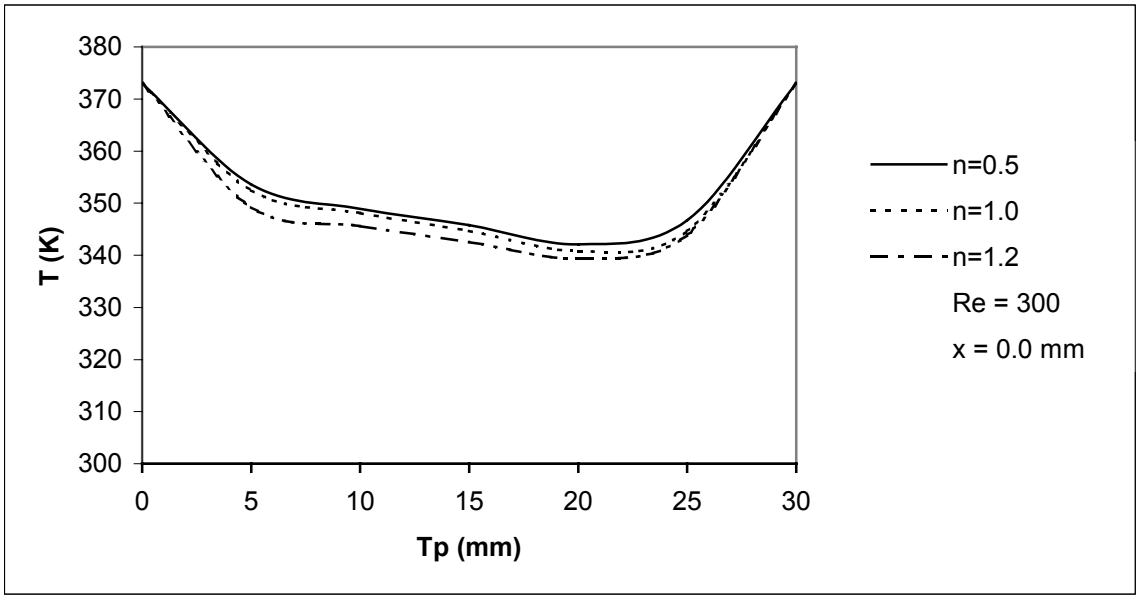

Figure 54. The Effect of Flow Index on Temperature Profile at Leading Edge (x = 0.0) of Long Plate (L1) for L1/L2 = 1.5, Tp = 30 mm, and $\theta = 25$

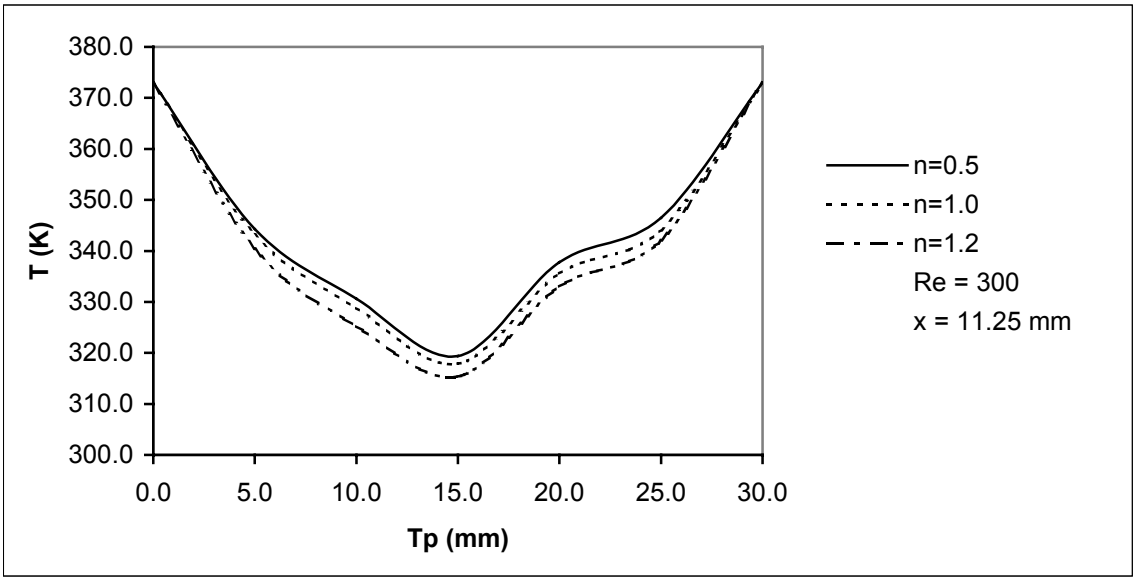

Figure 55. The Effect of Flow Index on Temperature Profile at Middle (x = 11.25) of Long Plate (L1) for L1/L2 = 1.5, Tp = 30 mm, and $\theta = 25$

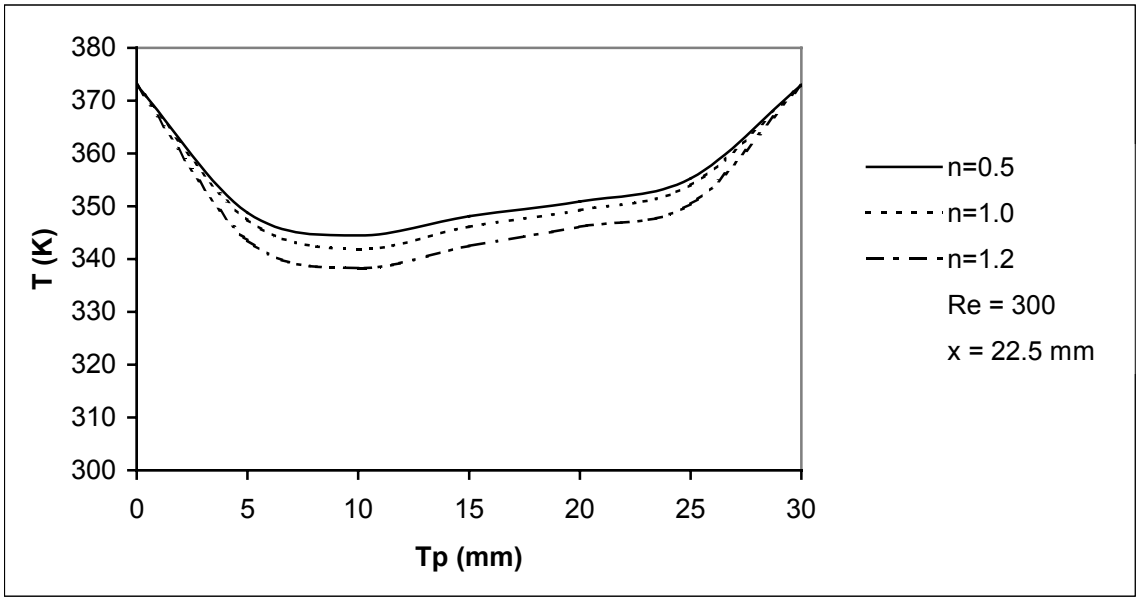

Figure 56. The Effect of Flow Index on Temperature Profile at Tailing Edge (x = 22.5) of Long Plate (L1) for L1/L2 = 1.5, Tp = 30 mm, and $\theta = 25$

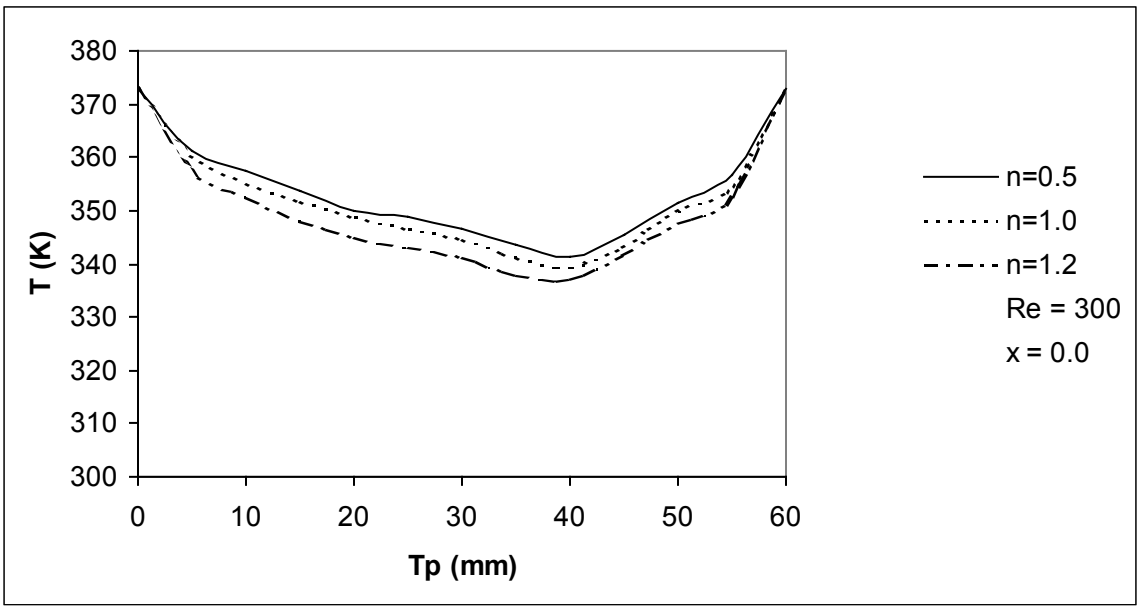

Figure 57. The Effect of Flow Index on Temperature Profile at Leading Edge (x = 0.0) of Long Plate (L1) for L1/L2 = 2.5, Tp = 60 mm, and $\theta = 25$

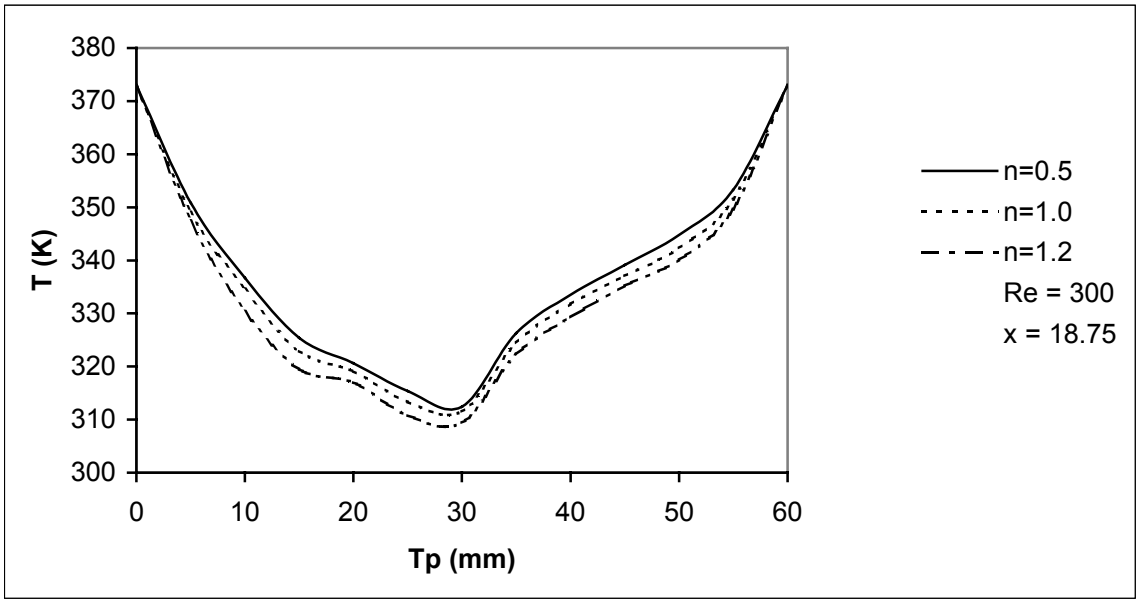

Figure 58. The Effect of Flow Index on Temperature Profile at Middle (x = 18.75) of Long Plate (L1) for L1/L2 = 2.5, Tp = 60 mm, and $\theta = 25$

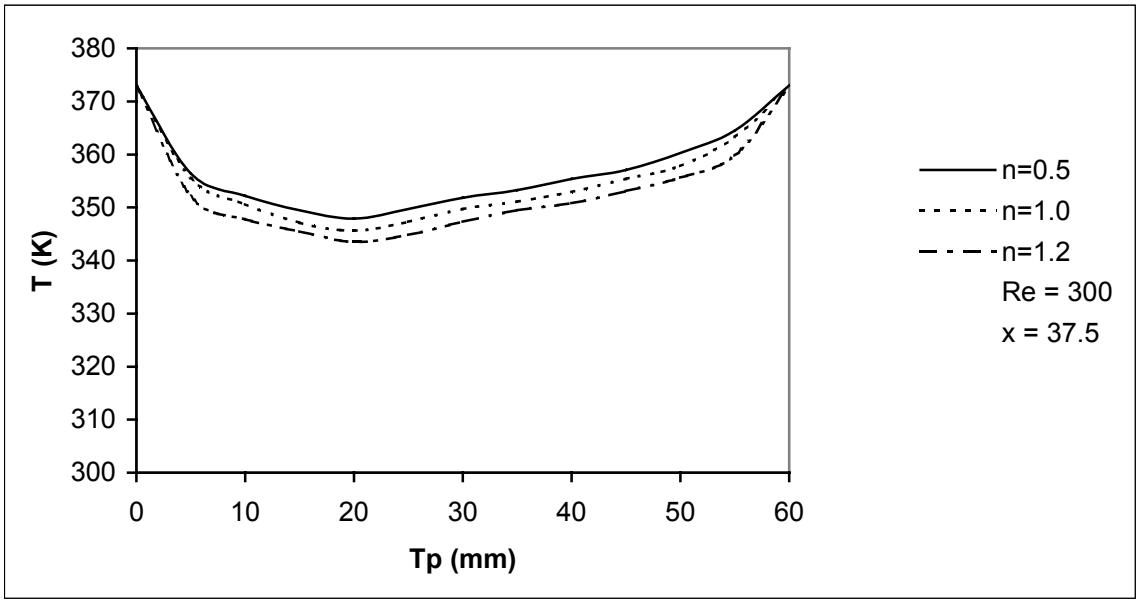

Figure 59. The Effect of Flow Index on Temperature Profile at Tailing Edge (x = 37.5) of Long Plate (L1) for L1/L2 = 2.5, Tp = 60 mm, and $\theta = 25$

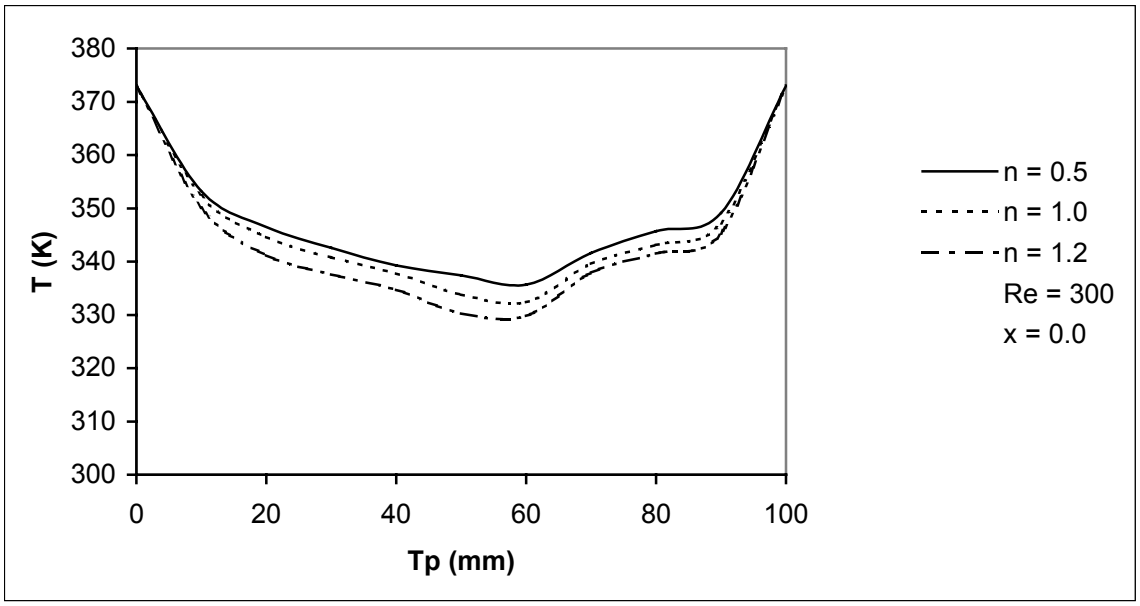

Figure 60. The Effect of Flow Index on Temperature Profile at Leading Edge (x = 0.0) of Long Plate (L1) for L1/L2 = 2.5, Tp = 100 mm, and $\theta = 25$

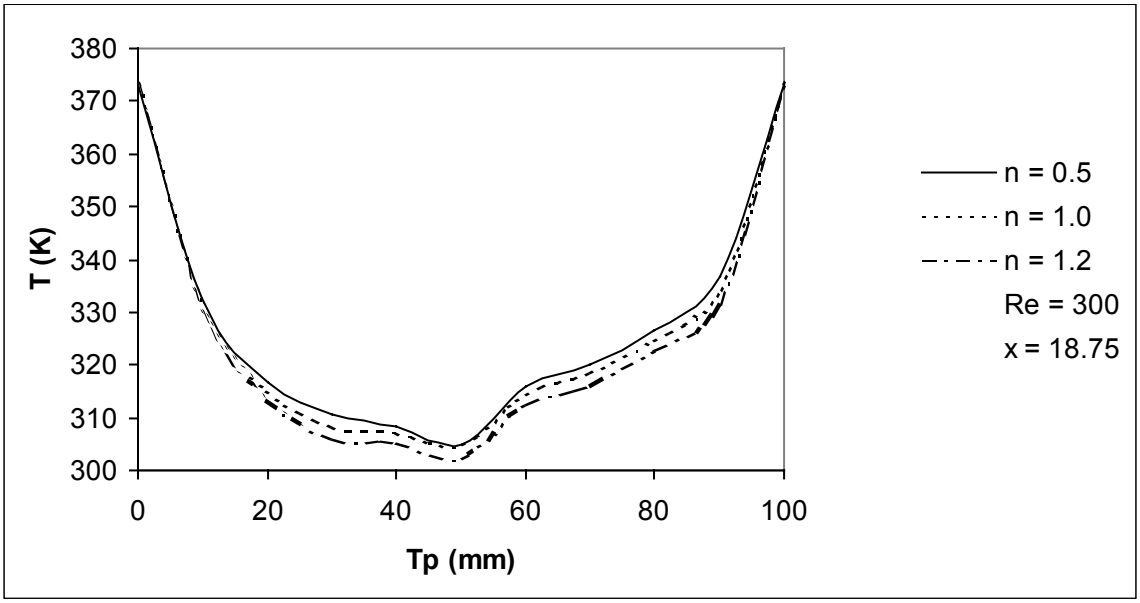

Figure 61. The Effect of Flow Index on Temperature Profile at Middle (x = 18.75) of Long Plate (L1) for L1/L2 = 2.5, Tp = 100 mm, and $\theta = 25$

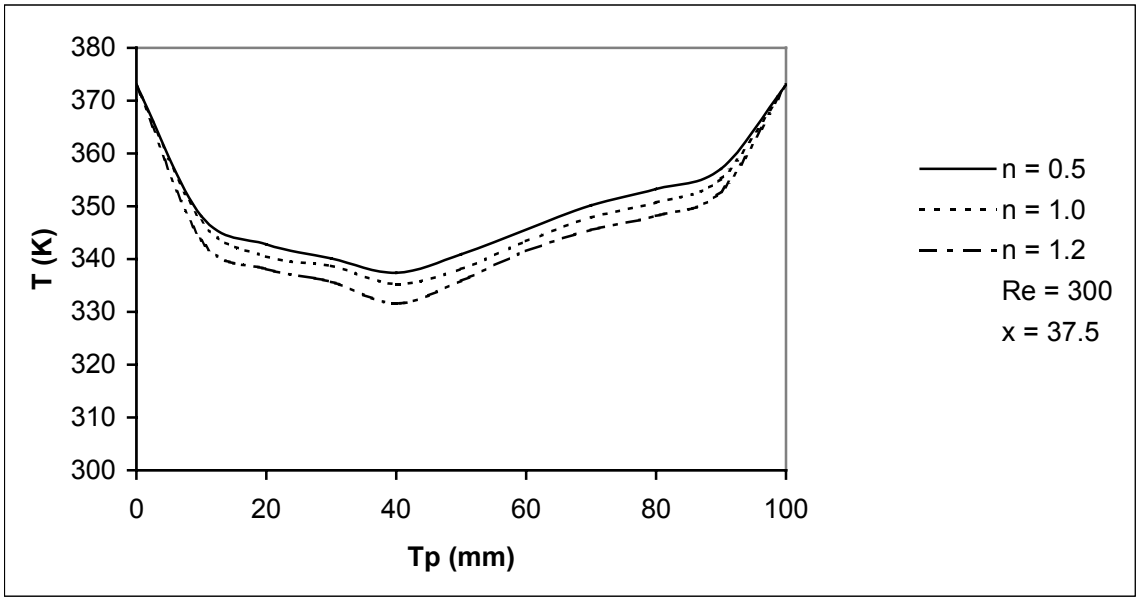

Figure 62. The Effect of Flow Index on Temperature Profile at Tailing Edge (x = 37.5) of Long Plate (L1) for L1/L2 = 2.5, Tp = 100 mm, and $\theta = 25$

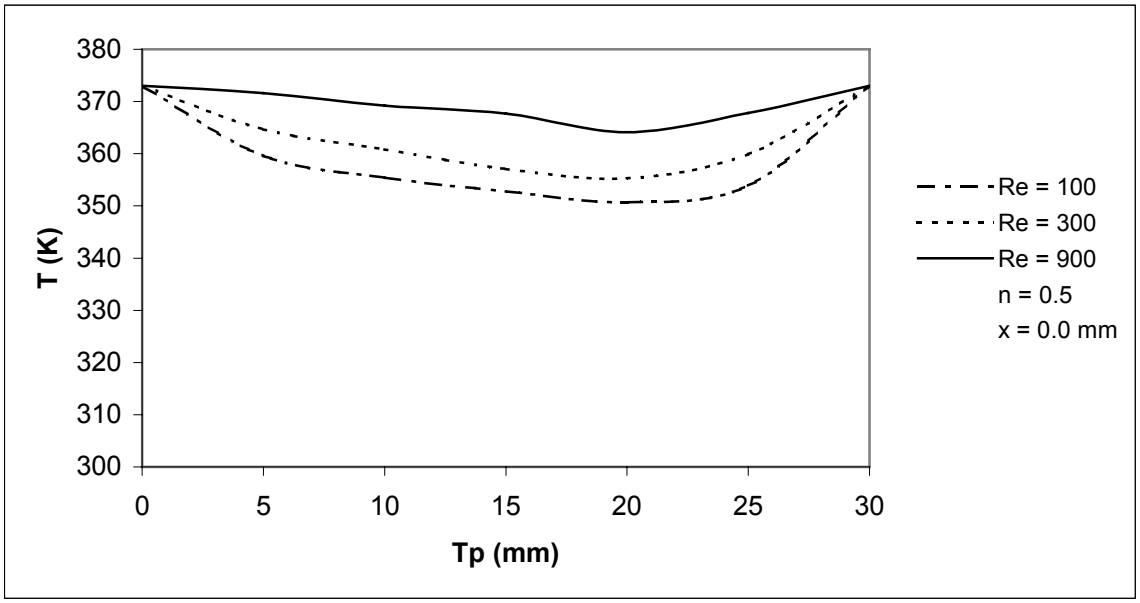

Figure 63. The Effect of Reynolds Number on Temperature Profile at Leading Edge (x = 0.0) of Long Plate (L1) for L1/L2 = 2.5, Tp = 30 mm, and $\theta = 25$

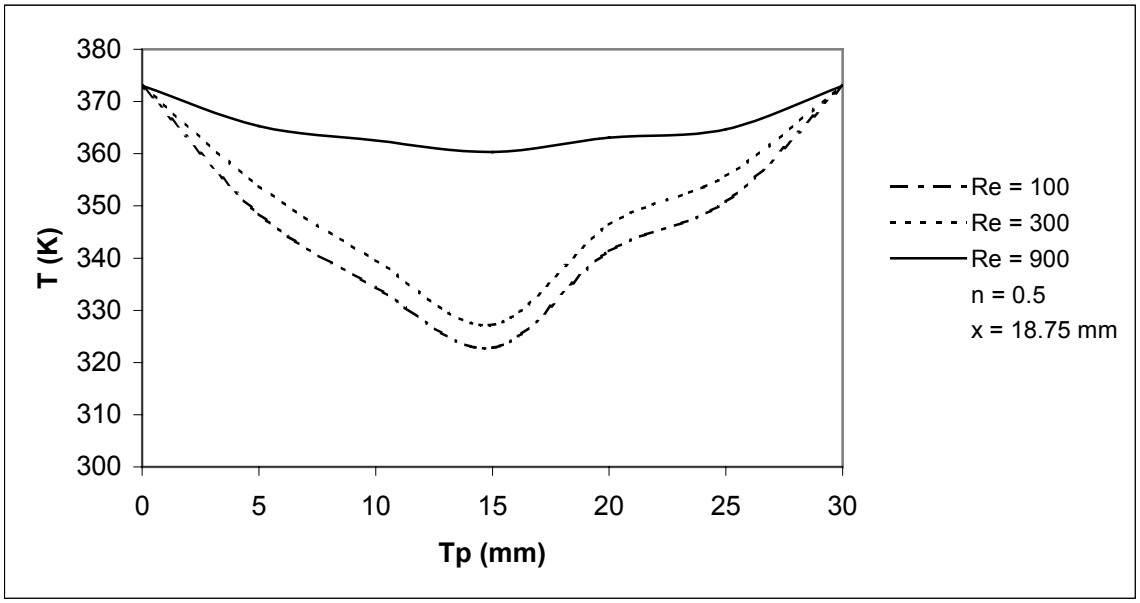

Figure 64. The Effect of Reynolds Number on Temperature Profile at Middle (x = 18.75) of Long Plate (L1) for L1/L2 = 2.5, Tp = 30 mm, and $\theta = 25$

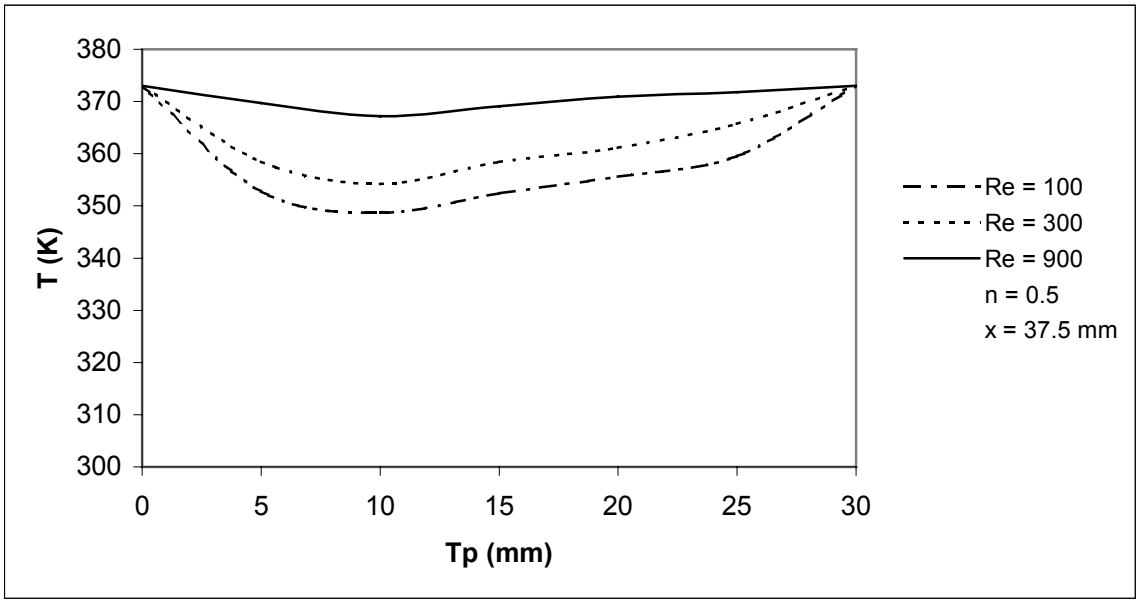

Figure 65. The Effect of Reynolds Number on Temperature Profile at Tailing Edge (x =37.5) of Long Plate (L1) for L1/L2 = 2.5, Tp = 30 mm, and $\theta = 25$

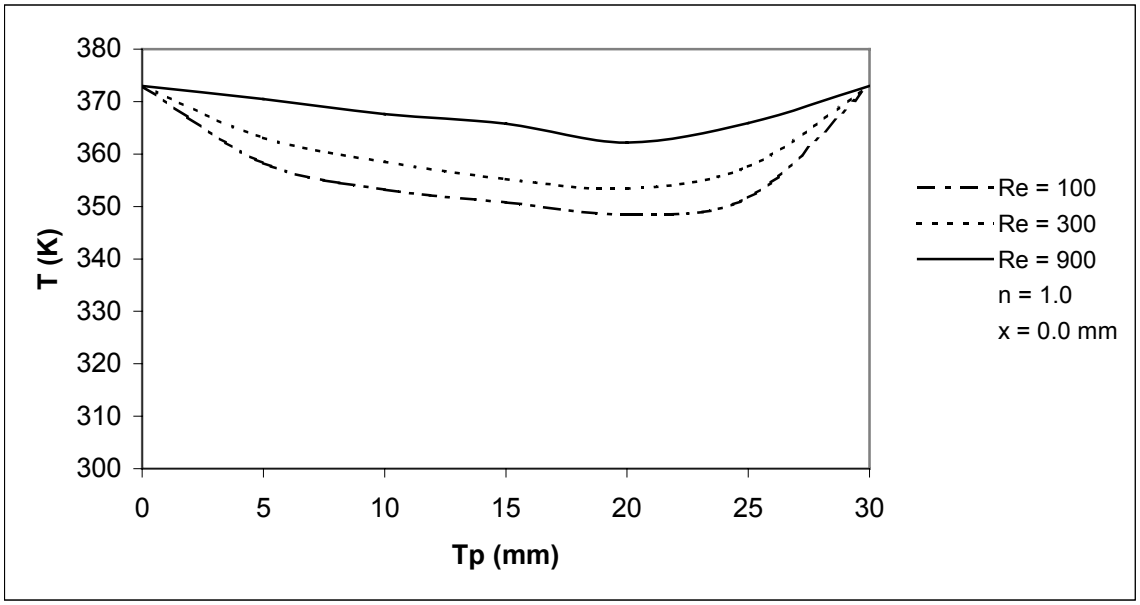

Figure 66. The Effect of Reynolds Number on Temperature Profile at Leading Edge (x = 0.0) of Long Plate (L1) for L1/L2 = 2.5, Tp = 30 mm, and $\theta = 25$

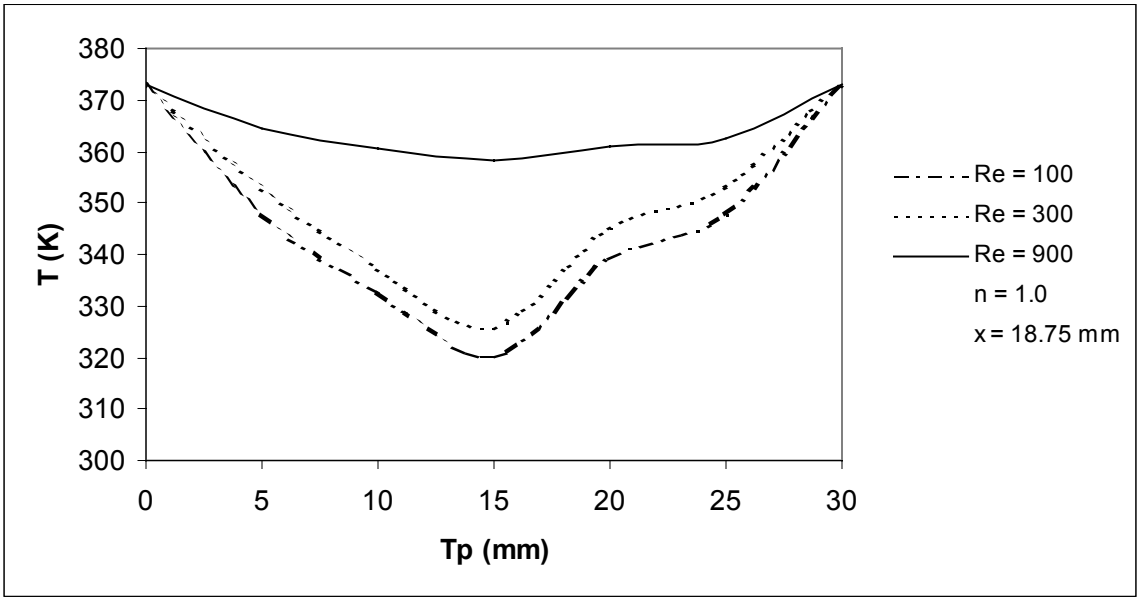

Figure 67. The Effect of Reynolds Number on Temperature Profile at Middle (x = 18.75) of Long Plate (L1) for L1/L2 = 2.5, Tp = 30 mm, and θ = 25

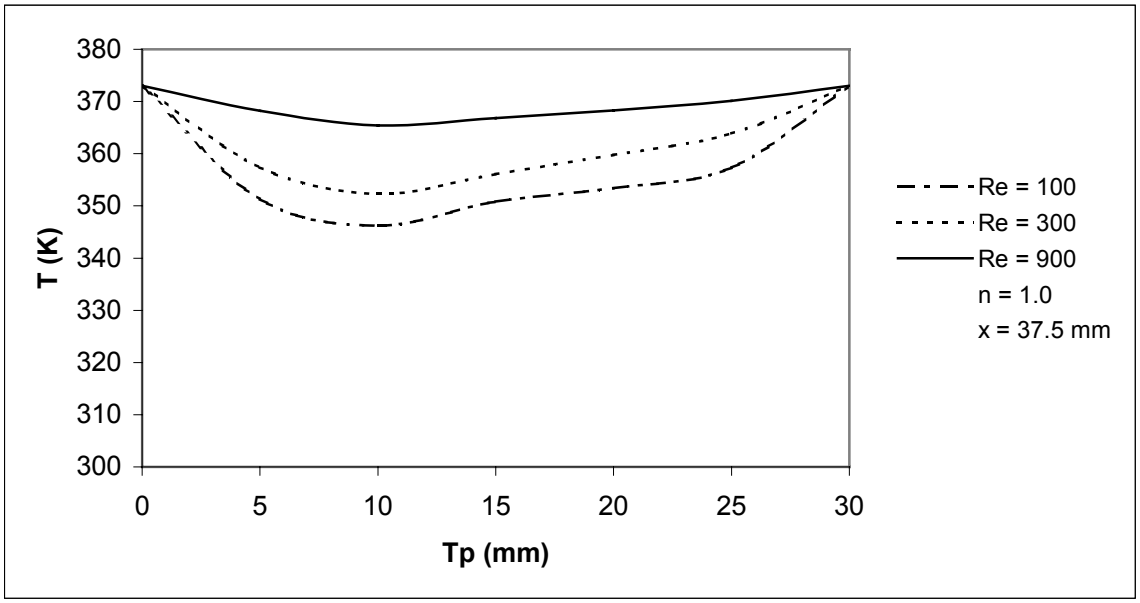

Figure 68. The Effect of Reynolds Number on Temperature Profile at Tailing Edge (x =37.5) of Long Plate (L1) for L1/L2 = 2.5, Tp = 30 mm, and $\theta = 25$

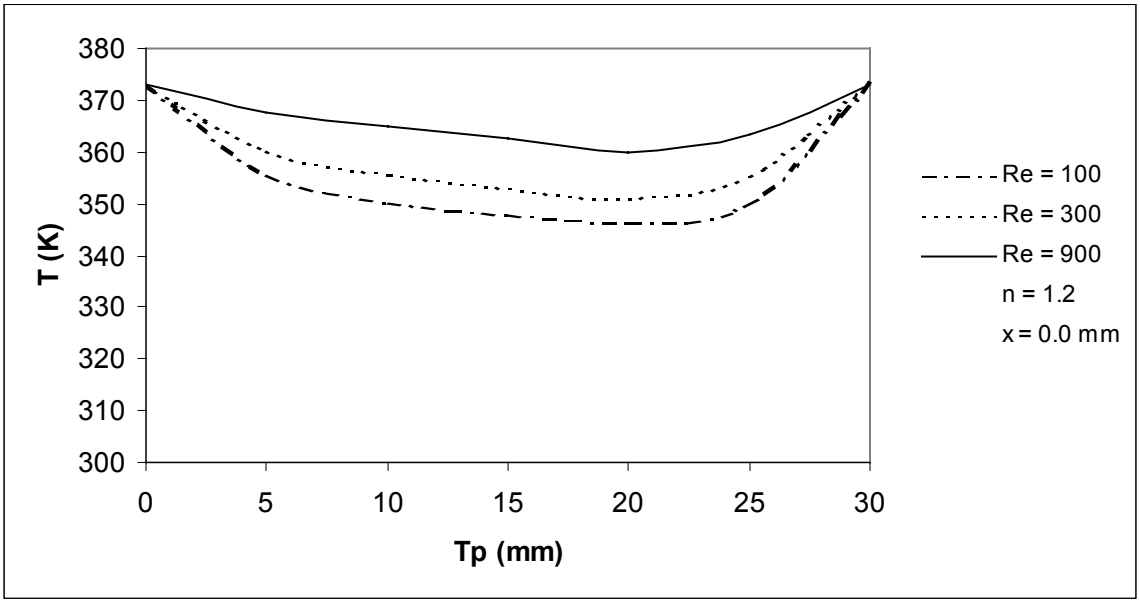

Figure 69. The Effect of Reynolds Number on Temperature Profile at Leading Edge (x = 0.0) of Long Plate (L1) for L1/L2 = 2.5, Tp = 30 mm, and $\theta = 25$

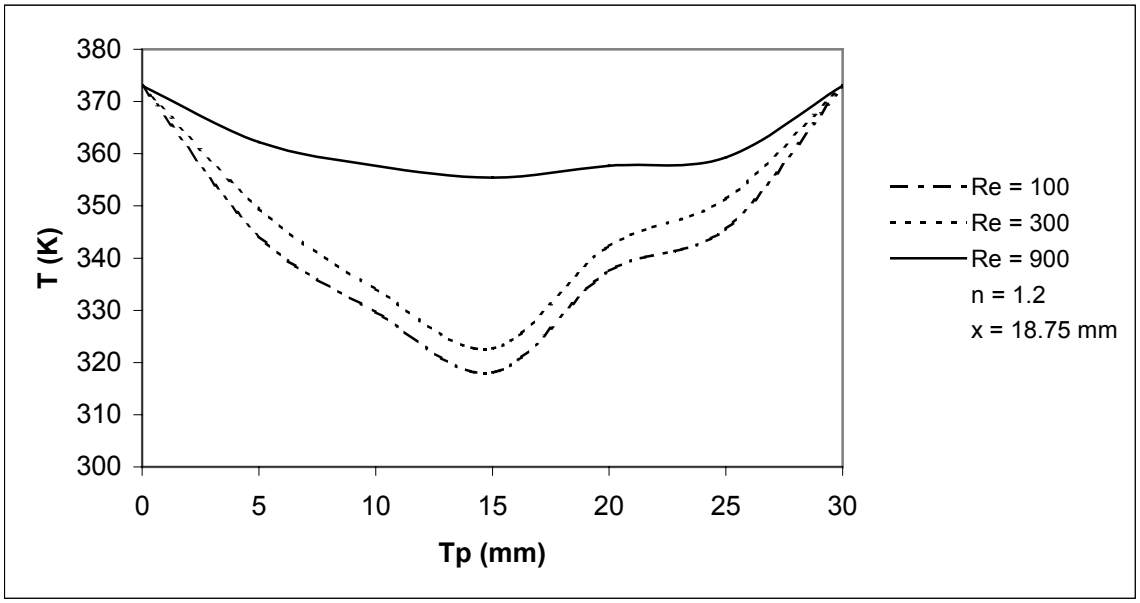

Figure 70. The Effect of Reynolds Number on Temperature Profile at Middle (x = 18.75) of Long Plate (L1) for L1/L2 = 2.5, Tp = 30 mm, and $\theta = 25$

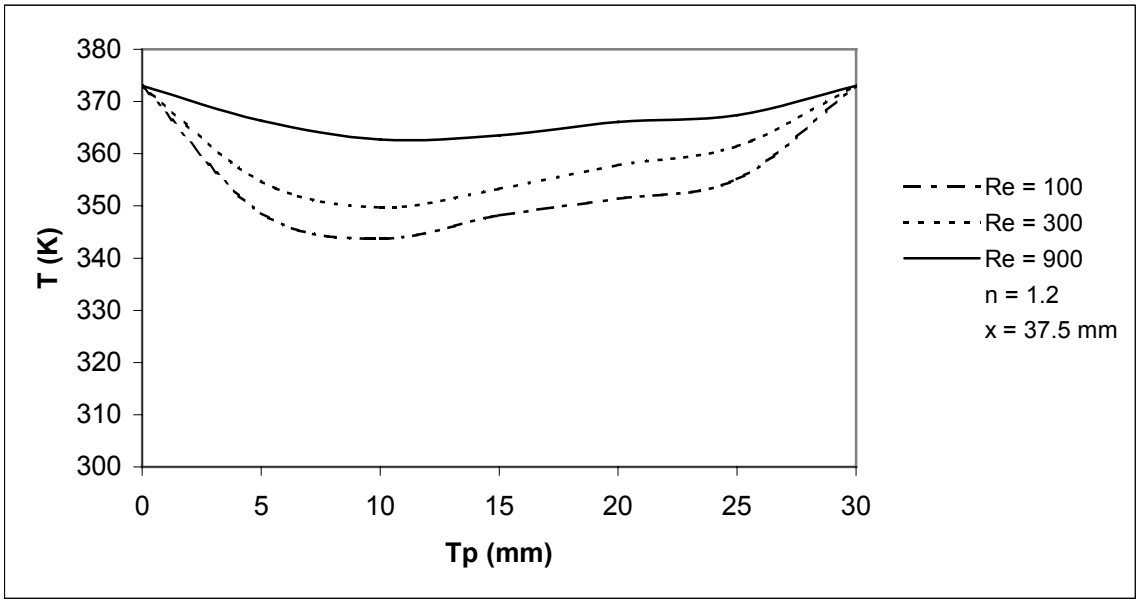

Figure 71. The Effect of Reynolds Number on Temperature Profile at Tailing Edge (x =37.5) of Long Plate (L1) for L1/L2 = 2.5, Tp = 30 mm, and $\theta = 25$

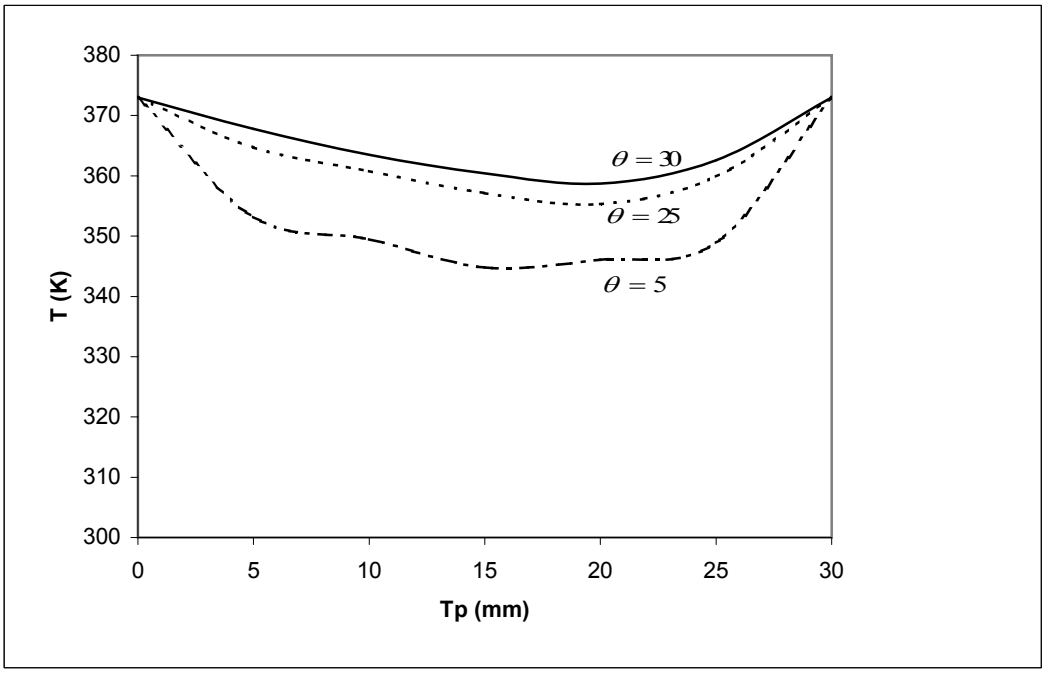

Figure 72. The Effect of Plate Angle on Temperature Profile at Leading Edge (x = 0.0) of Long Plate (L1) for L1/L2 = 2.5, Re = 300, and n = 0.5

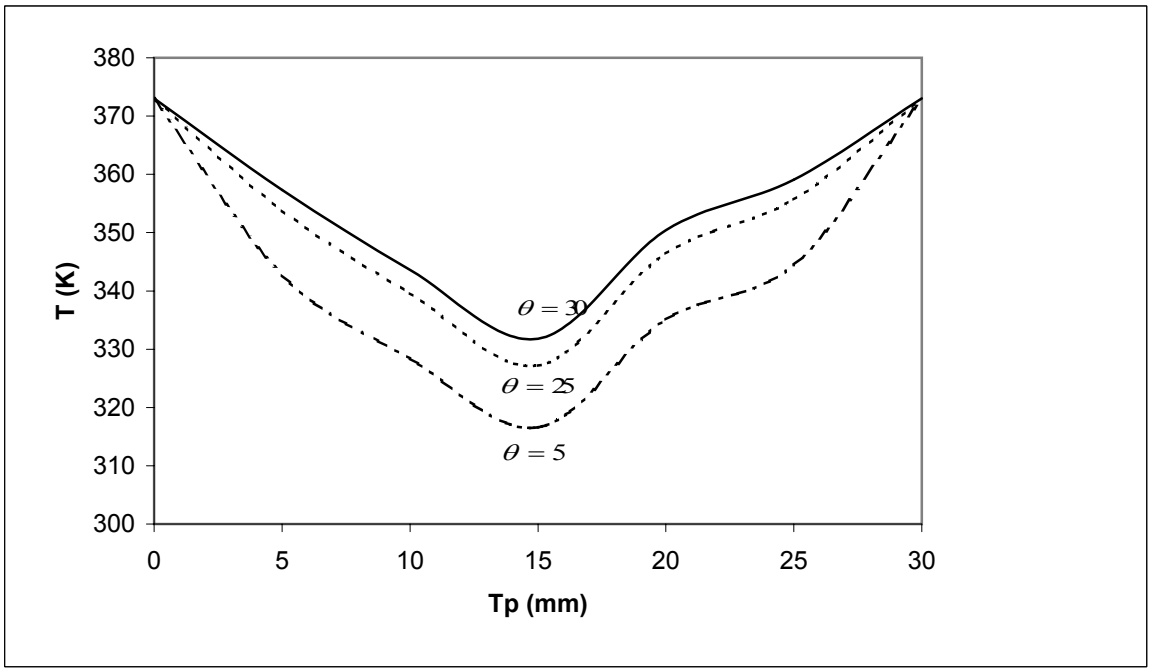

Figure 73. The Effect of Plate Angle on Temperature Profile at Middle (x = 18.75) of Long Plate (L1) for L1/L2 = 2.5, Re = 300, and n = 0.5

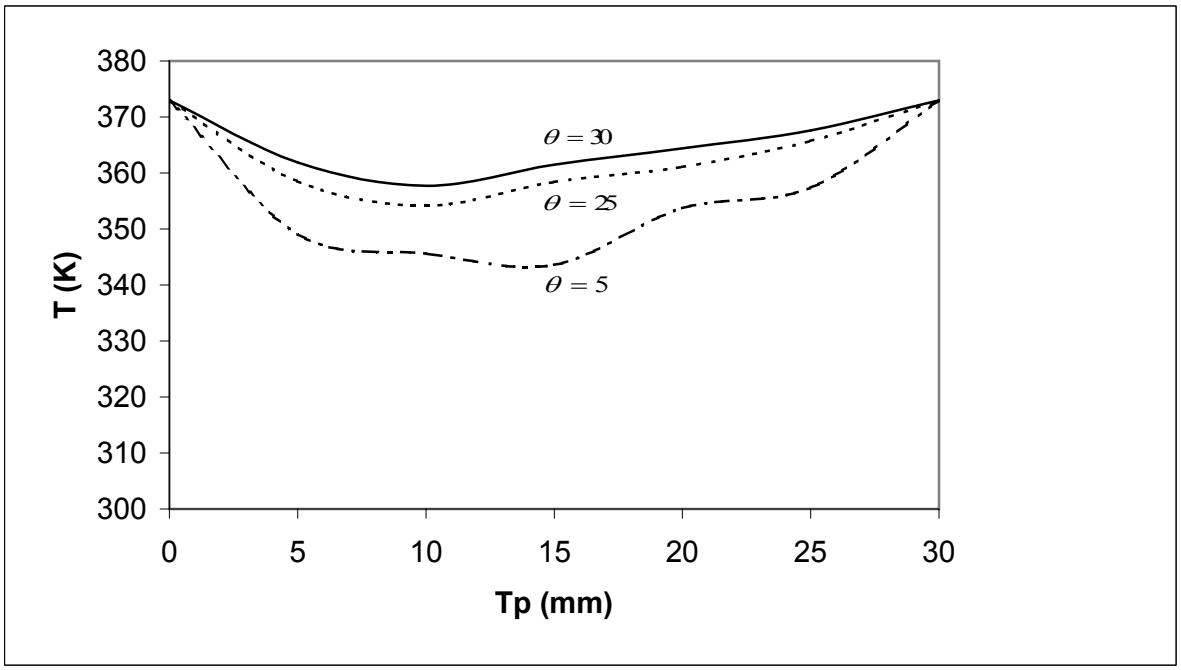

Figure 74. The Effect of Plate Angle on Temperature Profile at Tailing Edge (x = 37.5) of Long Plate (L1) for L1/L2 = 2.5, Re = 300, and n = 0.5

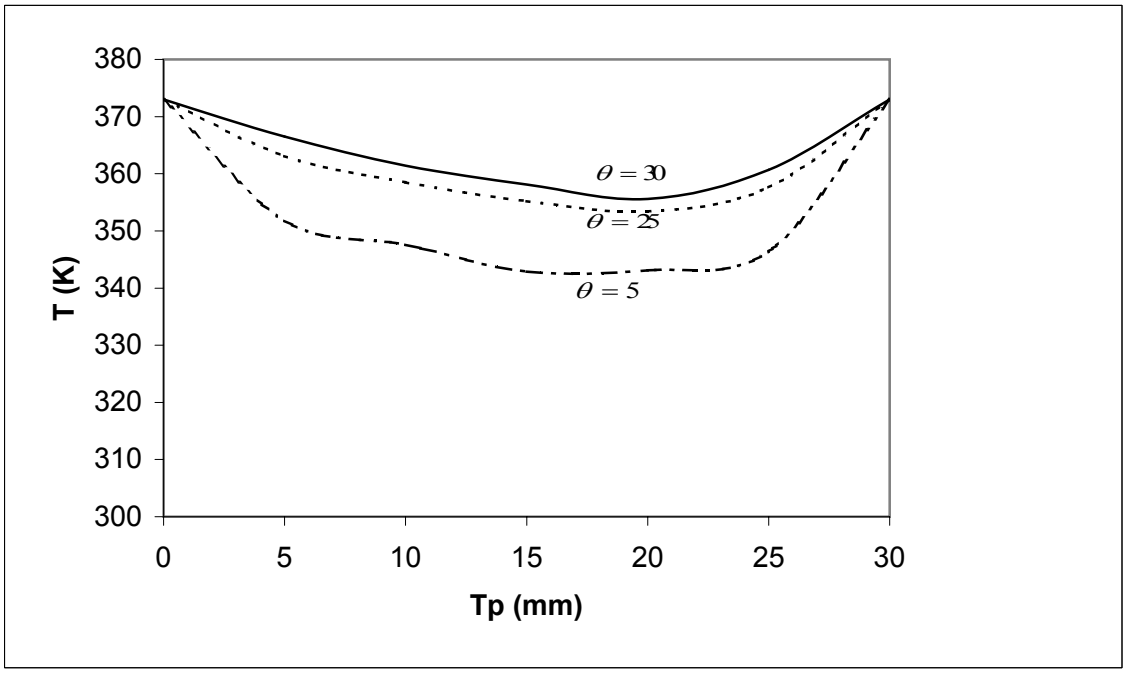

Figure 75. The Effect of Plate Angle on Temperature Profile at Leading Edge (x = 0.0) of Long Plate (L1) for L1/L2 = 2.5, Re = 300, and n = 1.0

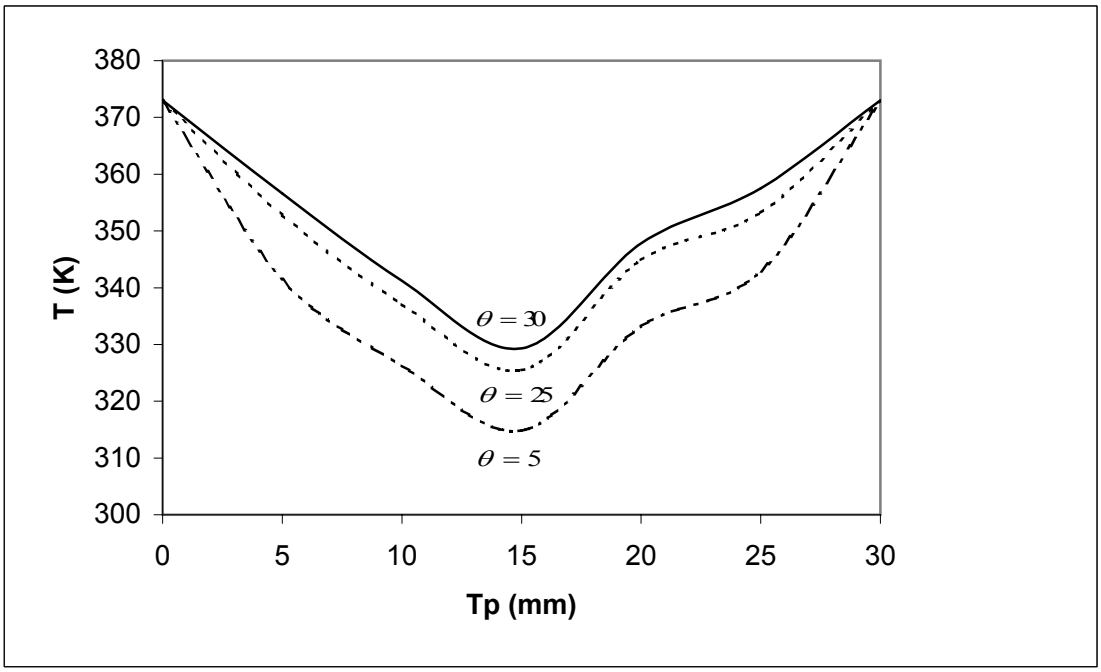

Figure 76. The Effect of Plate Angle on Temperature Profile at Middle (x = 18.75) of Long Plate (L1) for L1/L2 = 2.5, Re = 300, and n = 1.0

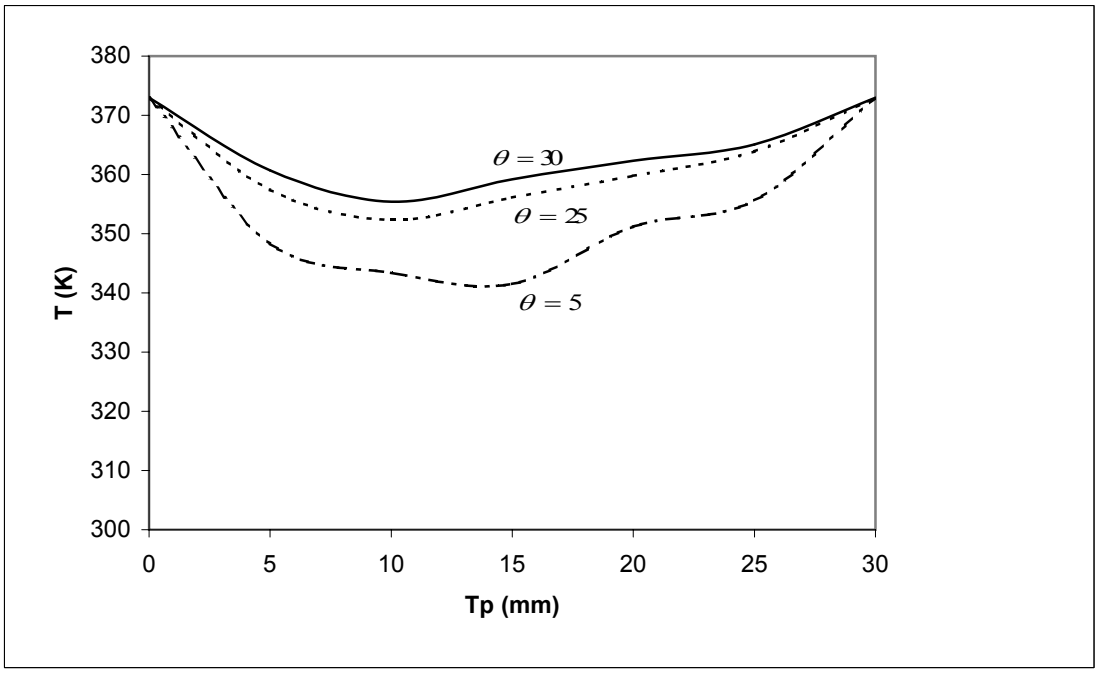

Figure 77. The Effect of Plate Angle on Temperature Profile at Tailing Edge (x = 37.5) of Long Plate (L1) for L1/L2 = 2.5, Re =300, and n = 1.0

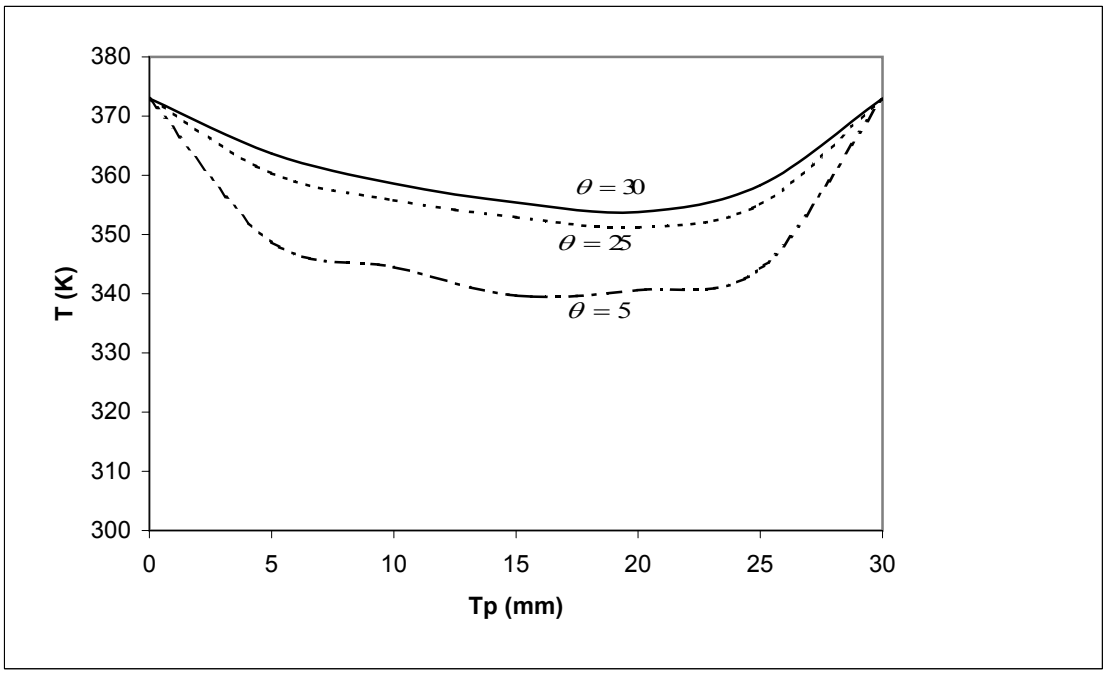

Figure 78. The Effect of Plate Angle on Temperature Profile at Leading Edge (x = 0.0) of Long Plate (L1) for L1/L2 = 2.5, Re = 300, and n = 1.2

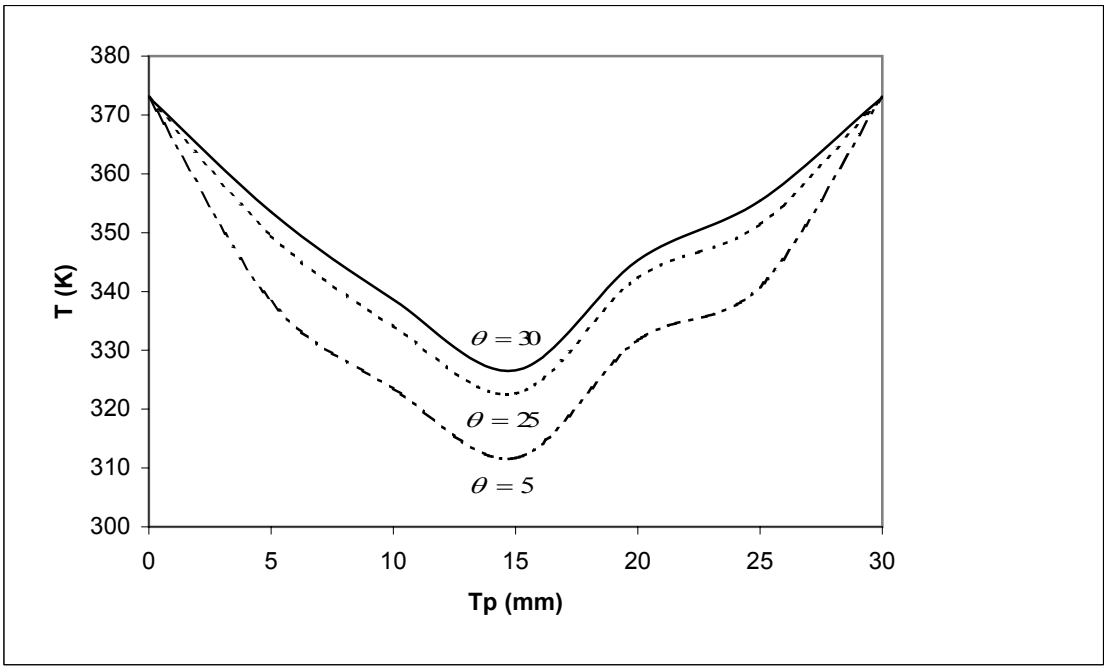

Figure 79. The Effect of Plate Angle on Temperature Profile at Middle (x = 18.75) of Long Plate (L1) for L1/L2 = 2.5, Re = 300, and n = 1.2

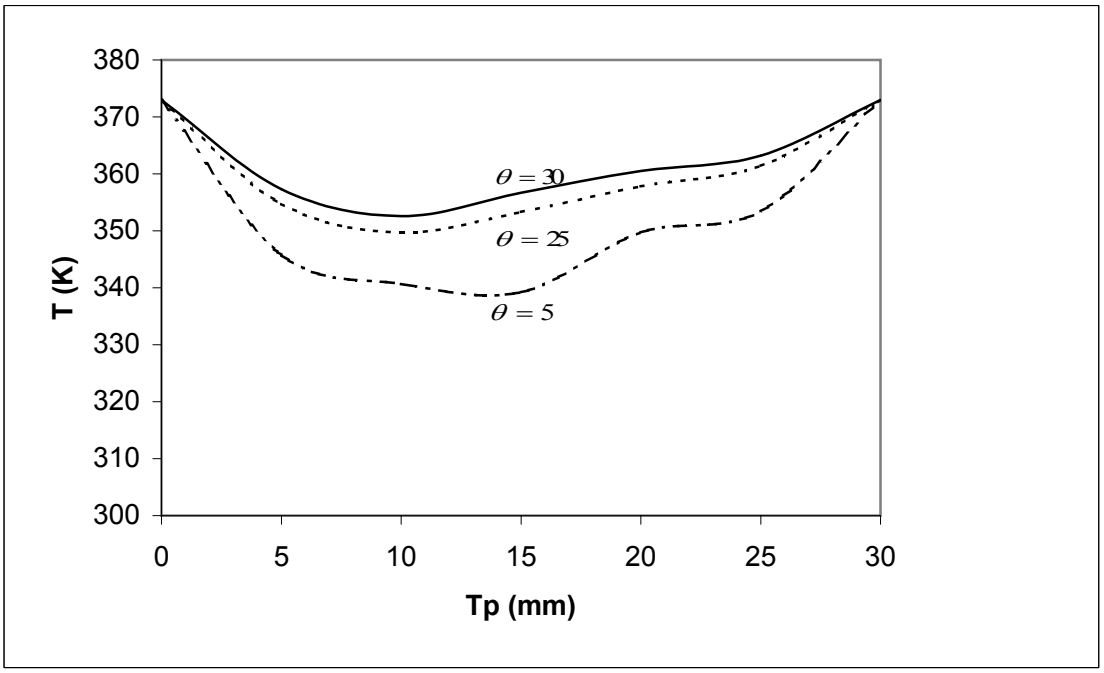

Figure 80. The Effect of Plate Angle on Temperature Profile at Tailing Edge (x = 37.5) of Long Plate (L1) for L1/L2 = 2.5, Re = 300, and n = 1.2

6. Conclusion

A parametric investigation on the fluid flow and heat transfer characteristics of the periodically fully developed flows in arrays with non-uniform plate length and oblique angle to the flow direction has been performed numerically by transforming the physical coordinate system to body-fitted coordinate system.

The following conclusion can be obtained from this study:

1. For Newtonian and non-Newtonian fluids that flow into this geometry, there is one circulating zone on the leeward side and windward side of long plate and there is another one circulating zone on the windward side of the short plate.
2. With the increase of the Reynolds number, the friction factor decreases until a certain value, after that the friction factor remains a constant value with increasing Reynolds number. However, Nusselt number increases with increasing Reynolds number throughout the range studied.
3. With the increase of flow index, the friction factor increases but the Nusselt numbers are no significant change at the same Reynolds number for each plate length ratio and transverse pitch ratio.
4. With the increase of plate length ratio (L_1 / L_2) that leads to the increase of long plate length (L_1), the friction factor, Nusselt number, and fluid temperature increase at the same Reynolds number for each flow index.

5. With the increase of transverse pitch ratio (T_p / L_p) that leads to the increase of transverse pitch spacing (T_p), the friction factor, Nusselt number, and fluid temperature decrease at the same Reynolds number and plate length ratio (L_1 / L_2) for each flow index.
6. The increment of the plate angle (θ) at a given Reynolds number leads to the increase of obstruction to flow, and hence the increases of friction factor, Nusselt number, and fluid temperature.
7. The pseudoplastic fluids promoted better heat transfer than Newtonian and dilatant fluids respectively.

From those results, heat exchanger may be re-designed by using oblique fin instead to improve thermal performance of heat exchanger. Auto radiator may use Pseudoplastic fluid instead of air or water to reduce the friction factor and improve thermal performance.

APPENDIX A

Table 1. The Effect of Flow Index on Friction Factor

$$L_1 / L_2 = 2.5, T_p / L_p = 0.571, \theta = 25$$

Re	n = 1.2	n = 1	n = 0.5
125	2.81	2.2	1.84
150	2.71	2.1	1.74
200	2.57	1.96	1.62
300	2.38	1.77	1.43
400	2.27	1.65	1.32
500	2.3	1.68	1.35
600	2.33	1.71	1.38
700	2.36	1.74	1.41
800	2.46	1.77	1.44
900	2.49	1.79	1.46

Re Generalized Reynolds number

Table 2. The Effect of Flow Index on Nu

$$L_1 / L_2 = 2.5, T_p / L_p = 0.571, \theta = 25$$

Re	n = 1.2	n = 1	n = 0.5
125	4.34	4.48	4.6
150	4.91	5.05	5.17
200	5.96	6.12	6.25
300	7.88	8.01	8.13
400	9.54	9.69	9.8
500	14.53	14.72	14.85
600	16.6	16.76	16.92
700	18.51	18.71	18.85
800	20.5	20.57	20.64
900	22.31	22.37	22.68

Re Generalized Reynolds number

Table 3. The Effect of Flow Index on Friction Factor

$$L_1 / L_2 = 2.0, T_p / L_p = 0.667, \theta = 25$$

Re	n=1.2	n=1	n=0.5
125	1.74	1.36	0.93
150	1.67	1.29	0.86
200	1.63	1.25	0.82
300	1.46	1.08	0.65
400	1.38	1	0.57
500	1.34	0.96	0.57
600	1.34	0.98	0.57
700	1.37	1	0.6
800	1.38	1.01	0.62
900	1.39	1.02	0.63

Re Generalized Reynolds number

Table 4. The Effect of Flow Index on Nu

$$L_1 / L_2 = 2.0, T_p / L_p = 0.667, \theta = 25$$

Re	n=1.2	n= 1	n=0.5
125	3.94	3.97	4.04
150	4.44	4.48	4.55
200	5.19	5.23	5.3
300	6.95	7.04	7.24
400	8.49	8.58	9.19
500	13.42	13.5	13.58
600	15.11	15.43	15.55
700	16.76	17.22	17.35
800	18.87	18.93	19.37
900	20.53	20.6	21.34

Re Generalized Reynolds number

Table 5. The Effect of Flow Index on Friction Factor

$$L_1 / L_2 = 1.5, T_p / L_p = 0.800, \theta = 25$$

Re	n = 1.2	n = 1	n = 0.5
125	1.34	0.77	0.4
150	1.29	0.73	0.36
200	1.24	0.68	0.31
300	1.17	0.61	0.24
400	1.13	0.57	0.2
500	1.06	0.5	0.15
600	1.07	0.51	0.14
700	1.08	0.52	0.15
800	1.08	0.52	0.15
900	1.09	0.53	0.16

Re Generalized Reynolds number

Table 6. The Effect of Flow Index on Nu

$$L_1 / L_2 = 1.5, T_p / L_p = 0.800, \theta = 25$$

Re	n = 1.2	n = 1	n = 0.5
125	3.3	3.46	3.62
150	3.74	3.9	4.06
200	4.56	4.72	4.88
300	6.02	6.18	6.33
400	7.32	7.48	7.63
500	12.17	12.35	12.5
600	13.88	14.06	14.21
700	15.51	15.69	15.85
800	17.07	17.25	17.41
900	18.56	18.77	18.97

Re Generalized Reynolds number

Table 7. The Effect of Plate Length Ratio on Friction Factor for n = 0.5

Re	case 1*	case 2*	case 3*
125	1.84	0.93	0.4
150	1.74	0.86	0.36
200	1.62	0.82	0.31
300	1.43	0.65	0.24
400	1.32	0.57	0.2
500	1.35	0.57	0.15
600	1.38	0.57	0.14
700	1.41	0.6	0.15
800	1.44	0.62	0.15
900	1.46	0.63	0.16

* case 1 $L_1 / L_2 = 2.5, T_p = 30mm, \theta = 25$

case 2 $L_1 / L_2 = 2.0, T_p = 30mm, \theta = 25$

case 3 $L_1 / L_2 = 1.5, T_p = 30mm, \theta = 25$

Re Generalized Reynolds number

Table 8. The Effect of Plate Length Ratio on Nu for n = 0.5

Re	case 1 *	case 2 *	case 3 *
125	4.6	4.04	3.62
150	5.17	4.55	4.06
200	6.25	5.3	4.88
300	8.13	7.24	6.33
400	9.8	9.19	7.63
500	14.85	13.58	12.5
600	16.92	15.55	14.21
700	18.85	17.35	15.85
800	20.64	19.37	17.41
900	22.68	21.34	18.97

* case 1 $L_1 / L_2 = 2.5, T_p = 30mm, \theta = 25$

case 2 $L_1 / L_2 = 2.0, T_p = 30mm, \theta = 25$

case 3 $L_1 / L_2 = 1.5, T_p = 30mm, \theta = 25$

Re Generalized Reynolds number

Table 9. The Effect of Plate Length Ratio on Friction Factor for n = 1.0

Re	case 1*	case 2*	case 3*
125	2.2	1.36	0.77
150	2.1	1.29	0.73
200	1.96	1.25	0.68
300	1.77	1.08	0.61
400	1.65	1	0.57
500	1.68	0.96	0.5
600	1.71	0.98	0.51
700	1.74	1	0.52
800	1.77	1.01	0.52
900	1.79	1.02	0.53

* case 1 $L_1 / L_2 = 2.5, T_p = 30mm, \theta = 25$

case 2 $L_1 / L_2 = 2.0, T_p = 30mm, \theta = 25$

case 3 $L_1 / L_2 = 1.5, T_p = 30mm, \theta = 25$

Re Generalized Reynolds number

Table 10. The Effect of Plate Length Ratio on Nu for n = 1.0

Re	case 1 *	case 2 *	case 3 *
125	4.48	3.97	3.46
150	5.05	4.48	3.9
200	6.12	5.23	4.72
300	8.01	7.04	6.18
400	9.69	8.58	7.48
500	14.72	13.5	12.35
600	16.76	15.43	14.06
700	18.71	17.22	15.69
800	20.57	18.93	17.25
900	22.37	20.6	18.77

* case 1 $L_1 / L_2 = 2.5, T_p = 30mm, \theta = 25$

case 2 $L_1 / L_2 = 2.0, T_p = 30mm, \theta = 25$

case 3 $L_1 / L_2 = 1.5, T_p = 30mm, \theta = 25$

Re Generalized Reynolds number

Table 11. The Effect of Plate Length Ratio on Friction Factor for n = 1.2

Re	case 1*	case 2*	case 3*
125	2.81	1.74	1.34
150	2.71	1.67	1.29
200	2.57	1.63	1.24
300	2.38	1.46	1.17
400	2.27	1.38	1.13
500	2.3	1.34	1.06
600	2.33	1.34	1.07
700	2.36	1.37	1.08
800	2.46	1.38	1.08
900	2.49	1.39	1.09

* case 1 $L_1 / L_2 = 2.5, T_p = 30mm, \theta = 25$

case 2 $L_1 / L_2 = 2.0, T_p = 30mm, \theta = 25$

case 3 $L_1 / L_2 = 1.5, T_p = 30mm, \theta = 25$

Re Generalized Reynolds number

Table 12. The Effect Plate Length Ratio on Nu for n = 1.2

Re	case 1 *	case 2 *	case 3 *
125	4.34	3.94	3.3
150	4.91	4.44	3.74
200	5.96	5.19	4.56
300	7.88	6.95	6.02
400	9.54	8.49	7.32
500	14.53	13.42	12.17
600	16.6	15.11	13.88
700	18.51	16.76	15.51
800	20.5	18.87	17.07
900	22.31	20.53	18.56

* case 1 $L_1 / L_2 = 2.5, T_p = 30mm, \theta = 25$

case 2 $L_1 / L_2 = 2.0, T_p = 30mm, \theta = 25$

case 3 $L_1 / L_2 = 1.5, T_p = 30mm, \theta = 25$

Re Generalized Reynolds number

Table 13. The Effect of Transverse Pitch Ratio on Friction Factor for n = 0.5

Re	case 1 *	case 2 *	case 3 *
125	0.93	1.85	3.61
150	0.86	1.75	3.43
200	0.82	1.59	3.16
300	0.65	1.41	2.81
400	0.57	1.28	2.59
500	0.57	1.38	3.2
600	0.57	1.42	3.27
700	0.6	1.44	3.33
800	0.62	1.47	3.38
900	0.63	1.49	3.43

* case 1 $L_1 / L_2 = 2.0, T_p / L_p = 0.667, \theta = 25$

case 2 $L_1 / L_2 = 2.0, T_p / L_p = 0.556, \theta = 25$

case 3 $L_1 / L_2 = 2.0, T_p / L_p = 0.444, \theta = 25$

Re Generalized Reynolds number

Table 14. The Effect of Transverse Pitch Ratio on Nu for n = 0.5

Re	case 1 *	case 2 *	case 3 *
125	4.04	5	6.26
150	4.55	5.61	7.03
200	5.3	6.75	8.46
300	7.24	8.76	11
400	9.19	10.56	13.33
500	13.58	15.81	18.64
600	15.55	17.97	21.19
700	17.35	20.03	23.32
800	19.37	21.99	25.95
900	21.34	23.88	28.19

* case 1 $L_1 / L_2 = 2.0, T_p / L_p = 0.667, \theta = 25$

case 2 $L_1 / L_2 = 2.0, T_p / L_p = 0.556, \theta = 25$

case 3 $L_1 / L_2 = 2.0, T_p / L_p = 0.444, \theta = 25$

Re Generalized Reynolds number

Table 15. The Effect of Transverse Pitch Ratio on Friction Factor for n = 1.0

Re	case 1 *	case 2 *	case 3 *
125	1.36	2.21	4.05
150	1.29	2.11	3.87
200	1.25	1.96	3.6
300	1.08	1.78	3.25
400	1	1.65	3.03
500	0.96	1.75	3.67
600	0.98	1.79	3.74
700	1	1.81	3.8
800	1.01	1.84	3.85
900	1.02	1.86	3.9

* case 1 $L_1 / L_2 = 2.0, T_p / L_p = 0.667, \theta = 25$

case 2 $L_1 / L_2 = 2.0, T_p / L_p = 0.556, \theta = 25$

case 3 $L_1 / L_2 = 2.0, T_p / L_p = 0.444, \theta = 25$

Re Generalized Reynolds number

Table 16. The Effect of Transverse Pitch Ratio on Nu for n = 1.0

Re	case 1 *	case 2 *	case 3 *
125	3.97	4.79	6.04
150	4.48	5.4	6.81
200	5.23	6.54	8.24
300	7.04	8.55	10.78
400	8.58	10.35	13.05
500	13.5	15.52	18.36
600	15.43	17.68	20.91
700	17.22	19.73	23.34
800	18.93	21.7	25.67
900	20.6	23.59	27.91

* case 1 $L_1 / L_2 = 2.0, T_p / L_p = 0.667, \theta = 25$

case 2 $L_1 / L_2 = 2.0, T_p / L_p = 0.556, \theta = 25$

case 3 $L_1 / L_2 = 2.0, T_p / L_p = 0.444, \theta = 25$

Re Generalized Reynolds number

Table 17. The Effect of Transverse Pitch Ratio on Friction Factor for n = 1.2

Re	case 1 *	case 2 *	case 3 *
125	1.74	2.78	4.66
150	1.67	2.68	4.48
200	1.63	2.53	4.21
300	1.46	2.35	3.86
400	1.38	2.22	3.64
500	1.34	2.32	4.28
600	1.34	2.36	4.35
700	1.37	2.37	4.41
800	1.38	2.4	4.46
900	1.39	2.42	4.51

* case 1 $L_1 / L_2 = 2.0, T_p / L_p = 0.667, \theta = 25$

case 2 $L_1 / L_2 = 2.0, T_p / L_p = 0.556, \theta = 25$

case 3 $L_1 / L_2 = 2.0, T_p / L_p = 0.444, \theta = 25$

Re Generalized Reynolds number

Table 18. The Effect of Transverse Pitch Ratio on Nu for n = 1.2

Re	case 1 *	case 2 *	case 3 *
125	3.94	4.63	5.89
150	4.44	5.24	6.66
200	5.19	6.38	8.09
300	6.95	8.39	10.63
400	8.49	10.2	12.8
500	13.42	15.36	18.11
600	15.11	17.5	20.66
700	16.76	19.6	23.09
800	18.87	21.54	25.42
900	20.53	23.43	27.66

* case 1 $L_1 / L_2 = 2.0, T_p / L_p = 0.667, \theta = 25$

case 2 $L_1 / L_2 = 2.0, T_p / L_p = 0.556, \theta = 25$

case 3 $L_1 / L_2 = 2.0, T_p / L_p = 0.444, \theta = 25$

Re Generalized Reynolds number

Table 19. The Effect of Plate Angle on Friction Factor at Re = 300

$$L_1 / L_2 = 2.5, T_p / L_p = 0.571$$

θ	n = 1.2	n = 1	n = 0.5
5	1.68	1.07	0.73
10	1.83	1.22	0.88
15	2.03	1.42	1.08
20	2.28	1.67	1.33
25	2.38	1.77	1.43
30	2.46	1.85	1.51

θ Plate angle

Table 20. The Effect of Plate Angle on Nu at Re = 300

$L_1 / L_2 = 2.5, T_p / L_p = 0.571$

θ	n = 1.2	n = 1	n = 0.5
5	7	7.48	7.62
10	7.15	7.55	7.71
15	7.43	7.78	7.91
20	7.65	7.86	7.96
25	7.88	8.01	8.13
30	8.03	8.2	8.58

θ Plate angle

Table 21. The Effect of Plate Angle on Friction Factor at Re = 300

$$L_1 / L_2 = 2.0, T_p / L_p = 0.667$$

θ	n = 1.2	n = 1	n = 0.5
5	0.71	0.33	0.13
10	0.91	0.53	0.22
15	1.11	0.73	0.35
20	1.36	0.98	0.58
25	1.46	1.08	0.65
30	1.54	1.16	0.73

θ Plate angle

Table 22. The Effect of Plate Angle on Nu at Re = 300

$L_1 / L_2 = 2.0, T_p / L_p = 0.667$

θ	n = 1.2	n = 1	n = 0.5
5	6.06	6.53	6.75
10	6.19	6.6	6.84
15	6.5	6.82	7.04
20	6.72	6.89	7.08
25	6.95	7.04	7.24
30	7.1	7.23	7.45

θ Plate angle

Table 23. The Effect of Plate Angle on Friction Factor at Re = 300

$L_1 / L_2 = 1.5, T_p / L_p = 0.800$

θ	n = 1.2	n = 1	n = 0.5
5	0.52	0.14	0.02
10	0.70	0.20	0.08
15	0.90	0.35	0.13
20	1.15	0.51	0.20
25	1.17	0.61	0.24
30	1.25	0.71	0.32

θ Plate angle

Table 24. The Effect of Plate Angle on Nu at Re = 300

$L_1 / L_2 = 1.5, T_p / L_p = 0.800$

θ	n = 1.2	n = 1	n = 0.5
5	5.49	5.67	5.81
10	5.56	5.72	5.87
15	5.79	5.94	6.1
20	5.87	6.03	6.18
25	6.02	6.18	6.33
30	6.21	6.37	6.52

θ Plate angle

Table 25. The Effect of Plate Length Ratio on Temperature Profile at Leading Edge of Long Plate (L1) for n = 0.5 at Re = 300 and θ = 25

Tp (mm)	L1/L2 = 2.5, x = 0.0 mm	L1/L2 = 2.0, x = 0.0 mm	L1/L2 = 1.5, x = 0.0 mm
0	373	373	373
5	364.7	361.2	353.6
10	360.8	357.6	348.9
15	357.1	354.2	345.8
20	355.3	351.7	342.1
25	359.9	355.5	346.7
30	373	373	373

Table 26. The Effect of Plate Length Ratio on Temperature Profile at Middle of Long Plate (L1) for n = 0.5 at Re = 300 and θ = 25

Tp (mm)	L1/L2 = 2.5, x = 18.75 mm	L1/L2 = 2.0, x = 15.00 mm	L1/L2 = 1.5, x = 11.25 mm
0	373	373	373
5	353.8	350.7	344.3
10	339.6	333.5	330.6
15	327.2	323.7	319.4
20	346.4	342.3	337.8
25	355.7	353.4	346.5
30	373	373	373

Table 27. The Effect of Plate Length Ratio on Temperature Profile at Tailing Edge of Long Plate (L1) for n = 0.5 at Re = 300 and θ = 25

Tp (mm)	L1/L2 = 2.5, x = 37.5 mm	L1/L2 = 2.0, x = 30.0 mm	L1/L2 = 1.5, x = 22.5 mm
0	373	373	373
5	358.5	354.4	348.8
10	354.2	350.8	344.5
15	358.4	354.2	348.1
20	361.1	357.5	350.9
25	365.7	361.9	355.3
30	373	373	373

Table 28. The Effect of Plate Length Ratio on Temperature Profile at Leading Edge of Long Plate (L1) for n = 1.0 at Re = 300 and θ = 25

Tp (mm)	L1/L2 = 2.5, x = 0.0 mm	L1/L2 = 2.0, x = 0.0 mm	L1/L2 = 1.5, x = 0.0 mm
0	373	373	373
5	363.1	359.7	352.5
10	358.5	355.3	348.1
15	355.2	352.5	344.7
20	353.4	350.1	340.8
25	357.6	353.6	344.6
30	373	373	373

Table 29. The Effect of Plate Length Ratio on Temperature Profile at Middle of Long Plate (L1) for n = 1.0 at Re = 300 and θ = 25

Tp (mm)	L1/L2 = 2.5, x = 18.75 mm	L1/L2 = 2.0, x = 15.00 mm	L1/L2 = 1.5, x = 11.25 mm
0	373	373	373
5	352.8	349.6	343.2
10	337.1	331.1	328.8
15	325.5	321.5	317.9
20	344.9	340.8	335.6
25	353.2	351.2	344.1
30	373	373	373

Table 30. The Effect of Plate Length Ratio on Temperature Profile at Tailing Edge of Long Plate (L1) for n = 1.0 at Re = 300 and θ = 25

Tp (mm)	L1/L2 = 2.5, x = 37.5 mm	L1/L2 = 2.0, x = 30.0 mm	L1/L2 = 1.5, x = 22.5 mm
0	373	373	373
5	357.4	353.3	347.4
10	352.3	348.2	341.9
15	356.1	352.4	346.1
20	359.8	355.7	349.3
25	363.9	359.1	354
30	373	373	373

Table 31. The Effect of Plate Length Ratio on Temperature Profile at Leading Edge of Long Plate (L1) for n = 1.2 at Re = 300 and θ = 25

Tp (mm)	L1/L2 = 2.5, x = 0.0 mm	L1/L2 = 2.0, x = 0.0 mm	L1/L2 = 1.5, x = 0.0 mm
0	373	373	373
5	360.3	356.4	349.2
10	355.8	351.6	345.6
15	352.9	348.2	342.5
20	351.2	347.2	339.4
25	355.1	350.8	343.9
30	373	373	373

Table 32. The Effect of Plate Length Ratio on Temperature Profile at Middle of Long Plate (L1) for n = 1.2 at Re = 300 and θ = 25

Tp (mm)	L1/L2 = 2.5, x = 18.75 mm	L1/L2 = 2.0, x = 15.00 mm	L1/L2 = 1.5, x = 11.25 mm
0	373	373	373
5	349.5	346.3	340.4
10	334.1	328.6	325.2
15	322.7	318.6	315.4
20	342.3	338.7	333
25	351.4	349.4	342.1
30	373	373	373

Table 33. The Effect of Plate Length Ratio on Temperature Profile at Tailing Edge of Long Plate (L1) for n = 1.2 at Re = 300 and θ = 25

Tp (mm)	L1/L2 = 2.5, x = 37.5 mm	L1/L2 = 2.0, x = 30.0 mm	L1/L2 = 1.5, x = 22.5 mm
0	373	373	373
5	354.7	349.9	343.6
10	349.7	344.5	338.3
15	353.3	348.2	342.5
20	357.8	349.7	346.1
25	361.4	354.8	350.4
30	373	373	373

Table 34. The Effect of Flow Index on Temperature Profile at Leading Edge of Long Plate (L1) for L1/L2 = 2.5, Re = 300, Tp = 30 mm, and θ = 25

Tp (mm)	n=0.5	n=1.0	n=1.2
0	373	373	373
5	364.7	363.1	360.3
10	360.8	358.5	355.8
15	357.1	355.2	352.9
20	355.3	353.4	351.2
25	359.9	357.6	355.1
30	373	373	373

Table 35. The Effect of Flow Index on Temperature Profile at Middle of Long Plate (L1) for L1/L2 = 2.5, Re = 300, Tp = 30 mm, and θ = 25

Tp (mm)	n=0.5	n=1.0	n=1.2
0	373	373	373
5	353.8	352.8	349.5
10	339.6	337.1	334.1
15	327.2	325.5	322.7
20	346.4	344.9	342.3
25	355.7	353.2	351.4
30	373	373	373

Table 36. The Effect of Flow Index on Temperature Profile at Tailing Edge of Long Plate (L1) for L1/L2 = 2.5, Re = 300, Tp = 30 mm, and θ = 25

Tp (mm)	n=0.5	n=1.0	n=1.2
0	373	373	373
5	358.5	357.4	354.7
10	354.2	352.3	349.7
15	358.4	356.1	353.3
20	361.1	359.8	357.8
25	365.7	363.9	361.4
30	373	373	373

Table 37. The Effect of Flow Index on Temperature Profile at Leading Edge of Long Plate (L1) for L1/L2 = 2.0, Re = 300, Tp = 30 mm, and θ = 25

Tp (mm)	n=0.5	n=1.0	n=1.2
0	373	373	373
5	361.2	359.7	356.4
10	357.6	355.3	351.6
15	354.2	352.5	348.2
20	351.7	350.1	347.2
25	355.5	353.6	350.8
30	373	373	373

Table 38. The Effect of Flow Index on Temperature Profile at Middle of Long Plate (L1) for L1/L2 = 2.0, Re = 300, Tp = 30 mm, and θ = 25

Tp (mm)	n=0.5	n=1.0	n=1.2
0	373	373	373
5	350.7	349.6	346.3
10	333.5	331.1	328.6
15	323.7	321.5	318.6
20	342.3	340.8	338.7
25	353.4	351.2	349.4
30	373	373	373

Table 39. The Effect of Flow Index on Temperature Profile at Tailing Edge of Long Plate (L1) for L1/L2 = 2.0, Re = 300, Tp = 30 mm, and θ = 25

Tp (mm)	n=0.5	n=1.0	n=1.2
0	373	373	373
5	354.4	353.3	349.9
10	350.8	348.2	344.5
15	354.2	352.4	348.2
20	357.5	355.7	349.7
25	361.9	359.1	354.8
30	373	373	373

Table 40. The Effect of Flow Index on Temperature Profile at Leading Edge of Long Plate (L1) for L1/L2 = 1.5, Re = 300, Tp = 30 mm, and θ = 25

Tp (mm)	n=0.5	n=1.0	n=1.2
0	373	373	373
5	353.6	352.5	349.2
10	348.9	348.1	345.6
15	345.8	344.7	342.5
20	342.1	340.8	339.4
25	346.7	344.6	343.9
30	373	373	373

Table 41. The Effect of Flow Index on Temperature Profile at Middle of Long Plate (L1) for L1/L2 = 1.5, Re = 300, Tp = 300mm, and θ = 25

Tp (mm)	n=0.5	n=1.0	n=1.2
0	373	373	373
5	344.3	343.2	340.4
10	330.6	328.8	325.2
15	319.4	317.9	315.4
20	337.8	335.6	333
25	346.5	344.1	342.1
30	373	373	373

Table 42. The Effect of Flow Index on Temperature Profile at Tailing Edge of Long Plate (L1) for L1/L2 = 1.5, Re = 300, Tp = 30 mm, and θ = 25

Tp (mm)	n=0.5	n=1.0	n=1.2
0	373	373	373
5	348.8	347.4	343.6
10	344.5	341.9	338.3
15	348.1	346.1	342.5
20	350.9	349.3	346.1
25	355.3	354	350.4
30	373	373	373

Table 43. The Effect of Flow Index on Temperature Profile at Leading Edge of Long Plate (L1) for L1/L2 = 2.5, Re = 300, Tp = 60 mm, and θ = 25

Tp (mm)	n=0.5	n=1.0	n=1.2
0	373	373	373
5	361.1	360.4	357.3
10	357.5	355.1	352.4
15	353.8	351.7	348.1
20	350.1	348.8	345.2
25	348.7	346.6	343.2
30	346.5	344.6	341.5
35	343.4	341.2	338.1
40	341.5	339.4	337.3
45	345.3	343.2	341.6
50	351.6	349.9	347.8
55	356.8	354.3	352.7
60	373	373	373

Table 44. The Effect of Flow Index on Temperature Profile at Middle of Long Plate (L1) for L1/L2 = 2.5, Re = 300, Tp = 60 mm, and θ = 25

Tp (mm)	n=0.5	n=1.0	n=1.2
0	373	373	373
5	350.8	349.1	347.5
10	336.7	334.6	330.4
15	325.4	322.9	319.5
20	320.6	319.1	317
25	315.4	313.3	310.8
30	312.4	311.5	309.4
35	326.3	324.5	322.3
40	333.5	331.8	329.3
45	339.1	337.1	335.2
50	344.8	342.3	340.1
55	353.3	351.5	349.6
60	373	373	373

Table 45. The Effect of Flow Index on Temperature Profile at Tailing Edge of Long Plate (L1) for L1/L2 = 2.5, Re = 300, Tp = 60 mm, and θ = 25

Tp (mm)	n=0.5	n=1.0	n=1.2
0	373	373	373
5	356.4	355.5	352.1
10	352.2	350.6	347.8
15	349.5	347.1	345.5
20	347.9	345.6	343.5
25	349.7	347.3	344.8
30	351.8	349.7	347.3
35	353.3	351.1	349.5
40	355.4	352.9	350.8
45	357.1	355.4	353.1
50	360.3	357.8	355.6
55	364.5	363.3	359.8
60	373	373	373

Table 46. The Effect of Flow Index on Temperature Profile at Leading Edge of Long Plate (L1) for L1/L2 = 2.5, Re = 300, Tp = 100 mm, and θ = 25

Tp (mm)	n = 0.5	n = 1.0	n = 1.2
0	373	373	373
10	353.2	352.4	350.1
20	346.5	344.6	341.2
30	342.6	340.8	337.6
40	339.3	337.8	334.7
50	337.4	333.8	330.3
60	335.7	332.4	329.8
70	341.6	339.6	337.9
80	345.7	343.1	341.5
90	349.1	347.2	345.3
100	373	373	373

Table 47. The Effect of Flow Index on Temperature Profile at Middle of Long Plate (L1) for L1/L2 = 2.5, Re = 300, Tp = 100 mm, and θ = 25

Tp (mm)	n = 0.5	n = 1.0	n = 1.2
0	373	373	373
10	332.6	331.3	329.8
20	316.5	315.1	313.4
30	310.8	308.5	306.2
40	308.5	307.1	305.3
50	305	304.9	302.1
60	315.9	314.3	312.4
70	320.2	318.6	315.8
80	326.4	324.7	322.7
90	336.8	334.3	331.6
100	373	373	373

Table 48. The Effect of Flow Index on Temperature Profile at Tailing Edge of Long Plate (L1) for L1/L2 = 2.5, Re = 300, Tp = 100 mm, and θ = 25

Tp (mm)	n = 0.5	n = 1.0	n = 1.2
0	373	373	373
10	348.1	347.2	343.5
20	342.8	340.5	338.1
30	340.1	338.7	335.7
40	337.4	335.3	331.6
50	340.9	338.1	335.9
60	345.6	343.4	341.5
70	350.2	347.9	345.5
80	353.3	350.7	348.2
90	357.1	355.2	352.8
100	373	373	373

Table 49. The Effect Reynolds Number on Temperature Profile at Leading Edge of Long Plate (L1) for L1/L2 = 2.5, n = 0.5, and θ = 25

Tp	Re = 100	Re = 300	Re = 900
0	373	373	373
5	359.6	364.7	371.6
10	355.4	360.8	369.2
15	352.8	357.1	367.7
20	350.7	355.3	364.1
25	353.9	359.9	367.8
30	373	373	373

Table 50. The Effect Reynolds Number on Temperature Profile at Middle of Long Plate (L1) for L1/L2 = 2.5, n = 0.5, and θ = 25

Tp	Re = 100	Re = 300	Re = 900
0	373	373	373
5	348.5	353.8	365.3
10	334.4	339.6	362.5
15	322.8	327.2	360.3
20	341.3	346.4	363.1
25	350.8	355.7	364.7
30	373	373	373

Table 51. The Effect Reynolds Number on Temperature Profile at Tailing Edge of Long Plate (L1) for L1/L2 = 2.5, n = 0.5, and θ = 25

Tp	Re = 100	Re = 300	Re = 900
0	373	373	373
5	352.8	358.5	369.7
10	348.7	354.2	367.2
15	352.4	358.4	369.1
20	355.6	361.1	370.9
25	359.5	365.7	371.8
30	373	373	373

Table 52. The Effect Reynolds Number on Temperature Profile at Leading Edge of Long Plate (L1) for L1/L2 = 2.5, n = 1.0, and θ = 25

Tp	Re = 100	Re = 300	Re = 900
0	373	373	373
5	358.3	363.1	370.5
10	353.2	358.5	367.6
15	350.8	355.2	365.8
20	348.5	353.4	362.2
25	351.7	357.6	365.9
30	373	373	373

Table 53. The Effect Reynolds Number on Temperature Profile at Middle of Long Plate (L1) for L1/L2 = 2.5, n = 1.0, and θ = 25

Tp	Re = 100	Re = 300	Re = 900
0	373	373	373
5	347.7	352.8	364.5
10	332.6	337.1	360.6
15	320.1	325.5	358.1
20	339.4	344.9	360.8
25	347.9	353.2	362.5
30	373	373	373

Table 54. The Effect Reynolds Number on Temperature Profile at Tailing Edge of Long Plate (L1) for L1/L2 = 2.5, n = 1.0, and θ = 25

Tp	Re = 100	Re = 300	Re = 900
0	373	373	373
5	351.3	357.4	368.2
10	346.2	352.3	365.4
15	350.8	356.1	366.8
20	353.4	359.8	368.3
25	357.3	363.9	370.1
30	373	373	373

Table 55. The Effect Reynolds Number on Temperature Profile at Leading Edge of Long Plate (L1) for L1/L2 = 2.5, n = 1.2, and θ = 25

Tp	Re = 100	Re = 300	Re = 900
0	373	373	373
5	355.7	360.3	367.6
10	350.1	355.8	365.1
15	348.1	352.9	362.7
20	346.5	351.2	359.8
25	349.8	355.1	363.2
30	373	373	373

Table 56. The Effect Reynolds Number on Temperature Profile at Middle of Long Plate (L1) for L1/L2 = 2.5, n = 1.2, and θ = 25

Tp	Re = 100	Re = 300	Re = 900
0	373	373	373
5	344.2	349.5	362.2
10	329.7	334.1	357.7
15	318.1	322.7	355.4
20	337.5	342.3	357.7
25	345.6	351.4	359.3
30	373	373	373

Table 57. The Effect Reynolds Number on Temperature Profile at Tailing Edge of Long Plate (L1) for L1/L2 = 2.5, n = 1.2, and θ = 25

Tp	Re = 100	Re = 300	Re = 900
0	373	373	373
5	348.6	354.7	366.3
10	343.7	349.7	362.7
15	348.2	353.3	363.5
20	351.4	357.8	366.1
25	355.1	361.4	367.4
30	373	373	373

Table 58. The Effect Plate Angle on Temperature Profile at Leading Edge of Long Plate (L1) for L1/L2 = 2.5, n = 0.5, and Re = 300

Tp (mm)	θ = 5	θ = 25	θ = 30
0	373	373	373
5	353.2	364.7	367.8
10	349.5	360.8	363.5
15	344.8	357.1	360.4
20	346.1	355.3	358.7
25	348.9	359.9	362.6
30	373	373	373

Table 59. The Effect Plate Angle on Temperature Profile at Middle of Long Plate (L1) for L1/L2 = 2.5, n = 0.5, and Re = 300

Tp (mm)	θ = 5	θ = 25	θ = 30
0	373	373	373
5	342.7	353.8	357.3
10	328.4	339.6	343.6
15	316.6	327.2	331.8
20	335.1	346.4	350.4
25	344.5	355.7	359.1
30	373	373	373

Table 60. The Effect Plate Angle on Temperature Profile at Tailing Edge of Long Plate (L1) for L1/L2 = 2.5, n = 0.5, and Re = 300

Tp (mm)	θ = 5	θ = 25	θ = 30
0	373	373	373
5	349.1	358.5	361.9
10	345.6	354.2	357.7
15	343.6	358.4	361.5
20	353.7	361.1	364.4
25	357.4	365.7	367.6
30	373	373	373

Table 61. The Effect Plate Angle on Temperature Profile at Leading Edge of Long Plate (L1) for L1/L2 = 2.5, n = 1.0, and Re = 300

Tp (mm)	θ = 5	θ = 25	θ = 30
0	373	373	373
5	351.8	363.1	366.5
10	347.6	358.5	361.4
15	342.9	355.2	358.1
20	343.1	353.4	355.6
25	346.4	357.6	360.7
30	373	373	373

Table 62. The Effect Plate Angle on Temperature Profile at Middle of Long Plate (L1) for L1/L2 = 2.5, n = 1.0, and Re = 300

Tp (mm)	θ = 5	θ = 25	θ = 30
0	373	373	373
5	341.5	352.8	356.6
10	326.3	337.1	341.2
15	314.8	325.5	329.3
20	333.2	344.9	347.8
25	342.9	353.2	357.5
30	373	373	373

Table 63. The Effect Plate Angle on Temperature Profile at Tailing Edge of Long Plate (L1) for L1/L2 = 2.5, n = 1.0, and Re = 300

Tp (mm)	θ = 5	θ = 25	θ = 30
0	373	373	373
5	348.3	357.4	360.7
10	343.4	352.3	355.4
15	341.5	356.1	359.2
20	351.2	359.8	362.3
25	355.6	363.9	365.1
30	373	373	373

Table 64. The Effect Plate Angle on Temperature Profile at Leading Edge of Long Plate (L1) for L1/L2 = 2.5, n = 1.2, and Re = 300

Tp (mm)	θ = 5	θ = 25	θ = 30
0	373	373	373
5	348.7	360.3	363.7
10	344.5	355.8	358.6
15	339.7	352.9	355.4
20	340.6	351.2	353.8
25	344.2	355.1	358.3
30	373	373	373

Table 65. The Effect Plate Angle on Temperature Profile at Middle of Long Plate (L1) for L1/L2 = 2.5, n = 1.2, and Re = 300

Tp (mm)	θ = 5	θ = 25	θ = 30
0	373	373	373
5	338.3	349.5	353.5
10	323.5	334.1	338.6
15	311.7	322.7	326.6
20	331.7	342.3	345.3
25	340.8	351.4	355.4
30	373	373	373

Table 66. The Effect Plate Angle on Temperature Profile at Tailing Edge of Long Plate (L1) for L1/L2 = 2.5, n = 1.2, and Re = 300

Tp (mm)	θ = 5	θ = 25	θ = 30
0	373	373	373
5	345.8	354.7	357.3
10	340.7	349.7	352.6
15	339.2	353.3	356.7
20	349.7	357.8	360.5
25	353.4	361.4	363.2
30	373	373	373

APPENDIX B

B.1 Momentum Equation Manipulation

This appendix presents a description of the numerical method developed to solve the governing equations (2) and (3) using power law scheme. The x-y momentum equations can be written as:

x -Momentum:

$$\rho(u\frac{\partial u}{\partial x}+v\frac{\partial u}{\partial y})=\frac{\partial}{\partial x}\left[m\left[\left|2\left(\left(\frac{\partial u}{\partial x}\right)^2+\left(\frac{\partial v}{\partial y}\right)^2\right)+\left(\frac{\partial u}{\partial y}+\frac{\partial v}{\partial x}\right)^2\right|^{\frac{n-1}{2}}\right]\frac{\partial u}{\partial x}\right]+\frac{\partial}{\partial y}\left[m\left[\left|2\left(\left(\frac{\partial u}{\partial x}\right)^2+\left(\frac{\partial v}{\partial y}\right)^2\right)+\left(\frac{\partial u}{\partial y}+\frac{\partial v}{\partial x}\right)^2\right|^{\frac{n-1}{2}}\right]\frac{\partial u}{\partial y}\right]-\frac{\partial P}{\partial x} \quad \text{(B-1)}$$

y-Momentum:

$$\rho(u\frac{\partial v}{\partial x}+v\frac{\partial v}{\partial y})=\frac{\partial}{\partial x}\left[m\left[\left|2\left(\left(\frac{\partial u}{\partial x}\right)^2+\left(\frac{\partial v}{\partial y}\right)^2\right)+\left(\frac{\partial u}{\partial y}+\frac{\partial v}{\partial x}\right)^2\right|^{\frac{n-1}{2}}\right]\frac{\partial v}{\partial x}\right]+\frac{\partial}{\partial y}\left[m\left[\left|2\left(\left(\frac{\partial u}{\partial x}\right)^2+\left(\frac{\partial v}{\partial y}\right)^2\right)+\left(\frac{\partial u}{\partial y}+\frac{\partial v}{\partial x}\right)^2\right|^{\frac{n-1}{2}}\right]\frac{\partial v}{\partial y}\right]-\frac{\partial P}{\partial y} \quad \text{(B-2)}$$

To non-dimensionalized x-momentum and y-momentum, the short length L_2 and mean velocity U_m are selected, and dimensionless variables are introduced as follow:

$$U=\frac{u}{u_m}$$

$$V=\frac{v}{u_m}$$

$$X=\frac{x}{L_2}$$

$$Y=\frac{y}{L_2}$$

$$\rho^*=\frac{\bar{\rho}}{\rho}$$

$$\bar{P} = \frac{P - P_{rc}}{\rho u_m^2}$$

The non-dimensionless form of x-momentum equation can be written by using those dimensionless variables. The first term, inertia forces, on the left hand side of x-momentum becomes

$$\frac{\rho u_m^2}{L_2}(U\frac{\partial U}{\partial X} + V\frac{\partial U}{\partial Y}) \tag{B-3}$$

The first term of viscous forces on the right hand side becomes:

$$\frac{m u_m^n}{L_2^{n+1}}\frac{\partial}{\partial X}\left[\left[\left|2\left(\left(\frac{\partial U}{\partial X}\right)^2 + \left(\frac{\partial V}{\partial Y}\right)^2\right) + \left(\frac{\partial U}{\partial Y}\right)^2 + \left(2\frac{\partial U}{\partial Y}\frac{\partial V}{\partial X}\right) + \left(\frac{\partial V}{\partial X}\right)^2\right|^{\frac{n-1}{2}}\right]\frac{\partial U}{\partial X}\right] \tag{B-4}$$

The second term of viscous forces on the right hand side becomes:

$$\frac{m u_m^n}{L_2^{n+1}}\frac{\partial}{\partial Y}\left[\left[\left|2\left(\left(\frac{\partial U}{\partial X}\right)^2 + \left(\frac{\partial V}{\partial Y}\right)^2\right) + \left(\frac{\partial U}{\partial Y}\right)^2 + \left(2\frac{\partial U}{\partial Y}\frac{\partial V}{\partial X}\right) + \left(\frac{\partial V}{\partial X}\right)^2\right|^{\frac{n-1}{2}}\right]\frac{\partial U}{\partial Y}\right] \tag{B-5}$$

The last term, pressure forces, of x-momentum equation becomes:

$$\frac{\rho u_m^2}{L_2}\frac{\partial \bar{P}}{\partial X} \tag{B-6}$$

To non-dimensionalized y-momentum equation, it can be written in similar to x-momentum. The first term, inertia forces, on the left hand side of y-momentum becomes:

$$\frac{\rho u_m^2}{L_2}(U\frac{\partial V}{\partial X} + V\frac{\partial V}{\partial Y}) \tag{B-7}$$

The first term of viscous forces on the right hand side becomes:

$$\frac{m u_m^n}{L_2^{n+1}}\frac{\partial}{\partial X}\left[\left[\left|2\left(\left(\frac{\partial U}{\partial X}\right)^2 + \left(\frac{\partial V}{\partial Y}\right)^2\right) + \left(\frac{\partial U}{\partial Y}\right)^2 + \left(2\frac{\partial U}{\partial Y}\frac{\partial V}{\partial X}\right) + \left(\frac{\partial V}{\partial X}\right)^2\right|^{\frac{n-1}{2}}\right]\frac{\partial V}{\partial X}\right] \tag{B-8}$$

The second term of viscous forces on the right hand side becomes:

$$\frac{mu_m^n}{L_2^{n+1}}\frac{\partial}{\partial Y}\left[\left[\left|2\left(\left(\frac{\partial U}{\partial X}\right)^2+\left(\frac{\partial V}{\partial Y}\right)^2\right)+\left(\frac{\partial U}{\partial Y}\right)^2+\left(2\frac{\partial U}{\partial Y}\frac{\partial V}{\partial X}\right)+\left(\frac{\partial V}{\partial X}\right)^2\right|^{\frac{n-1}{2}}\right]\frac{\partial V}{\partial Y}\right] \tag{B-9}$$

The last term, pressure forces, of x-momentum equation becomes:

$$\frac{\rho u_m^2}{L_2}\frac{\partial \bar{P}}{\partial Y} \tag{B-10}$$

To transform the dimensionless form of x and y momentum equations into the body-fitted coordinate system, the transformation parameters, equation (6), that described in chapter 3 are employed to above governing equations Thus the dimensionless form of governing equations are become:

x-Momentum:

$$\frac{\partial}{\partial\xi}(\phi_U U)+\frac{\partial}{\partial\eta}(\phi_V U)=[\frac{\partial}{\partial\xi}[\frac{A}{J\,\mathrm{Re}}(\alpha\frac{\partial U}{\partial\xi}-\beta\frac{\partial U}{\partial\eta})]+\frac{\partial}{\partial\eta}[\frac{A}{J\,\mathrm{Re}}(-\beta\frac{\partial U}{\partial\xi}+\gamma\frac{\partial U}{\partial\eta})]]+(\frac{\partial P}{\partial\eta}Y_\xi-\frac{\partial P}{\partial\xi}Y_\eta) \tag{B-11}$$

y-Momentum:

$$\frac{\partial}{\partial\xi}(\phi_U V)+\frac{\partial}{\partial\eta}(\phi_V V)=[\frac{\partial}{\partial\xi}[\frac{A}{J\,\mathrm{Re}}(\alpha\frac{\partial V}{\partial\xi}-\beta\frac{\partial V}{\partial\eta})]+\frac{\partial}{\partial\eta}[\frac{A}{J\,\mathrm{Re}}(-\beta\frac{\partial V}{\partial\xi}+\gamma\frac{\partial V}{\partial\eta})]]+(\frac{\partial P}{\partial\xi}X_\eta-\frac{\partial P}{\partial\eta}X_\xi) \tag{B-12}$$

where

$$\mathrm{Re}=\frac{\rho u_m^{2-n}L_2^n}{m}$$

$$A=\left[\left|\begin{array}{l}2\left(\left(\frac{\partial U}{\partial\xi}\frac{Y_\eta}{J}-\frac{\partial U}{\partial\eta}\frac{Y_\xi}{J}\right)^2+\left(\frac{\partial V}{\partial\eta}\frac{X_\xi}{J}-\frac{\partial V}{\partial\xi}\frac{X_\eta}{J}\right)^2\right)+\left(\frac{\partial U}{\partial\eta}\frac{X_\xi}{J}-\frac{\partial U}{\partial\xi}\frac{X_\eta}{J}\right)^2+ \\ \left(2\left(\frac{\partial U}{\partial\eta}\frac{X_\xi}{J}-\frac{\partial U}{\partial\xi}\frac{X_\eta}{J}\right)\left(\frac{\partial V}{\partial\xi}\frac{Y_\eta}{J}-\frac{\partial V}{\partial\eta}\frac{Y_\xi}{J}\right)\right)+\left(\frac{\partial V}{\partial\xi}\frac{Y_\eta}{J}-\frac{\partial V}{\partial\eta}\frac{Y_\xi}{J}\right)^2\end{array}\right|^{\frac{n-1}{2}}\right] \tag{B-13}$$

$$\Psi = \frac{k}{\rho c_p}$$

$$\phi_u = UY_\eta - VX_\eta$$

$$\phi_v = VX_\xi - UY_\xi$$

$$\alpha = X_\eta^2 + Y_\eta^2$$

$$\beta = X_\xi X_\eta + Y_\xi Y_\eta$$

$$\gamma = X_\xi^2 + Y_\xi^2$$

$$J = X_\xi Y_\eta - X_\eta Y_\xi$$

B.1.1 X-Momentum Equation Integration:

The x-momentum equation (B-11) can be integrated term by term over staggered control volume of axial velocity (u) in Fig. 5. The first term on the left hand side in x-momentum equation, inertia forces, becomes

$$\int_{sx}^{nx}\int_{P}^{E} \frac{\partial}{\partial \xi}\left(U\frac{\partial Y}{\partial \eta}U - V\frac{\partial X}{\partial \eta}U \right) d\xi d\eta$$

Then, this integrated term can be solved by using numerical integration and linear interpolation

$$= \frac{(U_{ee} + U_e)}{2}\Delta\eta U_E - \frac{(U_e + U_w)}{2}\Delta\eta U_P . \qquad \text{(B-14)}$$

The second term on the left hand side in x-momentum equation becomes

$$\int_{sx}^{nx}\int_{P}^{E} \frac{\partial}{\partial \eta}\left(V\frac{\partial X}{\partial \xi}U - U\frac{\partial Y}{\partial \xi}U \right) d\xi d\eta$$

$$= \left[V_n \Delta\xi \cos\theta - U_n \Delta\xi \sin\theta\right]\left(\frac{U_{Nx} + U_e}{2}\right) + \left[U_s \Delta\xi \sin\theta - V_s \Delta\xi \cos\theta\right]\left(\frac{U_e + U_{Sx}}{2}\right) \qquad \text{(B-15)}$$

The first term of viscous forces on the right hand side in x-momentum equation becomes

$$\int_{nx}^{sx}\int_{P}^{E} \frac{1}{\mathrm{Re}}\frac{\partial}{\partial\xi}\left(\frac{A}{J}\left(\alpha\frac{\partial U}{\partial\xi}-\beta\frac{\partial U}{\partial\eta}\right)\right)d\xi d\eta$$

$$=\frac{1}{\mathrm{Re}}\int_{nx}^{sx}\int_{P}^{E} \frac{\partial}{\partial\xi}\left(\frac{A\alpha}{J}\frac{\partial U}{\partial\xi}\right)d\xi d\eta \;-\; \frac{1}{\mathrm{Re}}\int_{nx}^{sx}\int_{P}^{E} \frac{\partial}{\partial\xi}\left(\frac{A\beta}{J}\frac{\partial U}{\partial\eta}\right)d\xi d\eta \qquad \text{(B-16)}$$

Now, consider the first integral term so that numerical integration, linear interpolation, and element analysis (Fig. 8) is used.

$$=\frac{\Delta\eta}{\Delta\xi\,\mathrm{Re}\cos\theta}\left[A_E^*\left(U_{ee}-U_e\right)-A_P^*\left(U_e-U_w\right)\right] \qquad \text{(B-17)}$$

where

$$A_E^* = \left[\left|2\left(\left(\left(\frac{U_{ee}^*-U_e^*}{\Delta\xi\cos\theta}\right)-\left(\left(\frac{U_{nE}^*-U_{sE}^*}{\Delta\eta}\right)\tan\theta\right)\right)^2+\left(\left(\frac{V_{nE}^*-V_{sE}^*}{\Delta\eta}\right)\right)^2\right)+\left(\left(\frac{U_{nE}^*-U_{sE}^*}{\Delta\eta}\right)\right)^2+\left|\frac{n-1}{2}\right|\right]$$

$$\left[\left|\left(2\left(\left(\left(\frac{U_{nE}^*-U_{sE}^*}{\Delta\eta}\right)\right)*\left(\left(\frac{V_{ee}^*-V_e^*}{\Delta\xi\cos\theta}\right)-\left(\left(\frac{V_{nE}^*-V_{sE}^*}{\Delta\eta}\right)\tan\theta\right)\right)\right)\right|+\right.$$

$$\left.\left|\left(\left(\frac{V_{ee}^*-V_e^*}{\Delta\xi\cos\theta}\right)-\left(\left(\frac{V_{nE}^*-V_{sE}^*}{\Delta\eta}\right)\tan\theta\right)\right)^2\right|\right]$$

$$A_P^* = \left[\left|2\left(\left(\left(\frac{U_e^*-U_w^*}{\Delta\xi\cos\theta}\right)-\left(\left(\frac{U_n^*-U_s^*}{\Delta\eta}\right)\tan\theta\right)\right)^2+\left(\left(\frac{V_n^*-V_s^*}{\Delta\eta}\right)\right)^2\right)+\left(\left(\frac{U_n^*-U_s^*}{\Delta\eta}\right)\right)^2+\left|\frac{n-1}{2}\right|\right]$$

$$\left[\left|\left(2\left(\left(\left(\frac{U_n^*-U_s^*}{\Delta\eta}\right)\right)*\left(\left(\frac{V_e^*-V_w^*}{\Delta\xi\cos\theta}\right)-\left(\left(\frac{V_n^*-V_s^*}{\Delta\eta}\right)\tan\theta\right)\right)\right)\right|+\right.$$

$$\left.\left|\left(\left(\frac{V_e^*-V_w^*}{\Delta\xi\cos\theta}\right)-\left(\left(\frac{V_n^*-V_s^*}{\Delta\eta}\right)\tan\theta\right)\right)^2\right|\right]$$

Now, consider term $\frac{A\beta}{J}$ in the second integral term. From element analysis

(Fig. 8), $\beta = \sin\theta$ and $J = \cos\theta$. Thus, $\frac{A\beta}{J} = A\tan\theta$

The $\frac{A\beta}{J}$ term gives a very small number [26] that is compared to $\frac{A\alpha}{J}$. Thus the β term doesn't effect to velocity and pressure profiles and it is neglected in this thesis.

Continuing the integration, the second term of viscous forces on the right hand side in x-momentum equation becomes

$$\int_{nx}^{sx}\int_{P}^{E} \frac{1}{\mathrm{Re}}\frac{\partial}{\partial\eta}\left(\frac{A}{J}\left(\gamma\frac{\partial U}{\partial\eta}-\beta\frac{\partial U}{\partial\xi}\right)\right)d\xi d\eta$$

$$= \frac{1}{\mathrm{Re}}\int_{nx}^{sx}\int_{P}^{E} \frac{\partial}{\partial\eta}\left(\frac{A\gamma}{J}\frac{\partial U}{\partial\eta}\right)d\xi d\eta \;-\; \frac{1}{\mathrm{Re}}\int_{nx}^{sx}\int_{P}^{E} \frac{\partial}{\partial\eta}\left(\frac{A\beta}{J}\frac{\partial U}{\partial\xi}\right)d\xi d\eta$$

In similar manner, the first integral can be written

$$= \frac{\Delta\xi}{\Delta\eta\,\mathrm{Re}\cos\theta}\left[A^{*}_{nx}\left(U_{eN}-U_{e}\right)-A^{*}_{sx}\left(U_{e}-U_{eS}\right)\right] \qquad \text{(B-18)}$$

where

$$A^{*}_{nx} = \left[\left|2\left(\left(\frac{U^{*}_{nn}-U^{*}_{n}}{\Delta\xi\cos\theta}\right)-\left(\left(\frac{U^{*}_{Ne}-U^{*}_{e}}{\Delta\eta}\right)\tan\theta\right)\right)^{2}+\left(\left(\frac{V^{*}_{Ne}-V^{*}_{e}}{\Delta\eta}\right)\right)^{2}+\left(\left(\frac{U^{*}_{Ne}-U^{*}_{e}}{\Delta\eta}\right)\right)^{2}+\right.\right.$$
$$\left(2\left(\left(\frac{U^{*}_{Ne}-U^{*}_{e}}{\Delta\eta}\right)\right)*\left(\left(\frac{V^{*}_{nn}-V^{*}_{n}}{\Delta\xi\cos\theta}\right)-\left(\left(\frac{V^{*}_{Ne}-V^{*}_{e}}{\Delta\eta}\right)\tan\theta\right)\right)\right)+$$
$$\left.\left.\left(\left(\frac{V^{*}_{nn}-V^{*}_{n}}{\Delta\xi\cos\theta}\right)-\left(\left(\frac{V^{*}_{Ne}-V^{*}_{e}}{\Delta\eta}\right)\tan\theta\right)\right)^{2}\right|^{\frac{n-1}{2}}\right]$$

$$A_{sx}^{*} = \left[\left| \begin{array}{l} 2\left(\left(\left(\frac{U_{ss}^{*} - U_{s}^{*}}{\Delta\xi \cos\theta}\right) - \left(\left(\frac{U_{e}^{*} - U_{Se}^{*}}{\Delta\eta}\right)\tan\theta\right)\right)^{2} + \left(\left(\frac{V_{e}^{*} - V_{Se}^{*}}{\Delta\eta}\right)\right)^{2}\right) + \left(\left(\frac{U_{e}^{*} - U_{Se}^{*}}{\Delta\eta}\right)\right)^{2} + \\ \left(2\left(\left(\left(\frac{U_{e}^{*} - U_{Se}^{*}}{\Delta\eta}\right)\right) * \left(\left(\frac{V_{ss}^{*} - V_{s}^{*}}{\Delta\xi \cos\theta}\right) - \left(\left(\frac{V_{e}^{*} - V_{Se}^{*}}{\Delta\eta}\right)\tan\theta\right)\right)\right)\right) + \\ \left(\left(\frac{V_{ss}^{*} - V_{s}^{*}}{\Delta\xi \cos\theta}\right) - \left(\left(\frac{V_{e}^{*} - V_{Se}^{*}}{\Delta\eta}\right)\tan\theta\right)\right)^{2} \end{array} \right|^{\frac{n-1}{2}} \right]$$

The β term can be considered in similar manner to the previous β term in the first term of viscous forces. Thus the β term in second integral is also neglected in this thesis.

Now integrate the pressure forces, last term, in x-momentum equation. It is becomes

$$\int_{nx}^{sx}\int_{P}^{E} \left(\frac{\partial \bar{P}}{\partial\eta} Y_{\xi} - \frac{\partial \bar{P}}{\partial\xi} Y_{\eta}\right) d\xi d\eta$$

$$= \int_{nx}^{sx}\int_{P}^{E} \left(\frac{\partial \bar{P}}{\partial\eta}\frac{\partial Y}{\partial\xi}\right) d\xi d\eta - \int_{nx}^{sx}\int_{P}^{E} \left(\frac{\partial \bar{P}}{\partial\xi}\frac{\partial Y}{\partial\eta}\right) d\xi d\eta$$

In similar manner,

$$= \Delta\xi \sin\theta \left(\bar{P}_{n} - \bar{P}_{s}\right) - \Delta\eta \left(\bar{P}_{E} - \bar{P}_{P}\right) \qquad \text{(B-19)}$$

Thus the convection-diffusion term are treated by power-law profile of Patanka [13, 24]. The discretization equation of x- momentum can be written as follows:

The strength of convection:

$$F_{E} = \Delta\eta\left(\frac{U_{ee} + U_{e}}{2}\right)$$

$$F_{P} = \Delta\eta\left(\frac{U_{e} + U_{w}}{2}\right)$$

$$F_{nx} = \left(V_{nx}\Delta\xi\cos\theta - U_{nx}\Delta\xi\sin\theta\right)$$

$$F_{sx} = \left(U_{sx}\Delta\xi\sin\theta - V_{sx}\Delta\xi\cos\theta\right)$$

The diffusion conductance:

$$D_E = \left(\frac{\Delta\eta A_E^* u_m^{n-1}}{\Delta\xi\ \mathrm{Re}\cos\theta L_2^{n-1}}\right)$$

$$D_P = \left(\frac{\Delta\eta A_P^* u_m^{n-1}}{\Delta\xi\ \mathrm{Re}\cos\theta L_2^{n-1}}\right)$$

$$D_{nx} = \left(\frac{\Delta\xi A_{nx}^* u_m^{n-1}}{\Delta\eta\ \mathrm{Re}\cos\theta L_2^{n-1}}\right)$$

$$D_{sx} = \left(\frac{\Delta\xi A_{sx}^* u_m^{n-1}}{\Delta\eta\ \mathrm{Re}\cos\theta L_2^{n-1}}\right)$$

The peclet number::

$$P_E = \frac{F_E}{D_E}$$

$$P_P = \frac{F_P}{D_P}$$

$$P_{nx} = \frac{F_{nx}}{D_{nx}}$$

$$P_{sx} = \frac{F_{sx}}{D_{sx}}$$

The power-law scheme can be written as follow:

$$A|P| = \left\langle\left\langle 0, \left(1 - 0.1|P|\right)^5 \right\rangle\right\rangle$$

Then, apply this power-law scheme to staggered control volume of axial velocity (u).

$$A|P_E| = \left\langle\left\langle 0, \left(1 - 0.1|P_E|\right)^5 \right\rangle\right\rangle$$

$$A|P_P| = \left\langle\left\langle 0, \left(1 - 0.1|P_P|\right)^5 \right\rangle\right\rangle$$

$$A|P_{nx}| = \left\langle\left\langle 0, (1 - 0.1|P_{nx}|)^5 \right\rangle\right\rangle$$

$$A|P_{sx}| = \left\langle\left\langle 0, (1 - 0.1|P_{sx}|)^5 \right\rangle\right\rangle$$

The discretization equation of x-momentum equation is

$$a_e U_e = a_E U_{ee} + a_P U_w + a_{nx} U_{Nx} + a_{sx} U_{Sx} + \Delta\xi \sin\theta\left(\bar{P}_n - \bar{P}_s\right) + \Delta\eta\left(\bar{P}_P - \bar{P}_E\right) \qquad \text{(B-20)}$$

where coefficient is

$$a_E = D_E A|P_E| + \left\langle\left\langle -F_E, 0\right\rangle\right\rangle$$

$$a_P = D_P A|P_P| + \left\langle\left\langle F_P, 0\right\rangle\right\rangle$$

$$a_{nx} = D_{nx} A|P_{nx}| + \left\langle\left\langle -F_{nx}, 0\right\rangle\right\rangle$$

$$a_{sx} = D_{sx} A|P_{sx}| + \left\langle\left\langle F_{sx}, 0\right\rangle\right\rangle$$

$$a_e = a_E + a_P + a_{nx} + a_{sx}$$

B.1.2 Y-Momentum Equation Integration:

The y-momentum equation (B-12) can be integrated term by term over staggered control volume of transverse velocity (v) in Fig. 6. The first term on the left hand side in y-momentum equation, inertia forces, becomes

$$\int_{P}^{N}\int_{wy}^{ey} \frac{\partial}{\partial \xi}\left(U\frac{\partial Y}{\partial \eta}V - V\frac{\partial X}{\partial \eta}V \right) d\xi d\eta$$

Then this integrated term can be solved by using numerical integration and linear interpolation

$$= \frac{(U_e + U_{Ne})}{2}\Delta\eta V_{ey} - \frac{(U_w + U_{Nw})}{2}\Delta\eta V_{wy} . \tag{B-21}$$

The second term on the left hand side in y-momentum equation becomes

$$\int_{P}^{N}\int_{wy}^{ey} \frac{\partial}{\partial \eta}\left(V\frac{\partial X}{\partial \xi}V - U\frac{\partial Y}{\partial \xi}V \right) d\xi d\eta$$

$$= \left[V_N \Delta\xi \cos\theta - U_N \Delta\xi \sin\theta\right]\left(\frac{V_{nn} + V_n}{2}\right) + \left[U_P \Delta\xi \sin\theta - V_P \Delta\xi \cos\theta\right]\left(\frac{V_n + V_s}{2}\right) \tag{B-22}$$

The first term of viscous forces on the right hand side in y-momentum equation becomes

$$\int_{P}^{N}\int_{wy}^{ey} \frac{1}{\mathrm{Re}}\frac{\partial}{\partial \xi}\left(\frac{A}{J}\left(\alpha\frac{\partial V}{\partial \xi} - \beta\frac{\partial V}{\partial \eta} \right) \right) d\xi d\eta$$

$$= \frac{1}{\mathrm{Re}}\int_{P}^{N}\int_{wy}^{ey} \frac{\partial}{\partial \xi}\left(\frac{A\alpha}{J}\frac{\partial V}{\partial \xi} \right) d\xi d\eta \; - \; \frac{1}{\mathrm{Re}}\int_{P}^{N}\int_{wy}^{ey} \frac{\partial}{\partial \xi}\left(\frac{A\beta}{J}\frac{\partial V}{\partial \eta} \right) d\xi d\eta$$

Now, consider the first integral term so that numerical integration, linear interpolation, and element analysis (Fig. 8) is used.

$$= \frac{\Delta\eta}{\Delta\xi\,\mathrm{Re}\cos\theta}\left[A^*_{ey}\left(V_{nE} - V_n\right) - A^*_{wy}\left(V_n - V_{nW}\right) \right] \tag{B-23}$$

where

$$A^*_{ey} = \left[\left| 2\left(\left(\left(\frac{U^*_{nE} - U^*_n}{\Delta\xi \cos\theta} \right) - \left(\left(\frac{U^*_{Ne} - U^*_e}{\Delta\eta} \right) \tan\theta \right) \right)^2 + \left(\left(\frac{V^*_{Ne} - V^*_e}{\Delta\eta} \right) \right)^2 \right) + \left(\left(\frac{U^*_{Ne} - U^*_e}{\Delta\eta} \right) \right)^2 + \left| \left(2\left(\left(\left(\frac{U^*_{Ne} - U^*_e}{\Delta\eta} \right) \right) * \left(\left(\frac{V^*_{nE} - V^*_n}{\Delta\xi \cos\theta} \right) - \left(\left(\frac{V^*_{Ne} - V^*_e}{\Delta\eta} \right) \tan\theta \right) \right) \right) \right) + \left(\left(\frac{V^*_{nE} - V^*_n}{\Delta\xi \cos\theta} \right) - \left(\left(\frac{V^*_{Ne} - V^*_e}{\Delta\eta} \right) \tan\theta \right) \right)^2 \right|^{\frac{n-1}{2}} \right]$$

$$A^*_{wy} = \left[\left| 2\left(\left(\left(\frac{U^*_{nW} - U^*_n}{\Delta\xi \cos\theta} \right) - \left(\left(\frac{U^*_{Nw} - U^*_w}{\Delta\eta} \right) \tan\theta \right) \right)^2 + \left(\left(\frac{V^*_{Nw} - V^*_w}{\Delta\eta} \right) \right)^2 \right) + \left(\left(\frac{U^*_{Nw} - U^*_w}{\Delta\eta} \right) \right)^2 + \left| \left(2\left(\left(\left(\frac{U^*_{Nw} - U^*_w}{\Delta\eta} \right) \right) * \left(\left(\frac{V^*_n - V^*_{nW}}{\Delta\xi \cos\theta} \right) - \left(\left(\frac{V^*_{Nw} - V^*_w}{\Delta\eta} \right) \tan\theta \right) \right) \right) \right) + \left(\left(\frac{V^*_n - V^*_{nW}}{\Delta\xi \cos\theta} \right) - \left(\left(\frac{V^*_{Nw} - V^*_w}{\Delta\eta} \right) \tan\theta \right) \right)^2 \right|^{\frac{n-1}{2}} \right]$$

Now, consider term $\frac{A\beta}{J}$ in the second integral term. From element analysis (Fig. 8), $\beta = \sin\theta$ and $J = \cos\theta$. Thus, $\frac{A\beta}{J} = A\tan\theta$

The $\frac{A\beta}{J}$ term gives a very small number [26] that is compared to $\frac{A\alpha}{J}$. Thus the β term doesn't effect to velocity and pressure profiles and it is neglected in this thesis.

Continuing the integration, the second term of viscous forces on the right hand side in y-momentum equation becomes

$$\int_P^N \int_{wy}^{ey} \frac{1}{\mathrm{Re}} \frac{\partial}{\partial\eta}\left(\frac{A}{J}\left(\gamma \frac{\partial V}{\partial\eta} - \beta \frac{\partial V}{\partial\xi} \right) \right) d\xi d\eta$$

$$= \frac{1}{\mathrm{Re}} \int_{P}^{N} \int_{wy}^{ey} \frac{\partial}{\partial \eta}\left(\frac{A\gamma}{J} \frac{\partial V}{\partial \eta} \right) d\xi d\eta \; - \frac{1}{\mathrm{Re}} \int_{P}^{N} \int_{wy}^{ey} \frac{\partial}{\partial \eta}\left(\frac{A\beta}{J} \frac{\partial V}{\partial \xi} \right) d\xi d\eta$$

In similar manner, the first integral can be written

$$= \frac{\Delta\xi}{\Delta\eta \,\mathrm{Re} \cos\theta} \left[A_N^* (V_{nn} - V_n) - A_P^* (V_n - V_s) \right] \tag{B-24}$$

where

$$A_N^* = \left[\left| 2\left(\left(\frac{U_{Ne}^* - U_{Nw}^*}{\Delta\xi \cos\theta} \right) - \left(\left(\frac{U_{nn}^* - U_n^*}{\Delta\eta} \right) \tan\theta \right) \right)^2 + \left(\left(\frac{V_{nn}^* - V_n^*}{\Delta\eta} \right) \right)^2 \right) + \left(\left(\frac{U_{nn}^* - U_n^*}{\Delta\eta} \right) \right)^2 + \left| \left(2\left(\left(\frac{U_{nn}^* - U_n^*}{\Delta\eta} \right) \right) * \left(\left(\frac{V_{Ne}^* - V_{Nw}^*}{\Delta\xi \cos\theta} \right) - \left(\left(\frac{V_{nn}^* - V_n^*}{\Delta\eta} \right) \tan\theta \right) \right) \right) + \left(\left(\frac{V_{Ne}^* - V_{Nw}^*}{\Delta\xi \cos\theta} \right) - \left(\left(\frac{V_{nn}^* - V_n^*}{\Delta\eta} \right) \tan\theta \right) \right)^2 \right|^{\frac{n-1}{2}} \right]$$

$$A_P^* = \left[\left| 2\left(\left(\frac{U_e^* - U_w^*}{\Delta\xi \cos\theta} \right) - \left(\left(\frac{U_n^* - U_s^*}{\Delta\eta} \right) \tan\theta \right) \right)^2 + \left(\left(\frac{V_n^* - V_s^*}{\Delta\eta} \right) \right)^2 \right) + \left(\left(\frac{U_n^* - U_s^*}{\Delta\eta} \right) \right)^2 + \left| \left(2\left(\left(\frac{U_n^* - U_s^*}{\Delta\eta} \right) \right) * \left(\left(\frac{V_e^* - V_w^*}{\Delta\xi \cos\theta} \right) - \left(\left(\frac{V_n^* - V_s^*}{\Delta\eta} \right) \tan\theta \right) \right) \right) + \left(\left(\frac{V_e^* - V_w^*}{\Delta\xi \cos\theta} \right) - \left(\left(\frac{V_n^* - V_s^*}{\Delta\eta} \right) \tan\theta \right) \right)^2 \right|^{\frac{n-1}{2}} \right]$$

The β term can be considered in similar manner to the previous β term in the first term of viscous forces. Thus the β term in second integral is also neglected in this thesis.

Now integrate the pressure forces, last term, in y-momentum equation. It is becomes

$$\int_{P}^{N} \int_{wy}^{ey} \left(\frac{\partial \bar{P}}{\partial \xi} X_\eta - \frac{\partial \bar{P}}{\partial \eta} X_\xi \right) d\xi d\eta$$

$$= \int_{P}^{N} \int_{wy}^{ey} \left(\frac{\partial \bar{P}}{\partial \xi} \frac{\partial X}{\partial \eta} \right) d\xi d\eta - \int_{P}^{N} \int_{wy}^{ey} \left(\frac{\partial \bar{P}}{\partial \eta} \frac{\partial X}{\partial \xi} \right) d\xi d\eta$$

By using element analysis (Fig. 8), $\frac{\partial X}{\partial \eta} = 0$ so that the first term of pressure forces is equal to zero. The pressure forces can be written as follows:

$$= -\Delta \xi s \cos\theta \left(\bar{P}_N - \bar{P}_P \right) = \Delta \xi s \cos\theta \left(\bar{P}_P - \bar{P}_N \right) \quad \text{(B-25)}$$

Thus the convection-diffusion term are treated by power-law profile of Patanka [13, 24]. The discretization equation of y- momentum can be written as follows:

The strength of convection:

$$F_{ey} = \Delta\eta \left(\frac{U_e + U_{Ne}}{2} \right)$$

$$F_{wy} = \Delta\eta \left(\frac{U_w + U_{Nw}}{2} \right)$$

$$F_N = \left(V_N \Delta\xi \cos\theta - U_N \Delta\xi \sin\theta \right)$$

$$F_P = \left(U_P \Delta\xi \sin\theta - V_P \Delta\xi \cos\theta \right)$$

The diffusion conductance:

$$D_{ey} = \left(\frac{\Delta\eta A^*_{ey} u_m^{n-1}}{\Delta\xi \,\mathrm{Re} \cos\theta L_2^{n-1}} \right)$$

$$D_{wy} = \left(\frac{\Delta\eta A^*_{wy} u_m^{n-1}}{\Delta\xi \,\mathrm{Re} \cos\theta L_2^{n-1}} \right)$$

$$D_N = \left(\frac{\Delta\xi A^*_N u_m^{n-1}}{\Delta\eta \,\mathrm{Re} \cos\theta L_2^{n-1}} \right)$$

$$D_P = \left(\frac{\Delta\xi A^*_P u_m^{n-1}}{\Delta\eta \,\mathrm{Re} \cos\theta L_2^{n-1}} \right)$$

The peclet number

$$P_{ey} = \frac{F_{ey}}{D_{ey}}$$

$$P_{wy} = \frac{F_{wy}}{D_{wy}}$$

$$P_N = \frac{F_N}{D_N}$$

$$P_P = \frac{F_P}{D_P}$$

The power-law scheme can be written as follow:

$$A|P| = \left\langle\left\langle 0, (1 - 0.1|P|)^5 \right\rangle\right\rangle$$

Then, apply this power-law scheme to staggered control volume of transverse velocity (v).

$$A\left|P_{ey}\right| = \left\langle\left\langle 0, \left(1 - 0.1\left|P_{ey}\right|\right)^5 \right\rangle\right\rangle$$

$$A\left|P_{wy}\right| = \left\langle\left\langle 0, \left(1 - 0.1\left|P_{wy}\right|\right)^5 \right\rangle\right\rangle$$

$$A\left|P_N\right| = \left\langle\left\langle 0, (1 - 0.1|P_N|)^5 \right\rangle\right\rangle$$

$$A\left|P_P\right| = \left\langle\left\langle 0, (1 - 0.1|P_P|)^5 \right\rangle\right\rangle$$

The discretization equation of y-momentum equation is

$$a_n V_n = a_N V_{nn} + a_P V_s + a_{ey} V_{Ey} + a_{wy} V_{Wy} + \Delta\xi \cos\theta\left(\bar{P}_N - \bar{P}_P\right) \tag{B-26}$$

where coefficient is

$$a_{ey} = D_{ey} A\left|P_{ey}\right| + \left\langle\left\langle -F_{ey}, 0\right\rangle\right\rangle$$

$$a_{wy} = D_{wy} A\left|P_{wy}\right| + \left\langle\left\langle F_{wy}, 0\right\rangle\right\rangle$$

$$a_N = D_N A\left|P_N\right| + \left\langle\left\langle - F_N, 0\right\rangle\right\rangle$$

$$a_P = D_P A\left|P_P\right| + \left\langle\left\langle F_P, 0\right\rangle\right\rangle$$

$$a_n = a_N + a_P + a_{ey} + a_{wy}$$

B.2 Energy Equation Manipulation

This section presents a description of the numerical method developed to solve the energy equation with viscous energy dissipation (4) by using the upwind scheme. The energy equation (4) can be written as follows:

$$\rho c_p (u \frac{\partial T}{\partial x} + v \frac{\partial T}{\partial y}) = k(\frac{\partial^2 T}{\partial x^2} + \frac{\partial^2 T}{\partial y^2}) + m\left[\left|2\left(\left(\frac{\partial u}{\partial x}\right)^2 + \left(\frac{\partial v}{\partial y}\right)^2\right) + \left(\frac{\partial u}{\partial y} + \frac{\partial v}{\partial x}\right)^2\right|^{\frac{n-1}{2}}\right]\Phi \quad \text{(B-27)}$$

where

$$\Phi = 2\left(\left(\frac{\partial u}{\partial x}\right)^2 + \left(\frac{\partial v}{\partial y}\right)^2\right) + \left(\frac{\partial u}{\partial y} + \frac{\partial v}{\partial x}\right)^2$$

To transform the dimensionless form of energy equation into the body-fitted coordinate system, the transformation parameters, equation (6), that described in chapter 3 are employed to energy equation. Thus the energy equation is become:

$$\frac{\partial}{\partial \xi}(\phi_U T) + \frac{\partial}{\partial \eta}(\phi_V T) = \frac{\partial}{\partial \xi}[\frac{\Psi}{J}(\alpha \frac{\partial T}{\partial \xi} - \beta \frac{\partial T}{\partial \eta})] + \frac{\partial}{\partial \eta}[\frac{\Psi}{J}(-\beta \frac{\partial T}{\partial \xi} + \gamma \frac{\partial T}{\partial \eta})] + \frac{mB}{\rho c_p}\Phi \quad \text{(B-28)}$$

where

$$B = \left[\left|\begin{array}{l} 2\left(\left(\frac{\partial u}{\partial \xi}\frac{y_\eta}{J} - \frac{\partial u}{\partial \eta}\frac{y_\xi}{J}\right)^2 + \left(\frac{\partial v}{\partial \eta}\frac{x_\xi}{J} - \frac{\partial v}{\partial \xi}\frac{x_\eta}{J}\right)^2\right) + \left(\frac{\partial u}{\partial \eta}\frac{x_\xi}{J} - \frac{\partial u}{\partial \xi}\frac{x_\eta}{J}\right)^2 + \\ \left(2\left(\frac{\partial u}{\partial \eta}\frac{x_\xi}{J} - \frac{\partial u}{\partial \xi}\frac{x_\eta}{J}\right)\left(\frac{\partial v}{\partial \xi}\frac{y_\eta}{J} - \frac{\partial v}{\partial \eta}\frac{y_\xi}{J}\right)\right) + \left(\frac{\partial v}{\partial \xi}\frac{y_\eta}{J} - \frac{\partial v}{\partial \eta}\frac{y_\xi}{J}\right)^2 \end{array}\right|^{\frac{n-1}{2}}\right]$$

$$\Phi = \left[\left|\begin{array}{l} 2\left(\left(\frac{\partial u}{\partial \xi}\frac{y_\eta}{J} - \frac{\partial u}{\partial \eta}\frac{y_\xi}{J}\right)^2 + \left(\frac{\partial v}{\partial \eta}\frac{x_\xi}{J} - \frac{\partial v}{\partial \xi}\frac{x_\eta}{J}\right)^2\right) + \left(\frac{\partial u}{\partial \eta}\frac{x_\xi}{J} - \frac{\partial u}{\partial \xi}\frac{x_\eta}{J}\right)^2 + \\ \left(2\left(\frac{\partial u}{\partial \eta}\frac{x_\xi}{J} - \frac{\partial u}{\partial \xi}\frac{x_\eta}{J}\right)\left(\frac{\partial v}{\partial \xi}\frac{y_\eta}{J} - \frac{\partial v}{\partial \eta}\frac{y_\xi}{J}\right)\right) + \left(\frac{\partial v}{\partial \xi}\frac{y_\eta}{J} - \frac{\partial v}{\partial \eta}\frac{y_\xi}{J}\right)^2 \end{array}\right|\right]$$

The energy equation can be integrated term by term. The first term on the left hand side in energy equation becomes

$$\int_s^n \int_w^e \frac{\partial}{\partial \xi}\left(u\frac{\partial y}{\partial \eta}T - v\frac{\partial x}{\partial \eta}T \right) d\xi d\eta$$

Then this integrated term can be solved by using numerical integration and linear interpolation.

$$\Delta\eta u_e \frac{(T_E + T_P)}{2} - \Delta\eta u_w \frac{(T_P + T_w)}{2} \tag{B-29}$$

Then the second term on the left hand side in energy equation becomes

$$\int_s^n \int_w^e \frac{\partial}{\partial \eta}\left(v\frac{\partial x}{\partial \xi}T - u\frac{\partial y}{\partial \xi}T \right) d\xi d\eta$$

$$= \left[v_n \Delta\xi \cos\theta - u_n \Delta\xi \sin\theta \right]\left(\frac{T_N + T_P}{2} \right) + \left[u_s \Delta\xi \sin\theta - v_s \Delta\xi \cos\theta \right]\left(\frac{T_P + T_S}{2} \right) \tag{B-30}$$

The first term on the right-hand side in energy equation becomes

$$\int_s^n \int_w^e \frac{\partial}{\partial \xi}\left(\frac{\Psi}{J}\left(\alpha\frac{\partial T}{\partial \xi} - \beta\frac{\partial T}{\partial \eta} \right) \right) d\xi d\eta$$

$$= \int_s^n \int_w^e \frac{\partial}{\partial \xi}\left(\frac{\Psi\alpha}{J}\frac{\partial T}{\partial \xi} \right) d\xi d\eta \; - \int_s^n \int_w^e \frac{\partial}{\partial \xi}\left(\frac{\Psi\beta}{J}\frac{\partial T}{\partial \eta} \right) d\xi d\eta$$

Now, consider the first integral term so that numerical integration, linear interpolation, and element analysis in Fig. 8 is used.

$$= \frac{\Psi\Delta\eta}{\Delta\xi\cos\theta}\left[(T_E - T_P) - (T_P - T_W) \right] \tag{B-31}$$

Now, consider term $\frac{\Psi\beta}{J}$ in the second integral term. From element analysis in Fig. 8,

$\beta = \sin\theta$ and $J = \cos\theta$. Thus, $\frac{\Psi\beta}{J} = A\tan\theta$

The $\frac{\Psi\beta}{J}$ term gives a very small number [26] that is compared to $\frac{\Psi\alpha}{J}$. Thus the β term doesn't effect to velocity and pressure profiles and it is neglected in this thesis.

Continuing the integration, the second term on the right hand side in energy equation becomes

$$\int_s^n \int_w^e \frac{\partial}{\partial\eta}\left(\frac{\Psi}{J}\left(\gamma\frac{\partial T}{\partial\eta}-\beta\frac{\partial T}{\partial\xi}\right)\right)d\xi d\eta$$

$$=\int_s^n \int_w^e \frac{\partial}{\partial\eta}\left(\frac{\Psi\gamma}{J}\frac{\partial T}{\partial\eta}\right)d\xi d\eta - \int_s^n \int_w^e \frac{\partial}{\partial\eta}\left(\frac{\Psi\beta}{J}\frac{\partial T}{\partial\xi}\right)d\xi d\eta$$

In similar manner, the first integral can be written

$$= \frac{\Psi\Delta\xi}{\Delta\eta\cos\theta}\left[(T_N - T_P)-(T_P - T_S)\right] \qquad \text{(B-32)}$$

The β term can be considered in similar manner to the previous β term in the first term of energy equation. Thus the β term in second integral is also neglected in this thesis.

Now integrate the viscous energy dissipation, in the energy equation. It is become

$$\frac{m}{\rho c_p}\int_s^n \int_w^e B\Phi d\xi d\eta$$

$$=\frac{m}{\rho c_p}\int_s^n \int_w^e B\left[\left|\begin{array}{l} 2\left(\left(\frac{\partial u}{\partial\xi}\frac{y_\eta}{J}-\frac{\partial u}{\partial\eta}\frac{y_\xi}{J}\right)^2+\left(\frac{\partial v}{\partial\eta}\frac{x_\xi}{J}-\frac{\partial v}{\partial\xi}\frac{x_\eta}{J}\right)^2\right)+\left(\frac{\partial u}{\partial\eta}\frac{x_\xi}{J}-\frac{\partial u}{\partial\xi}\frac{x_\eta}{J}\right)^2+ \\ \left(2\left(\frac{\partial u}{\partial\eta}\frac{x_\xi}{J}-\frac{\partial u}{\partial\xi}\frac{x_\eta}{J}\right)\left(\frac{\partial v}{\partial\xi}\frac{y_\eta}{J}-\frac{\partial v}{\partial\eta}\frac{y_\xi}{J}\right)\right)+\left(\frac{\partial v}{\partial\xi}\frac{y_\eta}{J}-\frac{\partial v}{\partial\eta}\frac{y_\xi}{J}\right)^2 \end{array}\right|\right]d\xi d\eta$$

By using element analysis in Fig. 8, x_η or $\frac{\partial x}{\partial \eta} = 0$ then the integrated viscous

energy dissipation term becomes

$$\left[\frac{2\Delta\eta B}{\Delta\xi\cos^2\theta}(u_e-u_w)^2\right]-\left[\frac{4B(u_e-u_w)(u_n-u_s)\tan\theta}{\cos\theta}\right]+\left[\frac{2B\Delta\xi\tan^2\theta(u_n-u_s)^2}{\Delta\eta}\right]+$$
$$\left[\frac{B\Delta\xi(u_n-u_s)^2}{\Delta\eta}\right]+\left[\frac{2B\Delta\xi(v_n-v_s)^2}{\Delta\eta}\right]+\left[\frac{2B(u_n-u_s)(v_e-v_w)}{\cos\theta}\right]-\left[\frac{2B\Delta\xi(u_n-u_s)(v_n-v_s)\tan\theta}{\Delta\eta}\right]+$$
$$\left[\frac{\Delta\eta B(v_e-v_w)^2}{\Delta\xi\cos^2\theta}\right]-\left[\frac{2B(v_e-v_w)(v_n-v_s)\tan\theta}{\cos\theta}\right]+\left[\frac{B\Delta\xi(v_n-v_s)^2\tan^2\theta}{\Delta\eta}\right]$$

where

$$B=\left[\begin{array}{l}\left|2\left(\left(\left(\frac{u_e-u_w}{\Delta\xi\cos\theta}\right)-\left(\left(\frac{u_n-u_s}{\Delta\eta}\right)\Delta\xi\tan\theta\right)\right)^2+\left(\left(\frac{v_n-v_s}{\Delta\eta}\right)\Delta\xi\right)^2\right)+\left(\left(\frac{u_n-u_s}{\Delta\eta}\right)\right)^2+\right.^{\frac{n-1}{2}}\\ \left(2\left(\left(\left(\frac{u_n-u_s}{\Delta\eta}\right)\right)*\left(\left(\frac{v_e-v_w}{\Delta\xi\cos\theta}\right)-\left(\left(\frac{v_n-v_s}{\Delta\eta}\right)\tan\theta\right)\right)\right)\right)+\\ \left(\left(\frac{v_e-v_w}{\Delta\xi\cos\theta}\right)-\left(\left(\frac{v_n-v_s}{\Delta\eta}\right)\tan\theta\right)\right)^2\end{array}\right]$$

Thus the discretization of energy equation by using upwind scheme is

$$a_P T_P = a_E T_E + a_W T_W + a_N T_N + a_S T_S + \frac{mB}{\rho c_p}\Phi \qquad \text{(B-33)}$$

where coefficient is

$$a_E = D_e + \langle\langle -T_e, 0\rangle\rangle$$

$$a_W = D_w + \langle\langle T_w, 0\rangle\rangle$$

$$a_N = D_n + \langle\langle -T_n, 0\rangle\rangle$$

$$a_S = D_s + \langle\langle T_s, 0\rangle\rangle$$

$$T_e = \Delta\eta u_e$$

$$T_w = \Delta\eta u_w$$

$$T_n = \left(v_n \Delta\xi \cos\theta - u_n \Delta\xi \sin\theta\right)$$

$$T_s = \left(u_s \Delta\xi \sin\theta - v_s \Delta\xi \cos\theta\right)$$

$$D_e = \frac{\Delta\eta\Psi}{\Delta\xi \cos\theta}$$

$$D_w = \frac{\Delta\eta\Psi}{\Delta\xi \cos\theta}$$

$$D_n = \frac{\Delta\xi\Psi}{\Delta\eta \cos\theta}$$

$$D_s = \frac{\Delta\xi\Psi}{\Delta\eta \cos\theta}$$

B.3 The Pressure Correction Equation

From continuity equation (1), it is written in physical coordinated as follow

$$\frac{\partial u}{\partial x} + \frac{\partial v}{\partial y} = 0 \tag{B-34}$$

By using dimensionless variables and the transformation parameters, equation (6) that described in chapter 3, the continuity equation can be written in body-fitted coordinated as follows

$$\frac{\partial}{\partial \xi}(\phi_U) + \frac{\partial}{\partial \eta}(\phi_V) = 0 \tag{B-35}$$

By using definition of ϕ_U and ϕ_V that mention before, the continuity equation can be written in form of

$$\frac{\partial}{\partial \xi}\left(U\frac{\partial Y}{\partial \eta} - V\frac{\partial X}{\partial \eta}\right) + \frac{\partial}{\partial \eta}\left(V\frac{\partial X}{\partial \xi} - U\frac{\partial Y}{\partial \xi}\right) = 0$$

or

$$\frac{\partial}{\partial \xi}\left(U\frac{\partial Y}{\partial \eta}\right) - \frac{\partial}{\partial \xi}\left(V\frac{\partial X}{\partial \eta}\right) + \frac{\partial}{\partial \eta}\left(V\frac{\partial X}{\partial \xi}\right) - \frac{\partial}{\partial \eta}\left(U\frac{\partial Y}{\partial \xi}\right) = 0$$

The continuity equation can be integrated term by term over staggered pressure control volume (P) in Fig. 7. Then the integral term of continuity equation can be written as follow

$$\int_s^n \int_w^e \left[\frac{\partial}{\partial \xi}\left(U\frac{\partial Y}{\partial \eta}\right) - \frac{\partial}{\partial \xi}\left(V\frac{\partial X}{\partial \eta}\right) + \frac{\partial}{\partial \eta}\left(V\frac{\partial X}{\partial \xi}\right) - \frac{\partial}{\partial \eta}\left(U\frac{\partial Y}{\partial \xi}\right)\right] d\xi d\eta = 0$$

$$\int_s^n \int_w^e \frac{\partial}{\partial \xi}\left(U\frac{\partial Y}{\partial \eta}\right) d\xi d\eta - \int_s^n \int_w^e \frac{\partial}{\partial \xi}\left(V\frac{\partial X}{\partial \eta}\right) d\xi d\eta + \int_s^n \int_w^e \frac{\partial}{\partial \eta}\left(V\frac{\partial X}{\partial \xi}\right) d\xi d\eta - \int_s^n \int_w^e \frac{\partial}{\partial \eta}\left(U\frac{\partial Y}{\partial \xi}\right) d\xi d\eta = 0$$

By using element analysis in Fig. 8, $\frac{\partial X}{\partial \eta}=0$ then the integrated term of continuity equation can be written

$$\Delta\eta\left(U_e-U_w\right)+\Delta\xi\cos\theta\left(V_n-V_s\right)-\Delta\xi\sin\theta\left(U_n-U_s\right)=0 \tag{B-36}$$

By substitution of velocity corrections (30) and (31), the discretization of pressure correction equation can be written as follow

$$a_P\bar{P}_P^{\prime}=a_E\bar{P}_E^{\prime}+a_W\bar{P}_W^{\prime}+a_N\bar{P}_N^{\prime}+a_S\bar{P}_S^{\prime}+a_{NE}\bar{P}_{NE}^{\prime}+a_{NW}\bar{P}_{NW}^{\prime}+a_{SE}\bar{P}_{SE}^{\prime}+a_{SW}\bar{P}_{SW}^{\prime}+\mathrm{b} \tag{B-37}$$

According to above discretization of pressure correction equation, the equation presents nine-point formulation that is difficult to solve. To reduce nine-point formulation to five-point formulation that is basic formulation of numerical method, the rest of five terms on the right hand side of discretization pressure correction equation are included to the source term. Then the discretization of pressure correction can be written in form of

$$a_P\bar{P}_P^{\prime}=a_E\bar{P}_E^{\prime}+a_W\bar{P}_W^{\prime}+a_N\bar{P}_N^{\prime}+a_S\bar{P}_S^{\prime}+\mathrm{source} \tag{B-38}$$

where

$$\mathrm{source}=a_{NE}\bar{P}_{NE}^{\prime}+a_{NW}\bar{P}_{NW}^{\prime}+a_{SE}\bar{P}_{SE}^{\prime}+a_{SW}\bar{P}_{SW}^{\prime}+\mathrm{b}$$

$$a_E=\Delta\eta d_{2e}$$

$$a_W=\Delta\eta d_{2w}$$

$$a_N=\left(\Delta\xi\cos\theta d_{3n}+\frac{\Delta\xi\sin\theta}{4}\left(d_{22N}-d_{21N}\right)\right)$$

$$a_S=\left(\Delta\xi\cos\theta d_{3s}+\frac{\Delta\xi\sin\theta}{4}\left(d_{21s}-d_{22s}\right)\right)$$

$$a_{NE}=\left(-\frac{\Delta\xi\sin\theta}{4}d_{22N}\right)$$

$$a_{NW} = \left(\frac{\Delta\xi \sin\theta}{4} d_{21N} \right)$$

$$a_{SE} = \left(\frac{\Delta\xi \sin\theta}{4} d_{22S} \right)$$

$$a_{SW} = \left(-\frac{\Delta\xi \sin\theta}{4} d_{21S} \right)$$

$$a_P = a_E + a_W + \Delta\xi \cos\theta d_{3n} + \Delta\xi \cos\theta d_{3s}$$

$$\text{b} = \Delta\eta\left(U_e^* - U_w^*\right) + \Delta\xi \cos\theta\left(V_n^* - V_s^*\right) + \frac{\Delta\xi \sin\theta}{4}\left(U_{2S}^* + U_{1S}^* - U_{2N}^* - U_{1N}^*\right)$$

$$U_e = U_e^* + d_{1e}\left(\bar{P}_n' - \bar{P}_s' \right)$$

$$U_w = U_w^* + d_{1w}\left(\bar{P}_n' - \bar{P}_s' \right)$$

$$U_{2N} = U_{2N}^* + d_{22N}\left(\bar{P}_n' - \bar{P}_s' \right)$$

$$U_{1N} = U_{1N}^* + d_{21N}\left(\bar{P}_n' - \bar{P}_s' \right)$$

$$U_{2S} = U_{2S}^* + d_{22S}\left(\bar{P}_n' - \bar{P}_s' \right)$$

$$U_{1S} = U_{1S}^* + d_{21S}\left(\bar{P}_n' - \bar{P}_s' \right)$$

$$d_{2e} = \frac{\Delta\eta}{a_e}$$

$$d_{2w} = \frac{\Delta\eta}{a_w}$$

$$d_{21N} = \frac{\Delta\eta}{a_{Nw}}$$

$$d_{22N} = \frac{\Delta\eta}{a_{Ne}}$$

$$d_{21S} = \frac{\Delta\eta}{a_{Sw}}$$

$$d_{22S} = \frac{\Delta\eta}{a_{Se}}$$

$$d_{3n} = \frac{\Delta\xi\cos\theta}{a_n}$$

$$d_{3s} = \frac{\Delta\xi\cos\theta}{a_s}$$

B.4 Inlet Temperature and Outlet Temperature

According to periodic boundary condition (BC, HI, DE, JK) in Fig. 2, they can be calculated by using linear interpolation. But inlet and outlet temperature can not be directly calculated by using linear interpolation because the rushing-in and rushing-out effect of the flow field. Then as far as the temperature is concerned, the periodic boundary condition at the cycle inlet and outlet is only valid for the dimensionless values.

Thus the dimensionless temperature at the cycle inlet and outlet can be written as follows:

$$\Theta = \frac{1}{2}\left(\frac{T(\xi_{1-1},\eta) - T_w}{T_b(\xi_{1-1}) - T_w} + \frac{T(\xi_{2-2},\eta) - T_w}{T_b(\xi_{2-2}) - T_w} \right) \tag{B-39}$$

where

ξ_{1-1}, ξ_{2-2} can be found in Fig. 4

$$T_b(\xi) = \frac{\int_{\eta_1}^{\eta_{M_1}} T(\xi,\eta) u(\xi,\eta) \sqrt{\alpha}\, d\eta}{\int_{\eta_1}^{\eta_{M_1}} u(\xi,\eta) \sqrt{\alpha}\, d\eta} \tag{B-40}$$

The local temperature at the cycle inlet and outlet are calculated by

$$T(\xi_{AG},\eta) = T_w + \Theta(T_b(\xi_{AG}) - T_w) \tag{B-41}$$

$$T(\xi_{FL},\eta) = T_w + \Theta(T_b(\xi_{FL}) - T_w) \tag{B-42}$$

By substitute $T_b(\xi)$ into (B-41) and (B-42) and use composite trapezoid rule [29], then the local temperature at the cycle inlet and outlet can be written in form of set of linear equations as follow

$$a_{11}T_1 + a_{12}T_2 + a_{13}T_3 + a_{14}T_4 + ... = b_1$$

$$a_{21}T_1 + a_{22}T_2 + a_{23}T_3 + a_{24}T_4 + ... = b_2 \qquad \text{(B-43)}$$

$$a_{31}T_1 + a_{32}T_2 + a_{33}T_3 + a_{34}T_4 + ... = b_3$$

$$\vdots$$

Where each set of above linear equations is separately solved for inlet and outlet temperature distribution.

To solve the local temperature at the cycle inlet and outlet, the Jacobi iterative method [29] is adopted.

APPENDIX C

Flow Chart of Non-Newtonian . C

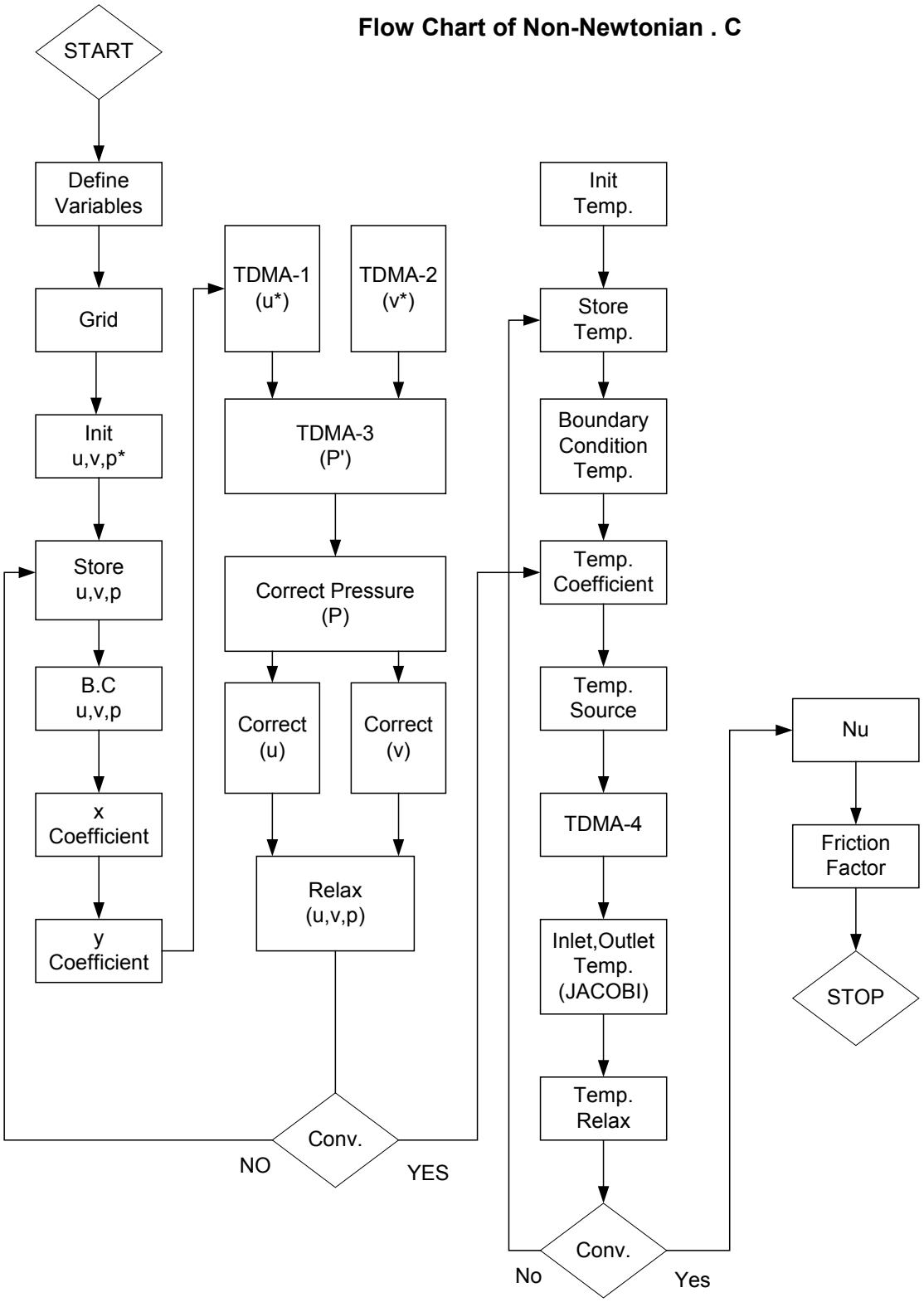

BIBLIOGRAPHY

BIBLIOGRAPHY

1. Huang, H.Z., and Tao, W.Q., 1993, "An Experimental Study on Heat/Mass Transfer and Pressure Drop Characteristics for Array of Non-Uniform Plate Length Positioned Obliquely to the Flow Direction," ASME Journal Of Heat Transfer, Vol. 115, pp. 568-575.
2. Lee, Y.N., 1986, "Heat Transfer and Pressure Drop Characteristics of an Array of Plates Aligned at Angles to the Flow in a Rectangle Duct," International Journal of Heat/Mass Transfer, Vol. 29, pp. 1553-1563.
3. Wang, L.B., and Tao, W.Q., 1995, "Heat Transfer and Fluid Flow Characteristics of Plated Array Aligned to the Flow Direction," International Journal Heat/Mass Transfer, Vol. 38, pp. 3053-3063.
4. Yan, X.J., Zhang, H.H., and Tao, W.Q., 1986, "An experimental Investigation of Heat Transfer and Pressure Drop Performance for Array of Staggered Plates Aligned with Air Flows," Proceedings of Eighth International Heat Transfer Conference, Vol. 4, pp. 2887-2896.
5. Sparrow, E.M., Baliga, B.R., and Patankar, S.V., 1977, "Heat Transfer and Fluid Flow Analysis of Interrupted-Wall Channel, With Application to Heat Exchanger" ASME Journal of Heat Transfer, Vol.99, pp. 4-11.
6. Sparrow, E.M., Liu, C.H., 1979, "Heat Transfer, Pressure Drop, and Performance Relationships for In-Line, Staggered, and Continuous Plate Heat Exchanger," International Journal Heat/Mass Transfer, Vol. 22, pp. 1613-1625.

7. Sparrow, E.M., and Cur, N., 1978, “Experiments Heat transfer and Pressure Drop for a Pair Colinear, Interrupted Plate Aligned with The Flow,” International Journal Heat/Mass Transfer, Vol. 21, pp. 1069-1080
8. Amano, R.S., 1985 “A Numerical Study of Laminar and Turbulent Heat Transfer in a Periodically Corrugated Wall Channel,” ASME Journal Of Heat Transfer, Vol. 107, pp. 564-569.
9. Lee, Y.N., 1989, “ Heat Transfer and Pressure Drop Characteristics of an Assembly of Partially Segmented Plates,” ASME Journal Of Heat Transfer, Vol. 111, pp. 44-50.
10. Lang, X.S., and Zhang, H.H., 1989, “The Investigation of Oblique Angles and Interrupted Plate Lengths for Louvered Fins in Compact Heat Exchanger,” Experimental Thermal Fluid Science, Vol. 2, pp.100-106.
11. Pang, K., Tao, W.Q, and Zhang, H.H., 1990, “Numerical Analysis of full developed Fluid Flow and Heat transfer for Array of Interrupted Plates Positioned Convergently-Divergently Along the Flow Direction,” Numerical Heat Transfer, Part A, Vol. 18, pp. 309-342.
12. Patankar, S.V., Prakash, C., 1981, “An Analysis of the Effect of Plate Thickness on Laminar Flow and Heat Transfer in Interrupted-Plate Passages,” International Journal Heat/Mass Transfer, Vol. 24, pp. 1801-1810.
13. Wang, L.B, Jiang, G.D, Tao, W.Q, and Ozoe, H., 1998,”Numerical Simulation on Heat Transfer and Fluid Flow Characteristics of Array of Non-Uniform Plate Length Positioned Obliquely to the Flow Direction,” Journal of Heat Transfer, Vol.120, pp. 991-998.

14. Wieting, A.R., 1975, “Empirical Correlation for Heat Transfer and Flow Friction Characteristics of Rectangular Offset-Fin-Plate-Fin Heat Exchangers,” Journal Of Heat Transfer, Vol. 97, pp. 488-490.
15. Xiao, Q., and Tao, W.Q., 1990, “Effect of Fin Spacing on Heat Transfer and Pressure Drop of Two-Row Corrugated Fin-and-Tube Heat Exchanger,” International Comm. Heat/Mass Transfer, Vol. 17, pp. 577-586.
16. Dewitt, D.P., and Incropera, F.P., 1990, Introduction to Heat Transfer, 2nd Edition, John-Wiley & Sons, New York, pp. 436-437.
17. Drake, R.M., and Eckert, E.R.G., 1959, Heat Mass Transfer, McGraw-Hill, New York.
18. Holman, J.P., 1989, Heat Transfer, SI Metric Edition, McGraw-Hill, New York, pp. 207-254.
19. Ozisik, N.M., 1985, Heat Transfer A Basic Approach, McGraw-Hill, New York, pp. 253-269.
20. Steward, W.E., Bird, R.B., and Lightfoot, E.N., 1962, “ Transport Phenomena,” New York, John Wiley, pp. 103.
21. Barletta, A., 1997, “ Fully Developed Laminar Forced Convection in Circular Ducts for Power-Law Fluids with Viscous Dissipation,” International Journal Heat/Mass transfer, Vol. 40, No. 1, pp. 15-26.
22. Mercer, W.E. et al., 1967, “Laminar Forced Convection in The Entrance region Between Parallel Flat Plates,” Journal Of Heat Transfer, Vol. 89, pp. 251-257.

23. Shahcheraghi, N., and Dwyer, H.A., A Generalized Laplacian Operator for Three-Dimension Geometry in Finite Volume Form, University of California, Davis, CA.
24. Patankar, S.V., 1980, Numerical Heat Transfer and Fluid Flow, Hemisphere, Washington, D.C., p. 126.
25. Frank, M.W., 1994, Fluid Mechanics 3Rd Edition, McGraw Hill, New York.
26. Chen, C.H, and Weng, F.B, 1990, "Heat Transfer for Incompressible and Compresssible Fluid Flows Over A Heat Cylinder," Numerical Heat Transfer, Part A, Vol 18, pp. 325-342.
27. Skelland, A.H.P., 1967, Non-Newtonian Flow and Heat Transfer, John Wiley &Sons, New York, pp. 1-12.
28. Schowalter, W.R, 1978, Mechanics of Non-Newtonian Fluids, Pergamon Press, New York, pp. 2-4
29. Fausett, L.V., 1999, Applied Numerical Analysis Using Matlab, Prentice Hall, New Jersey.
30. Sparrow, E.M., and Hajiloo, A., 1980,"Measurement of Heat Transfer and Pressure Drop for an Array of Staggered Plates Aligned Parallel to an Air Flow," International Journal Heat/Mass Transfer, Vol. 26, pp. 30-40.
31. Lang, X.S., and Zhang, H.H., 1989, "The Exprimental Investigation of Oblique Angles and Interrupted Plate Lengths for Louvered Fins in Compact Heat Exchanger," Experimental Thermal Fluid Science, Vol. 2, pp.100-106.